IN-38

359262

Final contract NAG3-1129 Report

Submitted to

NASA Lewis Research Center
Cleveland, Ohio 44135

Nondestructive Evaluation of Adhesively Bonded Joints

By
and

H. N. Hashemi
professor

J. N. Rossettos
Professor

Department of Mechanical, Industrial and Manufacturing Engineering
Northeastern University
Boston, MA 02115
617-373-5515

Our final report on contract #NAG3-1129 " Nondestructive Evaluation of Adhesively Bonded Joints," consists of the following documents. These include 5 published papers in referred journals and technical letters submitted to our monitor Dr. Alex Vary of NASA LRC. These publications are enclosed and listed as:

1. J. N. Rossettos, P. Lin, and H. Nayeb-Hashemi, "Comparison of the Effects of Debonds and Voids in Adhesive," J. of Eng. Mat. Tech., ASME Trans., 1994, pp. 533.

2. J. N. Rossettos and E. Zang, "On the Peak Shear Stresses in Adhesive Joints with Voids," J. Appl. Mech., Vol. 60, 1993, pp. 559.

3. H. Nayeb-Hashemi and J. N. Rossettos, "Nondestructive Evaluation of Adhesively Bonded Joints by Acousto-Ultrasonic Technique and Acoustic Emission," J. Acoustic Emission, Vol. 12, 1994, pp. 1.

4. H. Nayeb-Hashemi and J. N. Rossettos and A. P. Melo, "Multiaxial fatigue life evaluation of tubular adhesively bonded joints," Int. J. Adhesion and Adhesive 17, 1997, pp.55.

5. H. Nayeb-Hashemi and O. C. Jawad, "Theoretical and Experimental Evaluation of the Bond Strength Under Peeling Loads," J. Eng. Mat. Tech., Vol. 119, 1997. pp. 415.

6. H. Nayeb-Hashemi and J. N. Rossettos, "Progress report to NASA," 1994,

Comparison of the Effects of Debonds and Voids in Adhesive Joints

J. N. Rossettos

P. Lin

H. Nayeb-Hashemi

Department of Mechanical Engineering,
Northeastern University,
Boston, MA 02115

An analytical model is developed to compare the effects of voids and debonds on the interfacial shear stresses between the adherends and the adhesive in simple lap joints. Since the adhesive material above the debond may undergo some extension (either due to applied load or thermal expansion or both), a modified shear lag model, where the adhesive can take on extensional as well as shear deformation, is used in the analysis. The adherends take on only axial loads and act as membranes. Two coupled nondimensional differential equations are derived, and in general, five parameters govern the stress distribution in the overlap region. As expected, the major differences between the debond and the void occur for the stresses near the edge of the defect itself. Whether the defect is a debond or a void, is hardly discernible by the stresses at the overlap ends for central defect sizes up to the order of 70 percent of the overlap region. If the defect occurs precisely at or very close to either end of the overlap, however, differences of the order of 20 percent in the peak stresses can be obtained.

Introduction

Adhesive bonded joints for composite or metal joining are being used in many structural applications. Among the most significant concerns regarding the structural design and reliability of the joints are the possible defects like debonds or voids which occur during manufacturing or service. These defects can severely reduce the bond strength. Their presence will increase the peak stress levels which occur at the joint ends and near the flaw itself. The joint may fail at the ends of the joint at the ultimate stress or it may fail under cyclic loading where local debonding near the flaw can grow. Also, the subsequent redistribution of stress, due to debonding, may lead to possible delamination in the composite adherend itself. The stress concentration, therefore, near a void or disbond is important, and any thermal mismatch between the adherend and the adhesive will also contribute to the increased stress levels which occur.

Past work, related to the present study, was performed by Erdogan and Ratwani (1971), Hart-Smith (1973, 1981), Kan and Ratwani (1983, 1986), and Rossettos and Zang (1993). The aforementioned work, dealing with voids or disbonds in the adhesive, uses a shear lag model, where the adherends take on only axial load and the adhesive takes only shear. This is appropriate in bonded joints which are designed so that the net load path does not produce bending.

In the present work, which deals with simple lap joints, in order to properly compare the effects of debonds and voids, where the adhesive material above the debond may undergo some extension, it is necessary to allow the adhesive to take on axial stress as well as shear. A modified shear lag model used by Rossettos and Shishesaz (1987) is adopted here for this purpose. As such, a quadratic distribution of axial displacement is assumed in the adhesive. Based on appropriate equilibrium, stress-strain and strain-displacement relations, the problem is reduced to two coupled second order differential equations for the axial loads in the adherends. A subsequent nondimensionalization of quantities in the equation leads to several parameters which are seen to govern the stress distribution in the joint.

A structural mechanics rather than a continuum approach is used, where the loading mechanisms are restricted to net axial and shear deformation in the components, and where a given quadratic displacement distribution is taken over the thickness of the adhesive layer. This avoids the corner singularity at the overlap ends. Since the general solution of the structural model contains exponential terms, the steep stress gradients near the overlap ends and at the defect edges can be calculated accurately. It is also remarked that if transverse shear in the adherends is also included in a higher order analysis (Renton and Vinson, 1977) the peak shear stress values will occur very near the overlap ends, dropping sharply to zero at the ends themselves. The conclusions of the present paper, however, regarding these peak shear stresses, will change very little, if at all.

Analysis

The model consists of a simple lap joint as shown in Fig. 1(*a*, *b*) made of two plates, which take only axial loads, bonded by an adhesive layer. Plates 1 and 2 can be made of composite materials with orthotropic characteristics, although either ad-

Contributed by the Materials Division for publication in the JOURNAL OF ENGINEERING MATERIALS AND TECHNOLOGY. Manuscript received by the Materials Division July 26, 1993. Associate Technical Editor: V. K. Stokes.

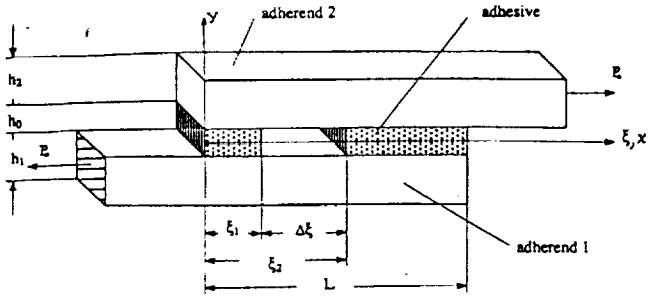

Fig. 1(*a*) Lap joint with a void

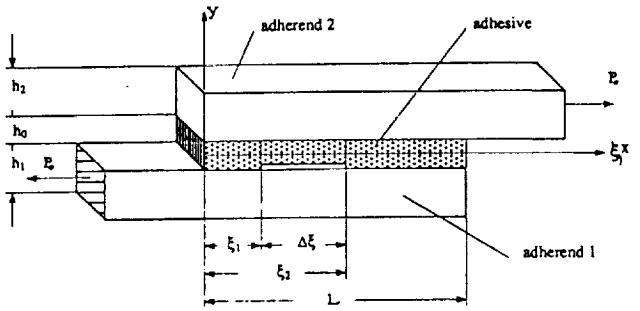

Fig. 1(*b*) Lap joint with a debond

herend could be specialized to an isotropic material with no change in the formulation or the general nondimensional solutions. Let $p_1(x)$, $p_2(x)$ and $p_3(x)$ be the resultant forces per unit width in adherend 1, adherend 2, and the adhesive respectively, while p_0 is the corresponding force applied to the adherends away from the joint. For any value of x we have

$$p_1(x) + p_2(x) + p_3(x) = p_0 \tag{1}$$

A quadratic displacement in the axial direction, $u_3(x, y)$, is assumed in the adhesive as

$$u_3(x, y) = u_0(x) + \frac{y}{h_0}[u_2(x) - u_1(x)] + \frac{2y^2}{h_0^2}[u_2(x) + u_1(x) - 2u_0(x)] \tag{2}$$

where u_1, u_2, and u_o are the axial displacements in adherend 1, adherend 2, and the center, ($y = 0$), of the adhesive, respectively, and are functions of x. In Eq. (2), the origin of the local x-y system is at the center of the adhesive as shown in Fig. 1, so that u_3 at $y = h_o/2$ and $y = -h_o/2$ has the value u_2 and u_1, respectively. In the adhesive, the lateral displacement in the x direction is taken uniform so that the shear stress is given by $\tau(x, y) = G_0 \partial u_3/\partial y$. On using Eq. (2), we obtain

$$\tau(x, y) = \frac{G_0}{h_0}[u_2(x) - u_1(x)] + \frac{4G_0 y}{h_0^2}[u_1(x) + u_2(x) - 2u_0(x)] \tag{3}$$

By considering the equilibrium of each adherend, the following equations are obtained

$$\frac{dp_2}{dx} - \tau_2(x) = 0 \quad \frac{dp_1}{dx} + \tau_1(x) = 0 \tag{4a, b}$$

where

$$\tau_2(x) = \tau\left(x, y = \frac{h_0}{2}\right) \quad \tau_1(x) = \tau_1\left(x, y = -\frac{h_0}{2}\right)$$

The shear stresses $\tau_2(x)$ and $\tau_1(x)$ are stresses in the adhesive just below adherend 2 and just above adherend 1 respectively, and can be calculated using Eq. (3). The net axial load in the adhesive is given by

$$p_3(x) = \int_{-\frac{h_0}{2}}^{\frac{h_0}{2}} \sigma_{x3}(x, y)\, dy \tag{5}$$

where σ_{x3} is the axial stress in the adhesive and is a function of x and y. The axial stresses in adherends 1 and 2 are $\sigma_{x1} = p_1/h_1$ and $\sigma_{x2} = p_2/h_2$, respectively. Since the thicknesses h_0, h_1, h_2 are small compared to other structural dimensions, we assume the stresses $\sigma_{y1} = \sigma_{y2} = \sigma_{y3} = 0$. We also assume generalized plane strain conditions to apply. These basic assumptions are also used by Kan and Ratwani (1983). The stress-strain relations are then given by

$$\epsilon_{x1} = \frac{p_1(x)}{E_{x1}h_1}(1 - \upsilon_{zx1}\upsilon_{xz1}) + \alpha_1 \Delta T \tag{6a}$$

$$\epsilon_{x2} = \frac{p_2(x)}{E_{x2}h_2}(1 - \upsilon_{zx2}\upsilon_{xz2}) + \alpha_2 \Delta T \tag{6b}$$

$$\epsilon_{x3} = \frac{\sigma_3(x, y)}{E_0}(1 - \upsilon_0^2) + \alpha_0 \Delta T \tag{6c}$$

where α_1, α_2, and α_0 are coefficients of thermal expansion in adherend 1, adherend 2 and adhesive, respectively. The strain displacement relations are

$$\epsilon_{x1} = \frac{du_1}{dx}; \quad \epsilon_{x2} = \frac{du_2}{dx}; \quad \epsilon_{x3} = \frac{du_1}{dx} \tag{7}$$

The principal equations for the problem can be derived as follows. If the derivative of Eqs. (4*a*, *b*) is taken, while observing Eq. (3), derivatives of the displacements u_0, u_1, u_2 appear. Equations (7) give these derivatives in terms of strains, and via Eqs. (6), (5), and (1), in terms of the loads p_1 and p_2. In the process, it works out that the strain ϵ_{x3} in the adhesive can be related to the derivatives of the displacements using Eqs. (6*c*) and (2), while the derivative of u_0 can be eliminated in terms of p_1 and p_2 using Eqs. (1), (5), (6*c*), and (7). In this way, the problem can be reduced to the solution of two coupled 2nd order differential equations for the adherend loads p_1 and p_2. The shear stresses at the interface between the adhesive and adherend are then given by the derivatives of these loads as indicated in Eqs. (4*a*, *b*).

Nondimensional quantities are next defined as follows:

$$(P_1, P_2) = \frac{(p_1, p_2)}{p_0}; \quad \xi = \frac{x}{L};$$

$$(U_1, U_2, U_0) = \frac{LG_0}{p_0 h_0}(u_1, u_2, u_0)$$

$$S = \pm\frac{dP}{d\xi} = \frac{L}{p_0}\frac{dp}{dx} = \frac{L}{p_0}\tau\left(x, y = \pm\frac{h_0}{2}\right) \tag{8}$$

where the quantities P, S represent nondimensional load, and shear stress, respectively, and will appear in what follows. With the definitions in Eqs. (8), the two differential equations are written in terms of the nondimensional loads P_1 and P_2 as,

$$\frac{d^2P_1}{d\xi^2} - \Omega(1 + \delta_1)P_1 - \Omega\left(1 + \frac{\delta_2}{2}\right)P_2 = -\Omega(1 - \phi_1) \tag{9a}$$

$$\frac{d^2P_2}{d\xi^2} - \Omega\left(1 + \frac{\delta_1}{2}\right)P_1 - \Omega(1 + \delta_2)P_2 = -\Omega(1 - \phi_2) \tag{9b}$$

where

$$\Omega = 3(1 - \upsilon_0)\left(\frac{L}{h_0}\right)^2 \qquad \delta_1 = \frac{2}{3}\frac{E_0 h_0}{E_{x1}h_1}\frac{1 - \upsilon_{zx1}\upsilon_{xz1}}{1 - \upsilon_0^2}$$

$$\delta_2 = \frac{2}{3}\frac{E_0 h_0}{E_{x2}h_2}\frac{1 - \upsilon_{zx2}\upsilon_{xz2}}{1 - \upsilon_0^2}$$

and

$$\phi_1 = \frac{2(2\alpha_1 + \alpha_2 - 3\alpha_0)}{3(1-\nu_0)} \frac{G_0 h_0 \Delta T}{p_0}$$

$$\phi_2 = \frac{2(\alpha_1 + 2\alpha_2 - 3\alpha_0)}{3(1-\nu_0)} \frac{G_0 h_0 \Delta T}{p_0}$$

The parameters δ_i ($i = 1, 2$) and Ω represent material and geometric properties of the adherends and the adhesive. The parameters ϕ_i ($i = 1, 2$), are thermal parameters which also include adhesive properties and the load p_0.

A solution to Eqs. (9) can be developed by means of an eigenvector expansion. As such the homogeneous form of Eqs. (9) can be written in the matrix form

$$\mathbf{U}'' - \mathbf{L}\mathbf{U} = 0 \tag{10}$$

where $\mathbf{U}^T = |P_1, P_2|$ and $\mathbf{L}$ is a square matrix involving Ω, δ_1, and δ_2. A solution to Eqs. (10) is then assumed in the form

$$\mathbf{U} = \mathbf{H}e^{\lambda\xi} \tag{11}$$

where $\mathbf{U}$ and $\mathbf{H}$ are vectors of second order. Substituting Eq. (11) into Eq. (10) results in the eigenvalue problem $(\mathbf{L} - \lambda^2\mathbf{I})\mathbf{H} = 0$ which leads to eigenvalues, λ_i^2, with corresponding eigenvectors, $\mathbf{H}^i$. For this problem, all the eigenvalues are real, and contain the parameters δ_1, δ_2, and Ω. The homogeneous solution can then be written as

$$\mathbf{U} = \mathbf{H}^{(1)}(C_1 e^{\lambda_1\xi} + C_2 e^{-\lambda_1\xi}) + \mathbf{H}^{(2)}(C_3 e^{\lambda_2\xi} + C_4 e^{-\lambda_2\xi}) \tag{12}$$

The particular solution, which is a constant, is easily obtained from Eqs. (9) and contains the parameters δ_i and ϕ_i.

In the solution procedure, the adhesive is divided into three regions. Equations (9) apply to the first and third regions, which border the ends of the overlap. In the second or defect region, which falls between the other two, the governing equations will differ from Eqs. (9). General solutions in all regions will give rise to constants of integration which are determined by appropriate boundary and continuity conditions.

The general solution to Eqs. (9) is

$$P_1(\xi) = C_1 e^{\lambda_1\xi} + C_2 e^{-\lambda_1\xi} + C_3 e^{\lambda_2\xi} + C_4 e^{-\lambda_2\xi} + A_1 \tag{13a}$$

$$P_2(\xi) = H_2^{(1)}(C_1 e^{\lambda_1\xi} + C_2 e^{-\lambda_1\xi}) + H_2^{(2)}(C_3 e^{\lambda_2\xi} + C_4 e^{-\lambda_2\xi}) + A_2 \tag{13b}$$

where A_1 and A_2 are particular solutions. The nondimensional shear stresses in the interface between the adhesive and adherends as determined from Eqs. (4) and (8) are given by

$$S_1(\xi) = -\frac{dP_1}{d\xi}; \quad S_2(\xi) = \frac{dP_2}{d\xi} \tag{14}$$

Void Model. The general solution, namely Eqs. (13), applies to regions I and III, and gives rise to 8 independent constants of integration. The boundary and continuity conditions are now given as follows. In the notation for the loads, P_{ij}, the first subscript $i = 1, 2$ represents the adherend, while the second subscript j = I, II, III represents the region number.

In region I ($0 \le \xi \le \xi_1$) we have

$$P_{1I}(0) = 1; \; P_{2I}(0) = 0; \; P_{1I}(\xi_1^-) = P_{1II}(\xi_1^+); \; P_{2I}(\xi_1^-) = P_{2II}(\xi_1^+) \tag{15}$$

In region II (void) ($\xi_1 \le \xi \le \xi_2$), since the shear stress on the adherends is zero, Eqs. (4*a*, *b*) imply that the loads are constant so $P_{1II} = C_5$ and $P_{2II} = C_6$. In this region the load in the adhesive is zero so that Eq. (1) leads to

$$P_{1II} + P_{2II} = C_5 + C_6 = 1 \tag{16}$$

In region III ($\xi_2 \le \xi \le 1$)

$$P_{1III}(\xi_2^-) = P_{1III}(\xi_2^+); \quad P_{2II}(\xi_2^-) = P_{2III}(\xi_2^+); \quad P_{1III}(1) = 0; \quad P_{2III}(1) = 1 \tag{17}$$

There are ten unknown constants of integration but only nine conditions in Eqs. (15), (16), and (17). An additional condition can be obtained as follows. The nondimensional shear quantities S_1 and S_2 can be written in terms of nondimensional displacements using Eqs. (3) and (8). When they are evaluated at ξ_2^+ and ξ_1^- they can be written as

$$S_1(\xi = \xi_2^+) = [4U_0(\xi_2^+) - 3U_1(\xi_2^+) - U_2(\xi_2^+)] \tag{18a}$$

$$S_2(\xi = \xi_2^+) = -[4U_0(\xi_2^+) - U_1(\xi_2^+) - 3U_2(\xi_2^+)] \tag{18b}$$

$$S_1(\xi = \xi_1^-) = [4U_0(\xi_1^-) - 3U_1(\xi_1^-) - U_2(\xi_1^-)] \tag{18c}$$

$$S_2(\xi = \xi_1^-) = -[4U_0(\xi_1^-) - U_1(\xi_1^-) - 3U_2(\xi_1^-)] \tag{18d}$$

The changes in the interfacial shear stresses, as we go from ξ_1^- to ξ_2^+ over the defect region, are given in terms of displacements as

$$\Delta S_1 = S_1(\xi = \xi_2^+) - S_1(\xi = \xi_1^-) = 4[U_0(\xi_2^+) - U_0(\xi_1^-)] - 3[U_1(\xi_2^+) - U_1(\xi_1^-)] - [U_2(\xi_2^+) - U_2(\xi_1^-)] \tag{19a}$$

and

$$\Delta S_2 = S_2(\xi = \xi_2^+) - S_2(\xi = \xi_1^-) = -4[U_0(\xi_2^+) - U_0(\xi_1^-)] + [U_1(\xi_2^+) - U_1(\xi_1^-)] + 3[U_2(\xi_2^+) - U_2(\xi_1^-)] \tag{19b}$$

Also, the change in the displacements of the adherends, as we go from ξ_1 to ξ_2, can be derived by noting, for the void case, that ϵ_{x1} and ϵ_{x2} are constants; this gives

$$U_1(\xi_2) - U_1(\xi_1) = \frac{G_0 L^2}{p_0 h_0}[u_1(x_2) - u_1(x_1)] = \frac{G_0 L^2}{p_0 h_0}\int_{x_1}^{x_2} \epsilon_{x1} dx = \left[\frac{1 - \nu_{zx1}\nu_{xz1}}{E_{x1} h_1} p_0 P_{1II} + \alpha_1 \Delta T\right] \frac{G_0 L^2}{p_0 h_0}(\xi_2 - \xi_1) \tag{20a}$$

$$U_2(\xi_2) - U_2(\xi_1) = \frac{G_0 L^2}{p_0 h_0}[u_1(x_2) - u_1(x_1)] = \frac{G_0 L^2}{p_0 h_0}\int_{x_1}^{x_2} \epsilon_{x2} dx = \left[\frac{1 - \nu_{zx2}\nu_{xz2}}{E_{x2} h_2} p_0 P_{2II} + \alpha_2 \Delta T\right] \frac{G_0 L^2}{p_0 h_0}(\xi_2 - \xi_1) \tag{20b}$$

Using continuity of displacements in the adherends, adding Eqs. (19*a*) and (19*b*) and using Eqs. (20) gives

$$\Delta S_1 + \Delta S_2 = \left\{-2\frac{1 - \nu_{zx1}\nu_{xz1}}{E_{x1} h_1} p_0 P_{1II} + 2\frac{1 - \nu_{zx2}\nu_{xz2}}{E_{x2} h_2} p_0 P_{2II} - 2\alpha_1 \Delta T + 2\alpha_2 \Delta T\right\} \frac{G_0 L^2}{p_0 h_0}(\xi_2 - \xi_1) \tag{21}$$

On noting the general solution (Eqs. (13)), and the computation of shears via Eqs. (14), Eq. (21) can be written in terms of the ten constants of integration, and so provides the additional equation needed for their determination.

Debond Model. An approach similar to the void model is used in the case of the debond, except now there is adhesive material above the debond in region II. Also, the quadratic displacement in this region is different from that in Eq. (2) which still applies to regions I and III. In region II, the quadratic displacement for u_3 must reflect the fact that the shear stress in the adhesive, at the debond (see Fig. 1(*b*)) location $y = -h_0/2$, is zero (i.e., $\partial u_3/\partial y = 0$). Using this condition, the displacement in the adhesive in region II can be derived to give

$$u_3(x, y) = u_0(x) + \frac{4}{3h_0}[u_2(x) - u_0(x)]y + \frac{4}{3h_0^2}[u_2(x) - u_0(x)]y^2 \tag{22}$$

With this relation, the shear stress between the adhesive and adherend 2 is given in region II as

$$\tau_2\left(x,\, y=\frac{h_0}{2}\right)=\frac{8G_0}{3h_0}\,(u_2-u_0) \tag{23}$$

The governing equation for adherend 2 in region II is then given by

$$\frac{d^2P_2}{d\xi^2}-\frac{1}{2}\,\Omega P_1-\frac{1}{2}\,\Omega\left(1+\frac{3}{2}\,\delta_2\right)P_2=-\frac{1}{2}\,\Omega[1-(2\phi_2-\phi_1)] \tag{24}$$

Since the shear stress on adherend 1 is zero (due to debond), the load there is still constant so $P_{1II} = C_5$. This is substituted into Eq. (24), and a solution for P_{2II} is easily obtained, with two additional constants of integration. There is therefore a total of 11 unknown constants ($C_1 \ldots C_4$ from region I, $C_5 \ldots C_7$ from region II and $C_8 \ldots C_{11}$ from region III) to be determined. The conditions in Eqs. (15) and (17) still apply, yielding eight equations. Two additional equations arise from the continuity of shear stress between adherend 2 and the adhesive at points ξ_1 and ξ_2, so

$$S_{2I}(\xi=\xi_1^-)=S_{2II}(\xi=\xi_1^+) \tag{25a}$$

and

$$S_{2II}(\xi=\xi_2^-)=S_{2III}(\xi=\xi_2^+) \tag{25b}$$

The eleventh required condition can be obtained in a manner similar to that of the void, except that in the debond model, in region II, ϵ_{x1} is constant but ϵ_{x2} is not. The change in the displacements of the adherends as we go from ξ_1 to ξ_2 are now as follows. For adherend 1, $U_1(\xi_2) - U_1(\xi_1)$ is the same as Eq. (20*a*) but for adherend 2 (using Eq. (6*b*) and the solution for P_{2II}) get

$$U_2(\xi_2)-U_2(\xi_1)=\frac{G_0L}{p_0h_0}\,[u_2(x_2)-u_2(x_1)]=\frac{G_0L}{p_0h_0}\int_{x_1}^{x_2}\epsilon_{x2}dx$$

$$=\left\{\frac{1-\upsilon_{zx2}\upsilon_{xz2}}{E_{x2}h_2}\,p_0\left(-\frac{1}{1+\frac{3}{2}\,\delta_2}\,(\xi_2-\xi_1)C_5\right.\right.$$

$$+\frac{e^{\sqrt{\frac{1}{2}\,\Omega\left(1+\frac{3}{2}\,\delta_2\right)}\,\xi_2}-e^{\sqrt{\frac{1}{2}\,\Omega\left(1+\frac{3}{2}\,\delta_2\right)}\,\xi_1}}{\sqrt{\frac{1}{2}\,\Omega\left(1+\frac{3}{2}\,\delta_2\right)}}\,C_6$$

$$-\frac{e^{-\sqrt{\frac{1}{2}\,\Omega\left(1+\frac{3}{2}\,\delta_2\right)}\,\xi_2}-e^{-\sqrt{\frac{1}{2}\,\Omega\left(1+\frac{3}{2}\,\delta_2\right)}\,\xi_1}}{\sqrt{\frac{1}{2}\,\Omega\left(1+\frac{3}{2}\,\delta_2\right)}}\,C_7$$

$$\left.\left.+A_3(\xi_2-\xi_1)\right)+\alpha_2\Delta T(\xi_2-\xi_1)\right\}\frac{G_0L^2}{p_0h_0} \tag{26}$$

Also, an equation, which is the counterpart of Eq. (21) for the void case, and which applies to the debond case can be derived to give

$$\Delta S_1+\Delta S_2=\left\{-2p_0\left[\frac{1-\upsilon_{zx1}\upsilon_{xz1}}{E_{x1}h_1}\right.\right.$$

$$\left.+\frac{1-\upsilon_{zx2}\upsilon_{xz2}}{E_{x2}h_2}\,\frac{1}{1+\frac{3}{2}\,\delta_2}\right](\xi_2-\xi_1)C_5$$

$$+\frac{2p_0}{\sqrt{\frac{1}{2}\,\Omega\left(1+\frac{3}{2}\,\delta_2\right)}}\,\frac{1-\upsilon_{zx2}\upsilon_{xz2}}{E_{x2}h_2}\left[\left(e^{\sqrt{\frac{1}{2}\,\Omega\left(1+\frac{3}{2}\,\delta_2\right)}\,\xi_2}\right.\right.$$

$$\left.-e^{\sqrt{\frac{1}{2}\,\Omega\left(1+\frac{3}{2}\,\delta_2\right)}\,\xi_1}\right)C_6-\left(e^{-\sqrt{\frac{1}{2}\,\Omega\left(1+\frac{3}{2}\,\delta_2\right)}\,\xi_2}-e^{-\sqrt{\frac{1}{2}\,\Omega\left(1+\frac{3}{2}\,\delta_2\right)}\,\xi_1}\right)C_7\Big]$$

$$\left.+2(\xi_2-\xi_1)\left[-\alpha_1\Delta T+\alpha_2\Delta T+\frac{1-\upsilon_{zx2}\upsilon_{xz2}}{E_{x2}h_2}\,p_0A_3\right]\right\}\frac{G_0L^2}{p_0h_0} \tag{27}$$

With this additional condition, all eleven unknown constants of integration can be found, and the interfacial shear stress quantities can be calculated. The algebraic details can be found in (Lin, 1992).

Results and Discussion

As indicated by the nondimensional differential equations, the stress distribution in the overlap region is governed by the five parameters Ω, δ_1, δ_2, ϕ_1, ϕ_2, and the size and position of the defect. These parameters contain both geometric and material properties of the adherends and adhesive. Peak shear stresses are therefore dependent on the selection of geometry or materials or both.

Typical distributions for the interfacial shear stresses S_1 and S_2 are given in Fig. 2 for Ω = 1000 and 4000. The defect is at the center of the overlap with size $\Delta\xi = \xi_2 - \xi_1 = 0.4$. Values of the other parameters are as shown. It is clear that there is very little difference in the stresses at the overlap ends for the void and the debond. Any differences occur at the edge of the defect itself, with steep boundary layer behavior. In fact, these stresses can have differences of 100–150 percent. Note, for

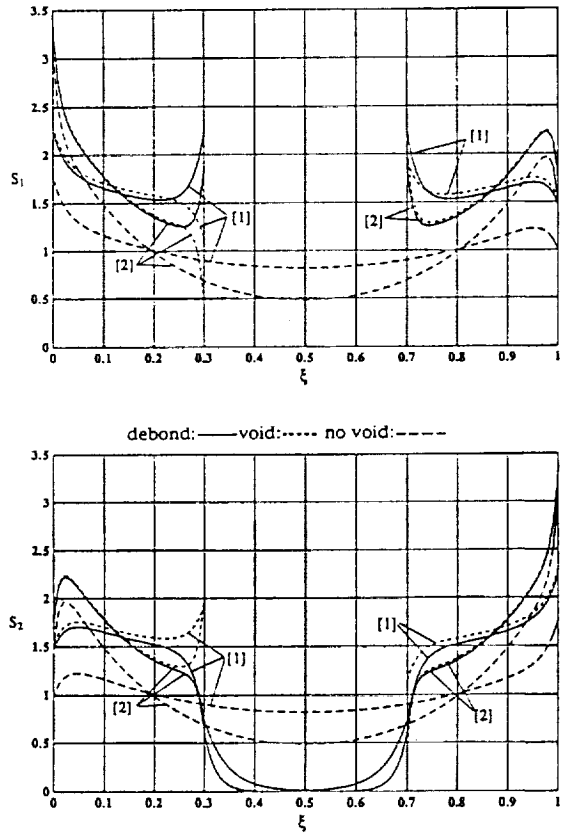

Fig. 2 Nondimensional shear stresses S_1, S_2 versus ξ for two Ω values. [1]: Ω = 1000; [2]: Ω = 4000; $\phi_1 = \phi_2 = 0.01$, $\delta_1 = \delta_2 = 0.01$, $\xi_1 = 0.3$, $\xi_2 = 0.7$. symmetric defect.

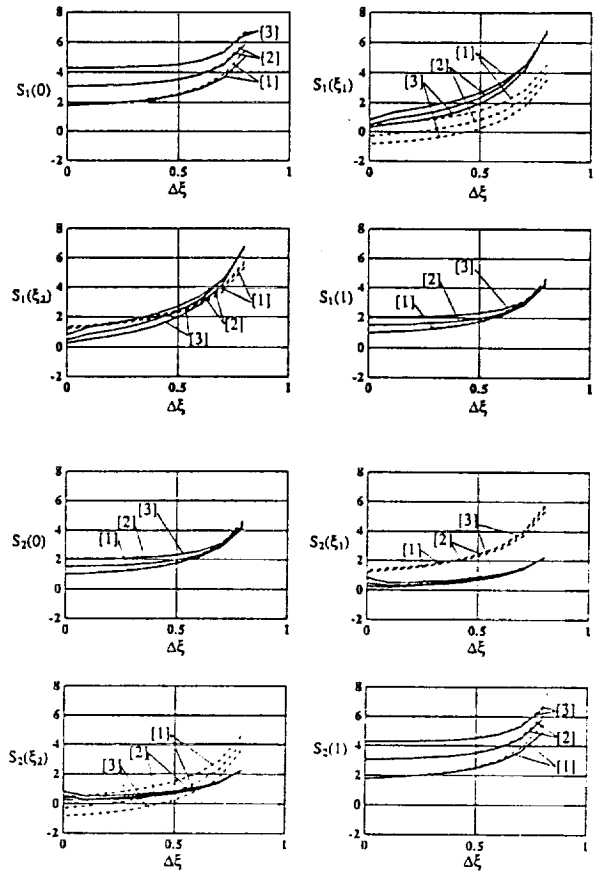

Fig. 3 Nondimensional shear stresses S_1, S_2 at special points versus $\Delta\xi$ for three Ω values. [1]: Ω = 1000, [2]: Ω = 4000, [3]: Ω = 8000; debond: —, void: · · · ·, $\phi_1 = \phi_2 = 0.01$, $\delta_1 = \delta_2 = 0.01$; symmetric defect.

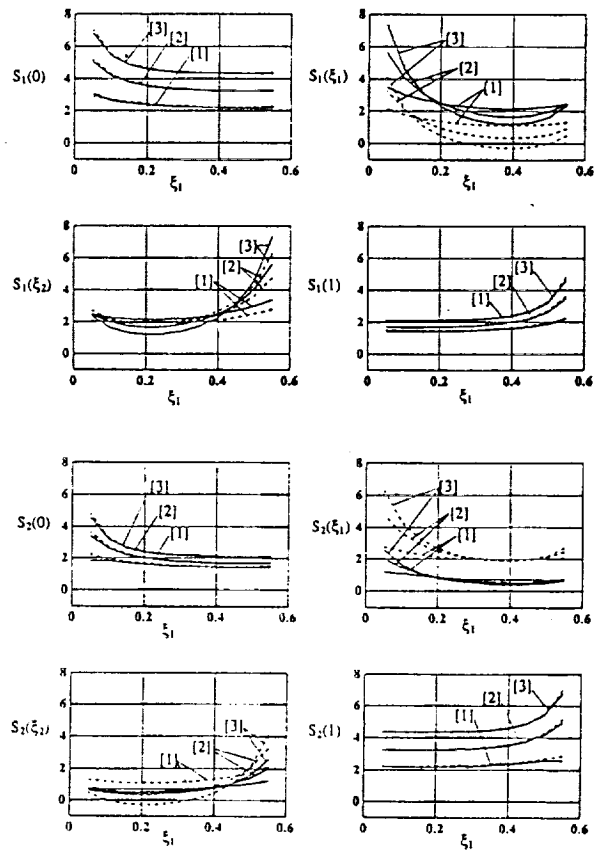

Fig. 4 Nondimensional shear stresses S_1, S_2 at special points versus ξ_1 for three Ω values. [1]: Ω = 1000, [2]: Ω = 4000, [3]: Ω = 8000; debond: —, void: · · · ·, $\phi_1 = \phi_2 = 0.01$, $\delta_1 = \delta_2 = 0.01$, nonsymmetric defect of size, $\Delta\xi = 0.4$.

instance, that at $\xi = \xi_1 = 0.3$, S_1 decreases for the void case while increasing for the debond case, and the reverse is true for S_2. Both stresses show a tendency for steep edge effects. The structural mechanics (rather than continuum) approach in this paper does not address the type of singularity that exists at these edges.

In Fig. 3, values for the shear stresses at the ends of the overlap and at the edges of the defect are plotted against center defect size, $\Delta\xi$. Again we see very little difference in the stresses at the overlap ends for the void and the debond, for a large range of defect sizes. Only when defect size is of the order of 70 percent of the overlap length can we find a difference of 5 percent in the case when Ω = 1000. The stress values at ξ_1 and ξ_2 (defect edges) are clearly substantially different for the debond and the void, for the full range of defect sizes.

Corresponding results for the nonsymmetric defect are shown in Fig. 4. Here the defect size, $\Delta\xi = 0.4$, is fixed and the left defect edge, ξ_1, moves from left to right (ξ_1 = 0.1 to 0.55). The same general conclusions on the small differences in the stresses at the ends of the overlap for the void and debond hold. Notice however, that in Fig. 3 (symmetric case) the curves for a given defect, for different Ω values, do not cross. But in the nonsymmetric case (Fig. 4) the curves for the stresses at the defect edges, do cross for different Ω values.

A special case occurs when the defect is at either end of the overlap. If a void occurs at the overlap ends, the result is just a shorter overlap length and a larger value of physical shear stress. In the debond case this is not so since the adhesive above the debond can take some axial load. The physical shear stress at $\xi = \xi_2$ is plotted against ξ_2, (the right edge of the defect) with $\xi_1 = 0$ in Fig. 5. While the peak stresses at $\xi = \xi_2$ in adherend 1 are larger for the debond than those for the cor-

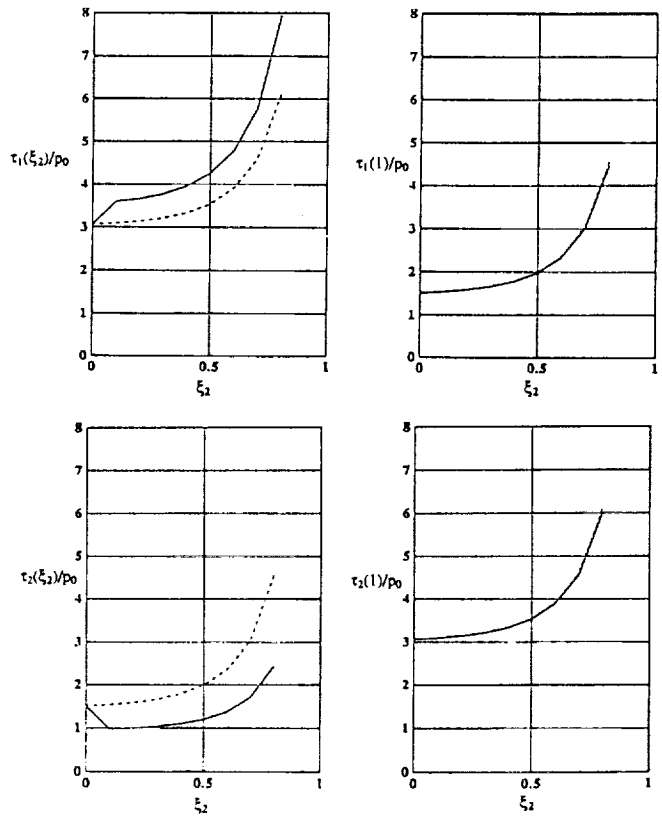

Fig. 5 Shear stresses, τ_1/p_0, τ_2/p_0, at special points versus ξ_2 for ξ_1 = 0. Ω = 4000, $\phi_1 = \phi_2 = 0.01$, $\delta_1 = \delta_2 = 0.01$. debond: —, void: · · · ·.

responding void, they are smaller at the same value of ξ_2 in adherend 2 for the debond. This is so, because the entire overlap length can share the shear stress.

Acknowledgment

This work has been supported by NASA LeRC Grant NAG3-1129, with Alex Vary as Monitor.

References

Erdogan, F., and Ratwani, M. M., 1971, "Stress Distribution in Bonded Joints," *Journal of Composite Materials*, Vol. 5, pp. 378-393.

Hart-Smith, L. J., 1973, "Adhesive Bonded Single Lap Joints," NASA CR 112236, National Aeronautics and Space Administration.

Hart-Smith, L. J., 1981, "Further Developments in the Design and Analysis of Adhesive-Bonded Structural Joints," *Joining of Composite Materials*, ASTM STP 749, K. T. Kedward, ed., pp. 3-31.

Kan, H. P., and Ratwani, M. M., 1983, "Stress Analysis of Stepped-Lap Joints with Bondline Flaws," *Journal of Aircraft*, Vol. 20, No. 10, pp. 848-852.

Lin, P., 1992, M.S. thesis, Dept. of Mech. Eng., Northeastern University.

Ratwani, M. M., and Kan, H. P., 1986, "Analysis of Delamination Propagation in the Composite Layer of Metal-to-Composite Stepped-Lap Joints," *Composite Materials: Testing and Design*, 7th Conference, J. M. Whitney, ed., ASTM, pp. 308-321.

Renton, W. J., and Vinson, J. R., 1977, "Analysis of Adhesively Bonded Joints Between Panels of Composite Materials," ASME *Journal of Applied Mechanics*, Vol. 44, No. 1, pp. 101-106.

Rossettos, J. N., and Zang, E., 1993, "On the Peak Stresses in Adhesive Joints with Voids," ASME *Journal of Applied Mechanics*, Vol. 60, No. 2, pp. 559-560.

Rossettos, J. N., and Shishesaz, M., 1987, "Stress Concentration in Fiber Composite Sheets Including Matrix Extension," ASME *Journal of Applied Mechancis*, Vol. 54, No. 3, pp. 723-724.

Transactions of the ASME

Published Quarterly by The American Society of Mechanical Engineers June 1993

On the Peak Shear Stresses in Adhesive Joints With Voids

J. N. Rossettos[3,5] and E. Zang[4,5]

Journal of

ISSN 0021-8936

JOURNAL CODE JE

ISSUE CODE 9302

[3]Professor. Fellow ASME.
[4]Graduate Student.
[5]Department of Mechanical Engineering, Northeastern University, Boston, MA 02115.

Hanson, M. T., 1992, "The Elastic Field for Conical Indentation Including Sliding Friction for Transverse Isotropy," ASME JOURNAL OF APPLIED MECHANICS, Vol. 59, No. 2, Pt. 2, pp. S123-S130.
Sneddon, I. N., 1948, "Boussinesq's Problem for a Rigid Cone," *Proceedings of the Cambridge Philosophical Society*, Vol. 44, pp. 492-507.

On the Peak Shear Stresses in Adhesive Joints With Voids

J. N. Rossettos[3,5] and E. Zang[4,5]

Introduction

Adhesive bonded joints have many advantages in terms of stress distribution, design flexibility, and simplicity of fabrication. It is known, however, that defects in the adhesive can severely reduce the bond strength. The presence of voids or disbond type flaws in the adhesive will increase the peak stress levels which occur at the joint ends and near the flaw itself.

Past work related to the present study was done by Hart-Smith (1981) and Kan and Ratwani (1983). The work deals with voids or disbonds in the adhesive, is a structural mechanics rather than a continuum approach, and uses a shear lag model where the adherends take on only axial load and the adhesive takes only shear. This is appropriate in bonded joints which are designed so that the net load path does not produce bending.

In the present Note, it is shown how the stresses in a single lap joint with a void are completely characterized by two nondimensional parameters. In particular, it is shown, how, for sufficiently large values of a parameter $\bar{\theta}$ (see Eq. 7), peak shear stresses can be essentially unaffected by relatively large central void sizes. Since the parameter $\bar{\theta}$ contains both geometric and material variables, it indicates explicitly how peak stresses can be controlled by selection of geometry and/or material. The influence of the location of the void is also indicated. It is remarked that if transverse shear is also included in a higher order analysis (Renton and Vinson, 1977), the peak shear stress values will occur very near the overlap ends-dropping sharply to zero at the ends (consistent with free adhesive ends). The conclusion of the present Note, however, will change very little if at all.

Analysis

The assumptions in the present model, with the geometry in Fig. 1, are similar to those by Kan and Ratwani (1983), so that the thickness variation of the stresses in the adherends is neglected. Also, in the z direction it is assumed that $\epsilon_{1z} = \epsilon_{2z} = 0$. In what follows, $p_1(x)$ and $p_2(x)$ are resultant forces per unit width in the x-direction in adherends 1 and 2, respectively, and p_o is the resultant force in the adherends away from the joint region. The corresponding displacements are $u_1(x)$ and $u_2(x)$. Since the adhesive is assumed to take on only shear, the shear stress there is

$$\tau(x) = (G/h_o)(u_2 - u_1), \tag{1}$$

where G and h_o are the shear modulus and thickness of the adhesive, respectively. Relations for the forces and stresses in the adherends are written as

$$p_1 + p_2 = p_o; \quad \sigma_{1x} = p_1/h_1; \quad \sigma_{2x} = p_2/h_2. \tag{2}$$

Because of the assumptions ($\sigma_{1y} = \sigma_{2y} = 0$), the stress-strain relations for isotropic adherends are given by

$$\epsilon_{1x} = (1-\nu_1^2)(p_o - p_2)/E_1h_1$$
$$\epsilon_{2x} = (1-\nu_2^2)p_2/E_2h_2 \tag{3}$$

where E_1, E_2 are Young's moduli and ν_1, ν_2 are Poisson's ratios of the adherends. The strain-displacement relations are

$$\epsilon_{1x} = du_1/dx, \quad \epsilon_{2x} = du_2/dx \tag{4}$$

Equilibrium of an element of adherend 2 gives $dp_2/dx - \tau(x) = 0$. The derivative of this equation gives

$$d^2p_2/dx^2 - d\tau/dx = 0 \tag{5}$$

By then using Eqs. (1)-(4), Eq. (5) leads to an equation for p_2. It can be written in nondimensional form as

$$d^2P_2/d\xi^2 - \bar{\theta}^2P_2 = -\bar{\theta}^2/(1+R) \tag{6}$$

where

$$\bar{\theta}^2 = L^2G(1-\nu_1^2)(1+R)/h_oh_1E_1 \tag{7}$$

$$R = (1-\nu_2^2)E_1h_1/(1-\nu_1^2)E_2h_2 \tag{8}$$

and where the nondimensionalization is given by

$$(P_1, P_1) = (p_2, p_1)/p_o; \quad \xi = x/L$$
$$S = L\tau/p_o; \quad (U_2, U_1) = GL(u_2, u_1)/p_oh_o. \tag{9}$$

By observing Eqs. (7) and (8), the parameter, $\bar{\theta}$, involves overlap length and adhesive/adherend geometric and material properties, while R measures the degree to which the adherends are different. Normalized void size is given by $\xi_2 - \xi_1 = a_2/L - a_1/L$. Note that if plate 2 is an orthotropic composite, then without change in the basic Eq. (6), R is given by

$$R = (1-\nu_{2x}\nu_{2z})E_1h_1/(1-\nu_1^2)E_{2x}h_2. \tag{10}$$

In the solution procedure, the adhesive is divided into three regions. Equation (6) applies to the first and the third regions. In the void regions, $\tau = 0$, so Eq. (6) is replaced by $d^2P_2/d\xi^2 = 0$. The solutions to these equations in the three regions lead to six constants of integration which are determined by boundary conditions and appropriate continuity conditions between regions.

In region 1, $(0 \le \xi \le \xi_1)$

$$P_{21}(0) = 0; \quad P_{21}(\xi_1) = P_{22}(\xi_1). \tag{11a, b}$$

In region 2, (void) $(\xi_1 \le \xi \le \xi_2)$

$$P_{22} = \text{constant} \tag{12}$$

$$P'_{23}(\xi_2) = P'_{21}(\xi_1) + (\xi_2 - \xi_1)\bar{\theta}^2(P_{22} - 1/(1+R)), \tag{13}$$

where $(\,)' = d(\,)/d\xi$. Equation (13) represents the change in the shear stress from ξ_1 to ξ_2 because of unequal displacements of the adherends over the void region (Zang, 1990).

In region 3 $(\xi_2 \le \xi \le 1)$,

$$P_{22}(\xi_2) = P_{23}(\xi_2); \quad P_{23}(1) = 1. \tag{14a, b}$$

Note that in the notation, P_{2i}, the subscript, i, denotes the solution for P_2 in region i.

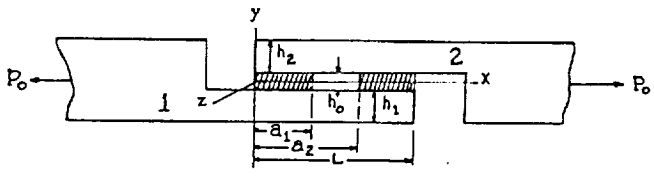

Fig. 1 Step lap joint with a void

[3]Professor. Fellow ASME.
[4]Graduate Student.
[5]Department of Mechanical Engineering, Northeastern University, Boston, MA 02115.

Contributed by the Applied Mechanics Division of THE AMERICAN SOCIETY OF MECHANICAL ENGINEERS for publication in the ASME JOURNAL OF APPLIED MECHANICS. Manuscript received by the ASME Applied Mechanics Division, June 11, 1992; final revision, Mar. 12, 1992. Associate Technical Editor: M. E. Fourney.

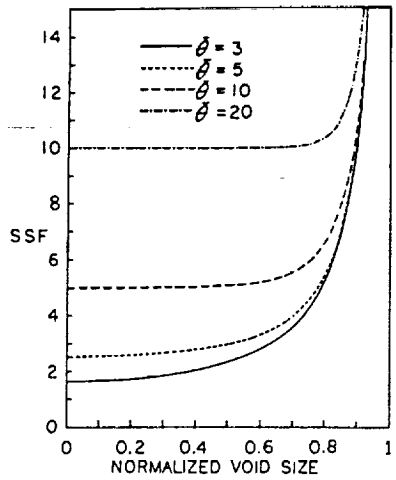

Fig. 2 Shear stress factor (SSF = ratio of peak shear stress to average shear stress) versus normalized void size, $\xi_2 - \xi_1$; symmetric void; $R = 1$

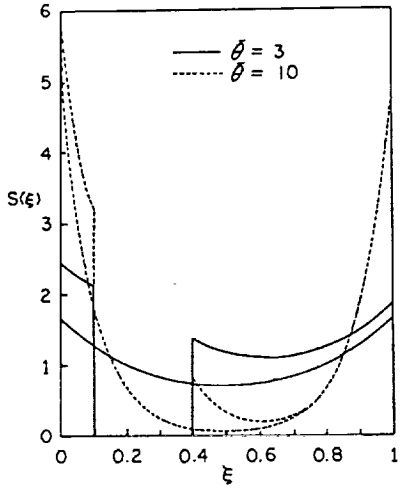

Fig. 3 Nondimensional shear stress, $S(\xi)$, versus ξ for both a void located near the left end of the overlap and no void (continuous curves); $R = 1$

Numerical Results and Discussion

As an example, for identical adherends ($R = 1$), the peak shear stress is shown to depend on both the location and size of the void and the value of $\bar{\theta}$. For the larger values of $\bar{\theta}$, such as $\bar{\theta} = 10$ or greater, a void located at the central portion of the overlap region with void sizes up to 70 percent of the overlap length (Fig. 2), will not affect the peak stress. For the same void located near one end of the overlap (Fig. 3), however, where a high stress gradient already exists, the peak stress can be increased by about 20 percent (for $\bar{\theta} = 10$). Note that even for the relatively large value of $\bar{\theta} = 10$ the stress at the void edge, although not the peak stress, does increase markedly (i.e., by over 35 percent in Fig. 3).

However, for smaller values of $\bar{\theta}$, say $\bar{\theta} = 3$, a void located at the central part of the overlap will also affect the peak stress. For example, when $\bar{\theta} = 3$, for a void one third the size of the overlap, an increase of 18 percent can be obtained for the peak stress, while the same void near one end (Fig. 3) can increase the stress by 39 percent.

By observation of Eq. (6), it is seen that the variation of $\bar{\theta}$ can be either due to changing the adhesive properties G and h_0, or the length of the overlap, L, or adherend properties. Yet, for a given value of $\bar{\theta}$ the non-dimensional shear stress distribution is the same.

Similar trends (Zang, 1990) of the effect of the parameter $\bar{\theta}$, also occur for values of R which differ from unity (i.e., different adherends such as composite/metal). In particular, a higher peak shear stress occurs at $\xi = 1$, when adherend 2 has a smaller stiffness than adherend 1, (i.e., $R > 1$). It turns out that as R increases from 1 to 10, the peak stress almost doubles in value. However, for larger R, the stress rapidly becomes asymptotic to a fixed value, suggesting that adherend 1 is essentially rigid relative to adherend 2.

References

Hart-Smith, L. J., 1981, "Further Developments in the Design and Analysis of Adhesive-Bonded Structural Joints," *Joining of Composite Materials*, ASTM-STP-749, K. T. Kedward, ed., p. 3-31.

Kan, H. P., and Ratwani, M. M., 1983, "Stress Analysis of Stepped-Lap Joints With Bondline Flaws," *Journal of Aircraft*, Vol. 20, No. 10, pp. 848-852.

Renton, W. J., and Vinson, J. R., 1977, "Analysis of Adhesively Bonded Joints Between Panels of Composite Materials," ASME JOURNAL OF APPLIED MECHANICS, Vol. 44, No. 1, pp. 101-106.

Zang, E., 1990, "Analysis of Step Lap Joints With Voids and Thermal Mismatch," M.S. Thesis, Dept. Mechanical Engineering, Northeastern University, Boston, MA.

First-Order Perturbation Analysis of Transient Interlaminar Thermal Stress in Composites

Y. R. Wang[6,8,9] and T.-W. Chou[7,8]

The first-order perturbation analysis of the three-dimensional transient interlaminar thermal stresses of a symmetric composite laminate has been performed in this paper. Numerical results for a four-layer angle-ply laminate have shown that the first-order analysis was necessary for the solution of thick laminate (thickness-to-width ratio $\epsilon \geq 0.02$).

Introduction

This study is a supplement to the work of Wang and Chou (1989), in which the three-dimensional transient interlaminar thermal stresses of a symmetric composite laminate were analyzed by a zeroth-order perturbation technique. Since the higher-order terms were neglected and it seems impossible to make an error analysis due to the mathematical difficulties, the present effort has been made to estimate the accuracy of the result obtained by Wang and Chou (1989) by including the first-order term in the solutions.

[6]Assistant Professor. Assoc. Mem. ASME.

[7]Mem. ASME.

[8]Center for Composite Materials and Department of Mechanical Engineering, University of Delaware, Newark, DE 19716.

[9]Present address: Department of Civil and Mechanical Engineering, McNeese State University, Lake Charles, LA 70609.

Contributed by the Applied Mechanics Division of THE AMERICAN SOCIETY OF MECHANICAL ENGINEERS for publication in the ASME JOURNAL OF APPLIED MECHANICS. Manuscript received by the ASME Applied Mechanics Division, Feb. 5, 1991; final revision, Aug. 14, 1991. Associate Technical Editor: G. J. Dvorak.

Nondestructive Evaluation of Adhesively Bonded Joints by Acousto-Ultrasonic Technique and Acoustic Emission

H. Nayeb-Hashemi and J. N. Rossettos

Abstract

Reliable applications of adhesively bonded joints require an effective nondestructive evaluation technique for their bond strength prediction. To properly evaluate factors affecting bond strength, effects of defects such as voids and disbonds on stress distribution in the overlap region must be understood. At the same time, in order to use acousto-ultrasonic (AU) technique to evaluate bond quality, the effect of these defects on dynamic response of single lap joints must be clear. The stress distribution in a single lap joint with and without defects (void or disbond) is analyzed. A $\bar{\theta}$ parameter which contains adherend and adhesive thickness and properties is introduced. It is shown for bonded joints with $\bar{\theta} \geq 10$, that a symmetric void or disbond in the middle of overlap up to the 70% of overlap length has negligible effect on bond strength. In contrast frequency response analyses by a finite element technique showed that the dynamic response is affected significantly by the presence of voids or disbonds. These results have direct implication in the interpretations of AU results. Through transmission attenuation and a number of AU parameters for various specimens with and without defects are evaluated. It is found that although void and disbond have similar effects on bond strength (stress distribution), they have completely different effects on wave propagation characteristics. For steel-adhesive-steel specimens with voids, the attenuation changes are related to the bond strength. However, the attenuation changes for specimens with disbond are fairly constant over a disbond range. In order to incorporate the location of defects in AU parameters, a weighting function is introduced. Using an immersion system with focused transducers, a number of AU parameters are evaluated. It is found that by incorporating weighting functions in these parameters better sensitivities (AU parameters vs. bond strength) are achieved.

Acoustic emission (AE) activities of steel-adhesive-steel specimens with $\bar{\theta} = 3.4$ are monitored. Two different formats of energy vs. time have resulted, each corresponding to the perfect specimens or the specimens with void or disbond. The relative acoustic energy and the number of events at failure are found to be a means for predicting the bond strength.

Received 24 June 1993. The authors are affiliated with Department of Mechanical Engineering, 334 Snell Engineering Center, Northeastern University, Boston, MA 02115.

1. Introduction

Over the past decade, much research effort has been expended and numerous test instruments have been developed in seeking a solution to the problem of nondestructively inspecting adhesively bonded joints (Williams and Zwicke, 1982; Rose, 1984; Dickstein et al., 1989, 1991, 1992; Rose et al., 1983; Subramanian et al., 1991; Williams et al., 1984). Several nondestructive evaluation (NDE) methods are recommended for the inspection of adhesively bonded joints, in addition to the well established methods for detecting localized flaws, voids, or delaminations. However, neither of these approaches nor more sophisticated ultrasonic methods (using frequency and time domain information), have been shown capable of absolutely assessing joint strength. This is due, in part, to the fact that no single ultrasonic measurement is a unique function of a single bond property; each ultrasonic measurement is sensitive to changes in several bond properties. However, the strength of the bond may or may not depend on these properties. A multidisciplinary approach is required that combines NDE, adhesive technology, and solid mechanics analyses to form a basis for a comprehensive quality assurance solution.

Many attempts have been made to advance the state-of-the-art in flaw classification analysis by using techniques and concepts from pattern recognition. The underlying premise is built upon linear system analysis, which assumes that the ultrasonic input energy, as it varies with time, is modified by the bond structure. The theory then asserts, that if one has the system input and output (echo), then the modifying mechanism can be found and characterized. Rose et al. (1983), using this concept, evaluated adhesively bonded aluminum-to-aluminum specimens by defining an "α" parameter as the ratio of received signal to the transmitted signal in immersion scanning experiments. The feature "α" was defined and was of known value for bond quality discrimination (Meyer and Rose, 1974; Rose and Meyer, 1973). A low value of "α" indicates good transmission of the stress wave energy, while the high value of "α" indicates most of the energy is reflected at the interface. The values of "α" at several locations of the bond area were evaluated and the feature "β" based on the surface integration of the "α" parameter was defined as

0730-0050/94/12001-014

$$\beta = \frac{1}{4h^2}\iint \alpha(x,y)dxdy$$
$$= \sum_{i=1}^{n} w_i \alpha_i(x,y) + R \qquad (1)$$

where h is the distance between scan points (square bond area), and w_i are the weighting factors. The surface integral values and log weighting function (Rose et al., 1983) from the center of each coupon were used to construct the feature data. These were related to the bond strength. The above equation and features can be modified by considering which area of adhesive is more responsible for the bond strength, and by proposing a weighting function which brings this factor into consideration.

The initial signature techniques were based on the analysis of ultrasonic signals in the time domain, and by making use of the arrival time and amplitudes. Gericke (1963) suggested that a source of additional discriminating characteristics might be found in the frequency spectrum of the returned echo. He indicated that if a short pulse, rich in spectral content, were used, the size, nature, and shape of flaws could be more readily determined from the frequency domain. He also proposed a method involving the use of two widely separated frequencies for inspection. The change of the returned pulse shape from one frequency range to the other could possibly yield information concerning the defect size, shape and orientation characteristics. Henneke and coworkers (Henneke et al., 1983; Duke et al., 1984, 1986; Sarrafzadeh-Khoee et al., 1986; Talreja et al., 1984; Govada et al., 1985) introduced several moments of the frequency spectrum as a means of damage evaluation in composite materials. A variety of additional signature techniques for ultrasonic examination both in time and frequency domains are introduced (Dickstein et al., 1990; Vary, 1987; Williams and Lee, 1987; Vary and Bowles, 1979; Vary and Lark, 1978; Nayeb-Hashemi et al., 1985). However, these parameters may not be effective when used in interrogation of the bond quality without understanding the effects of defects on both the received ultrasonic signature and bond strength.

The higher order crossing (HOC) method for signal analysis, often called the zero-crossing or level-crossing method, has been recently developed and applied in bond quality assessments (Dickstein et al., 1989, 1992). Ultrasonic echo signals were obtained from several specimens representing various adhesive or cohesive bond properties. HOC features were calculated from these signals and used to characterize the various conditions of the sample joints. However, no correlation between HOC parameters and bond strength were presented.

Acoustic emission is another nondestructive evaluation technique which has been projected to have potential of predicting structural integrity. AE has developed rapidly over the last two decades as a nondestructive evaluation technique and as a tool for materials research. AE signals can take many forms depending upon the material and the failure mechanism in the material. AE signals from defects in composites and geological materials generally contain information at low frequencies, 0.5-100 kHz, since attenuation is relatively high due to the complexity of these materials. Signals of significance in metals and brittle materials contain information between 100 kHz and 2 MHz. In this range a good compromise is found for most testing applications because ambient noise is low. A number of techniques are employed to isolate valid signals form noise in the time domain. Times of arrival can be used to permit geometric elimination of obvious noise through gating, and acceptance of only those signals which arrive from a particular region of the structure. At the present time, one can find many presentations of AE data in the literature. In time domain, these include: AE (ringdown) counts, rms voltage, number of events, energy rate, rise time, event duration, amplitude distribution, and numerous others.

It is also possible to analyze the frequency content of both burst and continuous types of AE. Relating such measurements to the source mechanism is an extremely complex problem, not only because of the specimen and transducer resonances and frequency dependent absorption effects, but also because of effects caused by the methods of analysis employed. Indeed, some investigators would argue that the information required to distinguish between different AE sources, or to describe the nature of operation of particular sources, is simply not available in the frequency content of the AE signals, particularly using piezoelectric transducers. Other investigators believe that spectral analysis can be of great value and that with proper methods of averaging and smoothing of data, spectral analysis can be used to identify and discriminate AE sources (Heiple and Carpenter, 1983; Egle et al., 1981).

As it was pointed out above, nondestructive evaluation of adhesively bonded joints requires comprehensive studies of the effects of defects, sizes, and their locations on the stress distribution and dynamic response of bonded joints. These analyses provide bases for more effective interpretation of various AU data. The purpose of this paper is to present our efforts toward understanding factors affecting (1) the bond strength and dynamic response of adhesively bonded joints, and (2) bond strength prediction by conducting various AU experiments. AE activities of steel-adhesive-steel, and graphite epoxy composite-adhesive-graphite epoxy composite specimens with various defects were also monitored during destructive tensile tests. The results of these investigations are presented in the following sections.

2. Stress Distribution in Bonded Joints-Theory

There are various bonded joint configurations. Most of the joint configurations are designed to transfer load in shear. Of all the various joints, the single lap joint is most

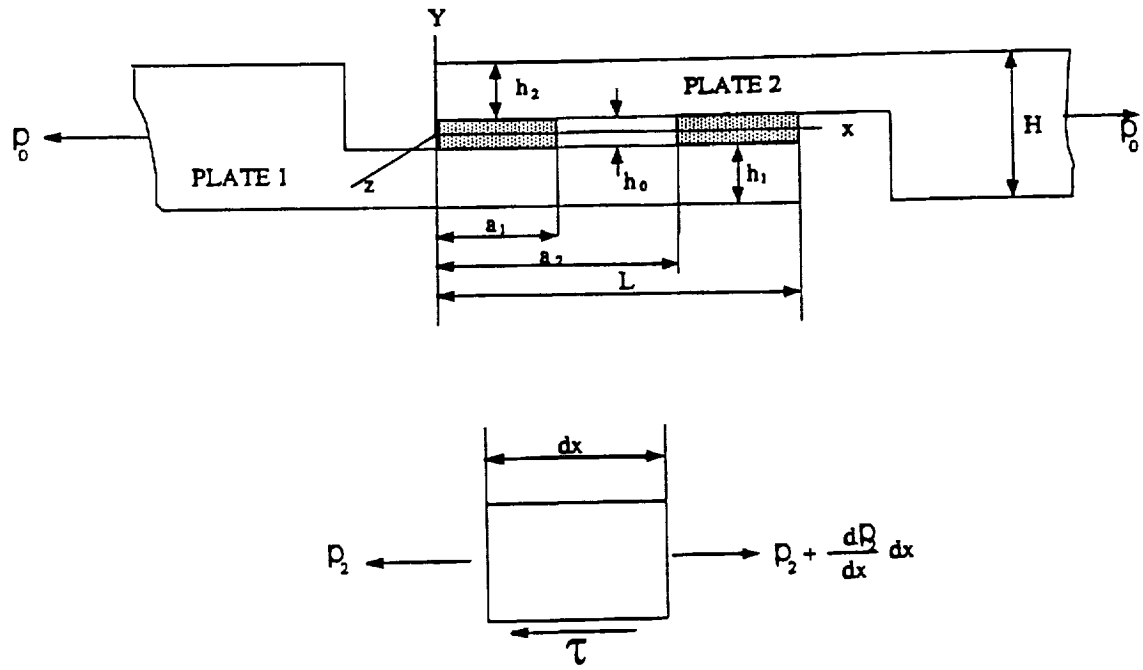

Fig. 1 Schematic diagrams of a step lap joint with a void, and a differential element.

commonly used in design. Also, theoretical and experimental investigations of the bond strength are less complicated with the single lap joint. For this reason, in this paper the effects of voids, disbond region, poor cohesive strength, and poor adhesive strength on the strength of the single lap joints are studied both experimentally and theoretically.

The strength of a given type of joint depends on the shear and peel stress distributions in the bonded area. These stresses depend on the adhesive and adherends' properties and geometries. Assuming the adhesive layer to be homogenous and free of defects Volkersen (1938) derived the shear stress distribution in single lap joints, using shear lag model assumptions. Goland and Reissner (1944) modified Volkersen's analysis by considering the bending moment and peel stresses in the theoretical analysis. Other researchers have also obtained the shear and peel stresses in the bond joints by finite element analyses (Ishai et al., 1977; Adams and Peppiatt, 1974; Hart-Smith, 1985, 1987; Cooper and Sawyer, 1979; Allman, 1977). There have been very limited theoretical investigations on the effects of defects on the stress distribution and bond strength in single lap joints. Since the bond strength may or may not depend on the defects, the stress distribution in a single lap joint with a void is derived in this section, using shear lag model assumptions. The details of the analyses can be found in Rossettos and Zang (1993) and Hashemi and Rossettos (1990). Here, some aspects of these analyses are briefly described and important conclusions are elaborated.

The two dimensional model consists of a simple lap joint as shown in Fig. 1, made of two plates bonded by a layer of adhesive. The problem is formulated under the following assumptions:

a) The thicknesses h_0, h_1, h_2, H are small compared to the other dimensions of the structure so that the individual layers may be under generalized plane stress (i.e. $\sigma_{1y} = \sigma_{2y} = 0$).

b) The thickness variation of the stresses in the plates will be neglected under the usual assumption that the surface shear stress transmitted through the adhesive layer acts as a body force.

c) In the z direction (i.e. transverse direction), plane strain conditions will prevail such that $\varepsilon_z = \varepsilon_{1z} = \varepsilon_{2z} = 0$.

Referring to Fig. 1, let $p_1(x)$ and $p_2(x)$ be the resultant forces per unit width in the x-direction in plates 1 and 2, respectively, and $u_1(x)$ and $u_2(x)$ be the displacements in the x direction. The elastic properties and thermal expansion coefficient of isotropic material 1 are donated by E_1, ν_1 and α_1, and those for isotropic material 2, are E_2, ν_2 and α_2. The shear modulus of the adhesive is given by G. The joint is divided into three regions. The following variables are defined as:

x_i = beginning of each region ($x_1 = 0$, $x_2 = a_1$, $x_3 = a_2$ in region 1, 2, 3, respectively).

region 1: $0 \le x \le a_1$

region 2: $a_1 \le x \le a_2$ (void)

region 3: $a_2 \le x \le L$.

The shear stress distribution in the lap joint can be obtained by writing the equilibrium equation of an incremental element in plate 2 (see Fig. 1) as

$$\frac{dp_2}{dx} - \tau(x) = 0 \qquad (2)$$

where $\tau(x)$ is the shear stress and p_2 is the normal force per unit width in the adherend #2. Assuming the displacements of the top and bottom of the adhesive layer are $u_2(x)$ and $u_1(x)$, and using strain-displacement relations of

$$\varepsilon_{1x} = \frac{du_1}{dx} \quad \text{and} \quad \varepsilon_{2x} = \frac{du_2}{dx},$$

equation (2) can be written in the form of

$$\frac{d^2p_2}{dx^2} - \frac{G}{h_o}(\varepsilon_{2x} - \varepsilon_{1x}) = 0. \qquad (3)$$

Because of the assumptions ($\sigma_{1y} = \sigma_{2y} = 0$), the stress-strain relations in the adherends are

$$\varepsilon_{1x} = \frac{1-\nu_1^2}{E_1 h_1}[p_o - p_2(x)] + \alpha_1 \Delta T, \qquad (4)$$

$$\varepsilon_{2x} = \frac{1-\nu_2^2}{E_2 h_2} p_2(x) + \alpha_2 \Delta T. \qquad (5)$$

Substituting equations (4) and (5) into equation (3), and presenting it in a nondimensionalized form results in,

$$\frac{d^2P_2}{d\xi^2} - \bar{\theta}^2 P_2 = \frac{-\bar{\theta}^2}{1+R} + \bar{\psi} \qquad (6)$$

where $\xi = x / L \qquad (7)$

$$(P_2, P_1) = \frac{1}{p_o}(p_2, p_1) \qquad (8)$$

$$R = \frac{1-\nu_2^2}{1-\nu_1^2}\frac{E_1 h_1}{E_2 h_2} \qquad (9)$$

$$\bar{\theta}^2 = \frac{L^2}{h_0 h_1}\frac{G}{E_1}(1-\nu_1^2)(1+R) \qquad (10)$$

$$\bar{\psi} = \frac{L^2 G}{p_o h_o}(\alpha_2 - \alpha_1)\Delta T. \qquad (11)$$

Equation (6) holds for region 1 and 3; in the void region $\tau = 0$, so

$$\frac{d^2P_2}{d\xi^2} = 0 \qquad (12)$$

The solution of equations (6) and (12) along with proper boundary conditions and continuity conditions between regions yields the normal and interfacial shear stress distribution in the adherends (Rossettos and Zang, 1993; Nayeb-Hashemi and Rossettos, 1990).

3. Theoretical Results of Void Effects on Shear Stress Distribution in a Single Lap Joint

The geometric configuration of the step lap joint is given in Fig. 1 and the three parameters R, $\bar{\theta}$ and $\bar{\psi}$, which appear in the governing equation (6), and influence the stress distribution, are given by equations (9), (10), and (11). The close observation of the aforementioned equations reveals that a change in $\bar{\theta}$ involves a change in geometry and material properties of both the adherends and the adhesive. An increase in $\bar{\theta}$ may be due to any number of possibilities, such as an increase in the length of the joint and/or an increase in the shear modulus of the adhesive, a decrease in the thicknesses of the adherend 1 and/or thickness of the adhesive layer, a decrease of the Young modulus of plate 1 and finally an increase in R.

The parameter, R, itself represents only the geometric and material properties of the adherends. The decrease of R involves the decrease of Young's modulus and thickness of plate 1 or the increase of the properties mentioned but applied to plate 2. For similar adherends, it is equal to unity.

The parameter, $\bar{\psi}$, can be seen as a thermal parameter. It involves the temperature difference between the two plates and their respective thermal coefficients of expansion. The parameter, $\bar{\psi}$, increases if the thermal mismatch increases, where the two plates have a large difference in coefficient of thermal expansion. It also increases when the joint length and shear modulus of the adhesive increases. Finally, $\bar{\psi}$, is inversely proportional to the thickness of the adhesive layer and the axial load.

The effect of $\bar{\theta}$ on shear stress $S(\xi) = (L/p_o)\,\tau$ distribution is shown in Fig. 2. For an adhesively bonded joint with the same adherend materials (R=1) the results show, that the higher $\bar{\theta}$ value causes very uniform (almost zero) stress over the bonded area with the peak shear stresses confined to the small region near the edge. Figure 3 shows the effect of a symmetric void on the shear stress distribution for different values of $\bar{\theta}$. Here again, the peak stress distribution is confined to the edge of the bonded joint.

To evaluate the degree of stress variation as it is affected by a void and $\bar{\theta}$, a shear stress factor, SSF, has been defined as the ratio of peak stress over the average stress. The SSF has been computed for a set of increasing symmetric void sizes. Figure 4 shows that the SSF is constant over most of the void size range (up to 70% of the overlap length) for the higher values of $\bar{\theta}$. So it is expected that the failure load would be independent of a void for this range of void size. Effects of thermal mismatch between adherends are reported in detail in Rossettos et al. (1991). The stress distribution is significantly changed for adherends with a large difference in thermal expansion coefficient. The effect of a disbond on the shear stress distribution is also investigated. Here again disbonds up to 70% of the overlap

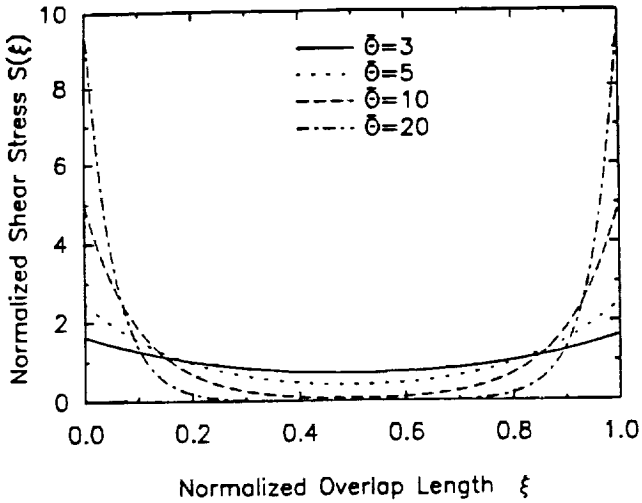

Fig. 2 Normalized shear stress S(ξ) versus normalized overlap length ξ, for adhesive joints with identical adherends (R=1) for several values of $\bar{\theta}$.

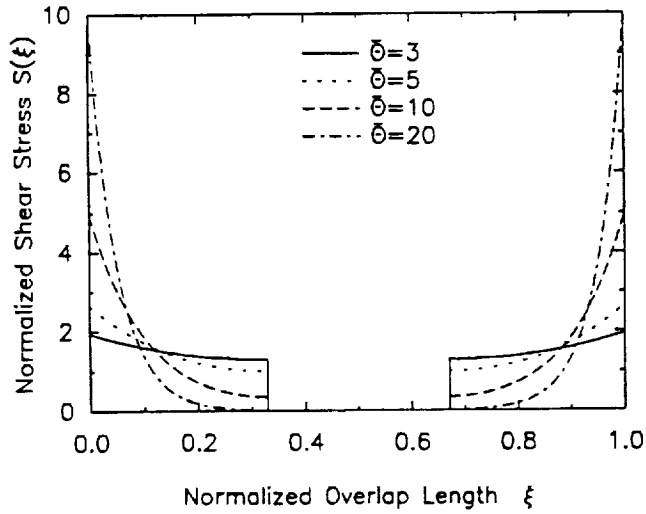

Fig. 3 Normalized shear stress S(ξ) versus normalized overlap length ξ, for adhesive joints with identical adherends (R=1) and a center void, for several values of $\bar{\theta}$.

length were found to have negligible effect on the peak shear stress for $\bar{\theta} \geq 10$.

5. Void Effects on Dynamic Response of Single Lap Joints - Theory

In order to understand the effects of voids on dynamic response of lap joints, we have studied the linear frequency response of an adhesive joint with a void, with particular attention given to the overlap region. This will be useful in the effective interpretation of ultrasonic data for the bond quality evaluation.

In the analysis, a finite element model is used to represent a simple adhesive lap joint. A harmonic force excitation is applied at one end of the joint near the overlap

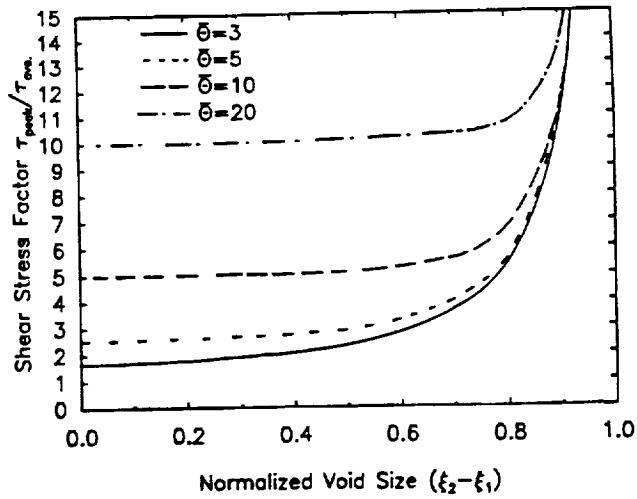

Fig. 4 Shear stress factor τ_{peak}/τ_{av} versus normalized void size $(\xi_2 - \xi_1)$, in adhesive joints with identical adherends, and a center void, for several values of $\bar{\theta}$.

region, and a displacement response at several output points is calculated over a frequency range. The modal analysis and frequency response calculation is performed for a joint with and without a void in the adhesive to determine changes in frequency response patterns caused by the void. The results indicate clear differences in the response patterns over a frequency range which covers all natural frequencies of the finite element model. The results presented here focus on the higher frequencies.

Beam elements are used for the adherends and lateral stiffness elements are used for the adhesive. Voids are created by removal of lateral stiffness elements. The model is simple and will indicate the important features to be expected. The NASTRAN code has been used. Material properties are for similar aluminum alloy adherends (E = 69 GPa and adherend thickness of 3.17 mm) and Hysol EA9689 adhesive (E = 2.2 GPa and thickness of 0.13 mm). The overlap was 25.4 mm x 25.4 mm and symmetric and unsymmetric voids were introduced in the overlap and dynamic responses for identical input harmonic force were evaluated.

The system equations formed for frequency response analysis include mass, damping and stiffness matrices and the system load vector. The equations may be written in matrix notations as follows:

$$M\ddot{U}(f) + C\dot{U}(f) + KU(f) = F(f) \qquad (13)$$

where f is the discrete frequency value.

The harmonic excitation is frequency dependent and the solution is obtained for the desired discrete frequencies. Since all nodal motion is assumed to be steady state, the velocities and accelerations are related to the displacements by

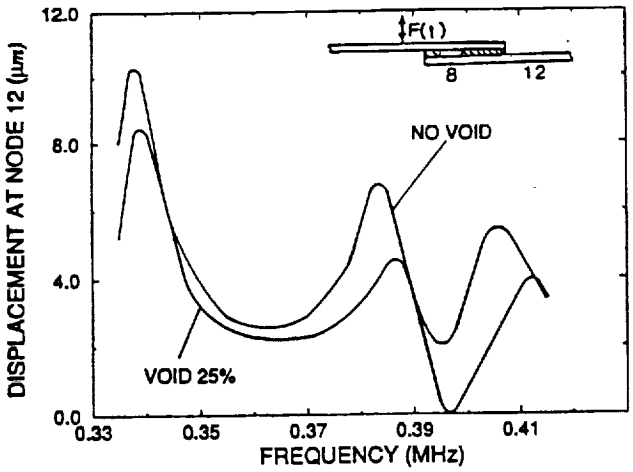

Fig. 5 Finite element model and frequency responses at node 12 for aluminum-adhesive-aluminum specimens with no void, and 6.35 mm void. Void starts at 3.18 mm from left end of 25.4 mm overlap.

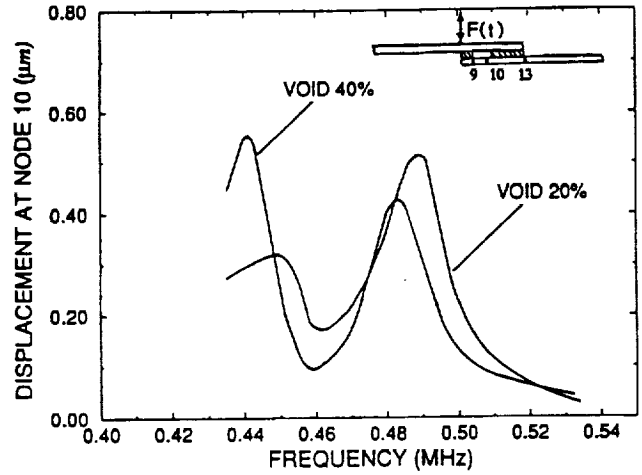

Fig. 6 Finite element model and frequency responses at node 10 for aluminum-adhesive-aluminum specimens with 5.08 mm and 10.16 mm void. Void starts at 2.54 mm from left end of overlap.

$$\ddot{U} = -(2\pi f)^2 U, \quad \dot{U} = i(2\pi f)U \tag{14}$$

The frequency response equation then becomes

$$[-(2\pi f)^2 M + i(2\pi f)C + K]U(f) = F(f) \tag{15}$$

Equation (15) represents a system of equations and the solution for U(f) can be found for every frequency point. Proportional damping is used so that

$$C = c_1 K + c_2 M. \tag{16}$$

In the present study $c_2 = 0$ and c_1 is given very small values (of the order of 0.001). Typical frequency response curves are given in Figs. 5 and 6. These are calculated for the two configurations indicated in the figures. For a given frequency, the ratio of the displacement with a void to the

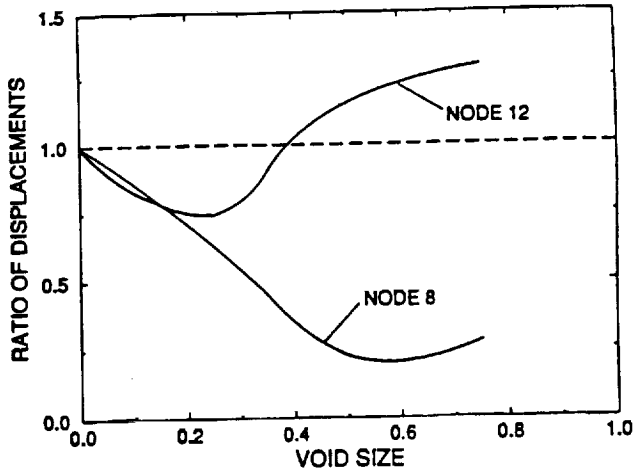

Fig. 7 Ratio of displacements at nodes 8 and 12 for specimens with and without void (Δ/Δ_o) versus void size at frequency of 0.39 MHz. Void starts at 3.17 mm from left end of overlap, and void size is given as percent of overlap length of 25.4 mm.

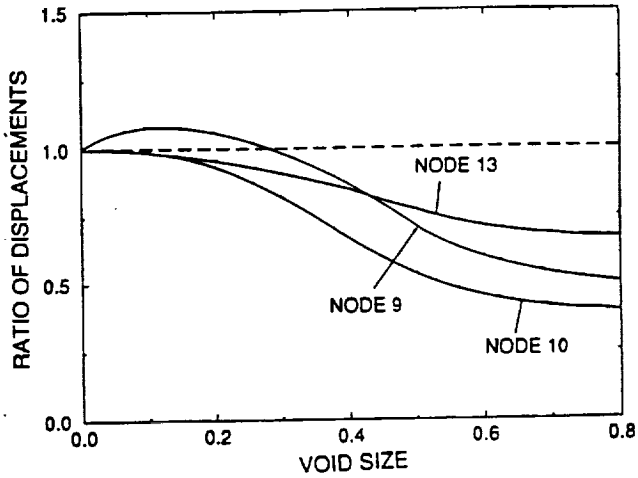

Fig. 8 Ratio of displacements at several locations for specimens with and without void (Δ/Δ_o) versus void size at frequency of 0.49 MHz. Void starts at 2.5 mm from left end of the overlap and size is given as percent of overlap length of 25.4 mm.

displacement without a void is plotted against void size in Figs. 7 and 8. It should be borne in mind that for different void sizes, the structural configuration changes and the natural or resonant frequencies will change, so that for a fixed frequency these curves need not be monotonic.

The results of this analysis indicate that, although there was little change in the peak shear stress in adhesively bonded joints with voids up to 70% of the overlap length ($\bar{\theta} \geq 10$), the dynamic response may be affected by the presence of voids significantly. These results have direct implication in the non-destructive evaluation of the adhesively bonded joints.

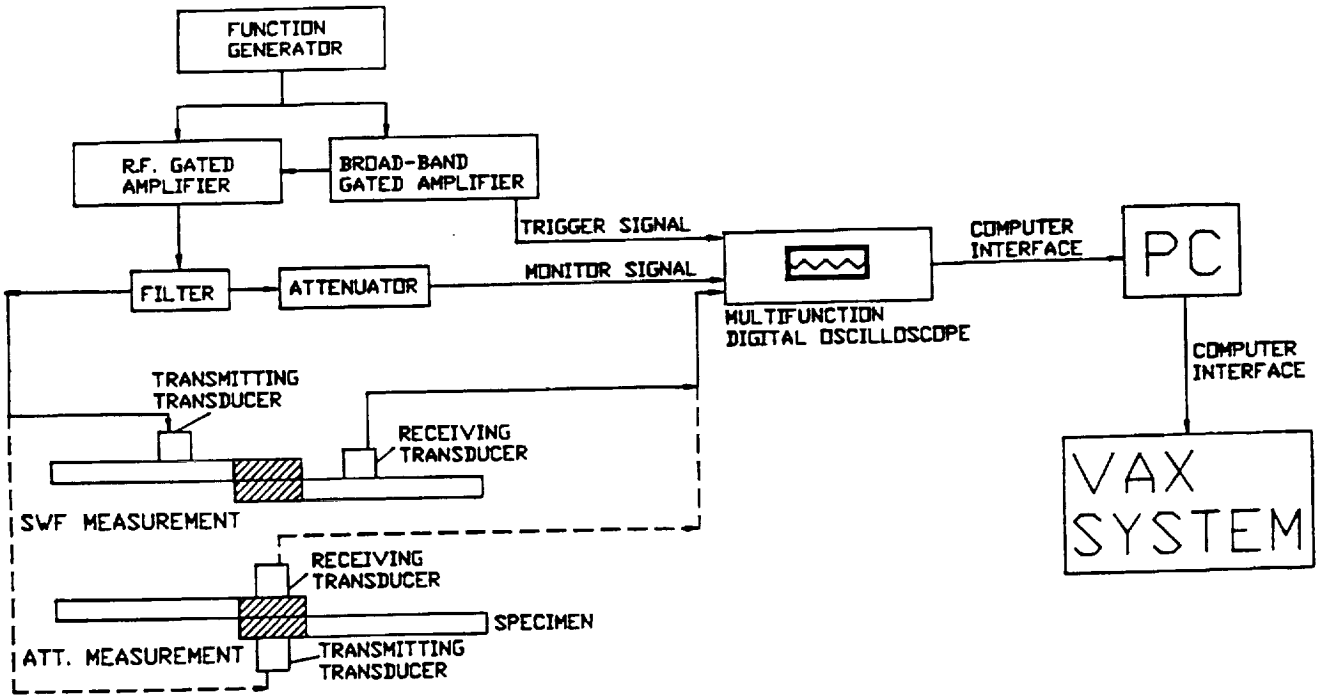

Fig. 9 System for attenuation and AU parameters measurements.

6. Experimental Investigations

Adhesively bonded joint specimens were prepared by using AISI 1018 cold rolled steel, unidirectional graphite epoxy composite material, and aluminum 6061-T6 as adherends. Identical adherends were joined together in a single lap joint configuration using Hysol EA9689 epoxy film of 0.13 mm thickness. For joints with steel as adherends, the adherend surfaces were prepared according to the ASTM standard D6251-79. For joints with aluminum as adherends, the adherend surfaces were either sanded and cleaned with acetone or were just cleaned with acetone prior to bonding. The composite adherends were slightly sanded in their overlap areas, in order to remove the residual mold release prior to their bonding. For metal adherends the overlap area was 25.4 mm x 25.4 mm and adherend thickness was 3.17 mm. Joints with graphite epoxy composite as adherend, had overlap dimensions of 50.8 mm x 25.4 mm and the thickness of the composite adherend was 1.07 mm. Various defects such as voids, disbonds were introduced in the overlap area in order to change the bond strength. Voids of different sizes were introduced by cutting the adhesive film. The disbond was created by spraying mold release agent over the disbond area.

Various ultrasonic setups and methodologies were used to measure longitudinal pulse-echo attenuation, through transmission longitudinal and shear waves attenuation, using both direct contact and immersion techniques, and acousto-ultrasonic parameters. In the attenuation experiments, narrow-band Panametrics transducers with center frequencies of 1 and 2 MHz were used both as transmitting and receiving transducers. Both narrow-band signal (pulse oscillator) and broad-band pulse were used in these experiments. In the AU experiments, narrow-band Panametric transducer with center frequency of 1 MHz and an FC-500 AET transducer with a flat sensitivity in the frequency range of 100 kHz-2 MHz, were used as transmitting and receiving transducers, respectively. The experiments were conducted by using a broad-band pulse with the center frequency of 1 MHz. The received signals were digitized in a Nicolet digital oscilloscope and stored in a PC computer and later analyzed in a SUN work station, Fig. 9. The signals were analyzed in both time and frequency domains.

In the time domain, attenuation, stress wave factor (SWF) and AU parameter (AUP) were measured for each specimen. Assuming the impedance between transmitting and receiving transducers and adherends are $F_1(\omega)$ and $F_2(\omega)$, the amplitude or peak amplitude of the received signal from a perfect and a defective specimens for an input pulse oscillator or pulse can be expresses as

$$(Ar)_p = F_1(\omega)F_2(\omega)A_t \exp(-\alpha_p t) \qquad (17)$$

$$(Ar)_d = F_1(\omega)F_2(\omega)A_t \exp(-\alpha_d t) \qquad (18)$$

where A_t is the transmitted signal amplitude, α_p and α_d are the attenuation in perfect and defective specimens, t is the bond thickness, and $(Ar)_p$ and $(Ar)_d$ are the amplitude of the received signals from perfect and defective specimens at angular frequency ω. The change in attenuation can be obtained from equations (17) and (18) as

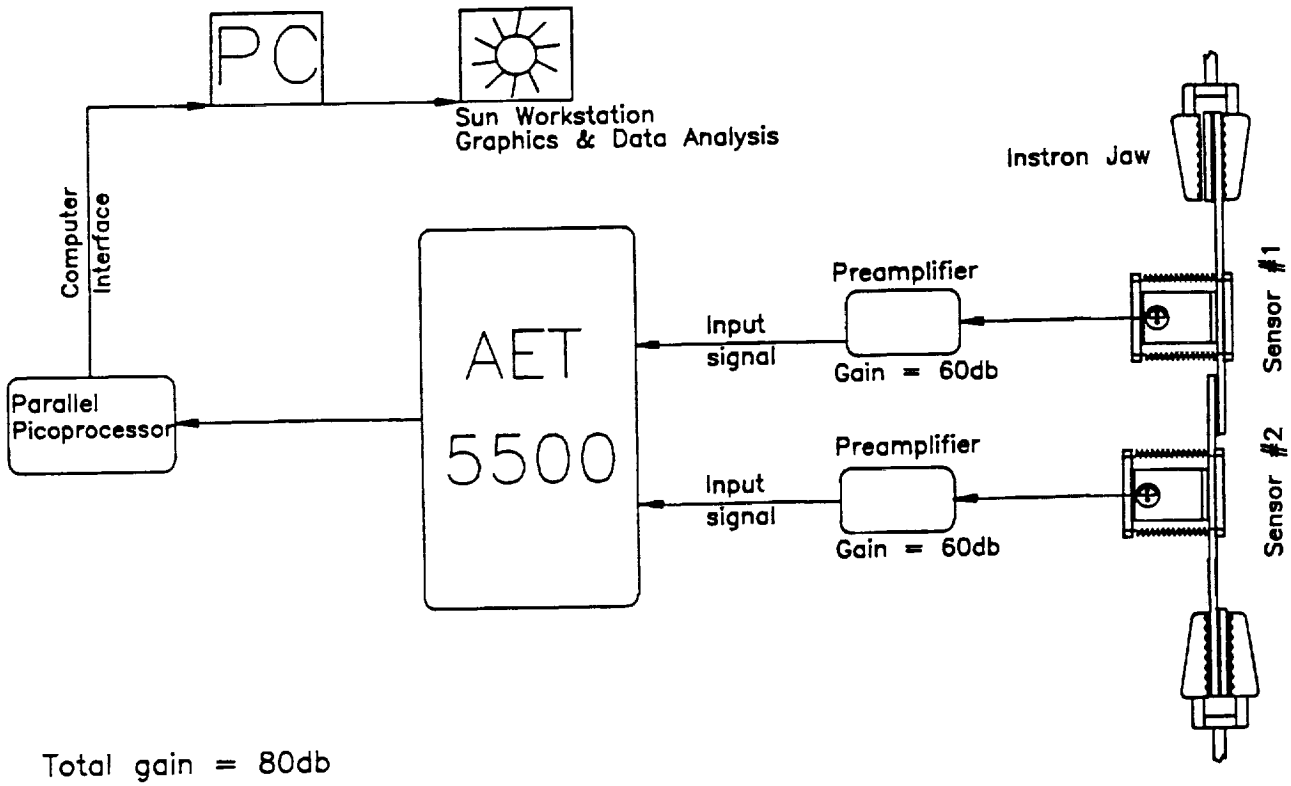

Fig. 10 Schematic diagram of the AE data acquisition system.

$$\alpha_d - \alpha_p = \Delta\alpha = \frac{1}{t}\ell n\left[\frac{(Ar)_p}{(Ar)_d}\right] \qquad (19)$$

Stress wave propagation efficiency was evaluated by evaluating SWF values (Vary, 1987; Vary and Bowles, 1979) at several threshold levels. The SWF is defined as the number of times a signal passes a threshold level. AUP were also measured for all specimens. This is defined as

$$AUP = \sum_{i=1}^{n}(A_i - Th) \qquad (20)$$

where A_i is amplitude of the signal passing threshold level of Th, and n is equal to the SWF. Data were analyzed at different threshold levels including one which was set just above the noise level and similar conclusions were drawn.

Upon completion of AU experiments, specimens were broken in an Instron testing machine by applying tensile load at the rate of 22 N/s. AE activities of steel-adhesive-steel and graphite epoxy composite-adhesive-graphite epoxy composite were monitored. Here the results of AE activities of the steel-adhesive-steel specimens will be discussed. Since the failure load in these specimens were much less than the load required for yielding adherends, all received activities were related to the bond failure. However, for graphite epoxy composite-adhesive-graphite epoxy composite specimens, bond failures were sometimes accompanied by fiber fracture and delamination. For this reason the correlation of these data with the bond strength was not clear.

For steel-adhesive-steel specimens, two AE transducers, each with a center frequency of 175 kHz (AC 175L), were utilized to detect the events emitted from the specimen at a distance of 7.6 cm apart. Each sensor was coupled with the workpiece through B-type Panametrics couplant and held in position with the aid of 4 stiff springs as shown in Fig. 10. The data were gathered and analyzed using an AET 5500 system. Data collection was focused on the lap joint portion only and all the other AE activities were thus discarded. For the lap joint, AE event locations were established using the difference in the arrival times of the signals received by the two sensors. Some of the parameters measured during the tensile tests were as follows; peak amplitude in decibels, event duration and rise time in μs, ringdown counts, slope, and AE energy. Here, the slope has been defined as peak amplitude/rise time while AE energy was defined as 10*log(event duration) + peak amplitude (in dB). It is notable that rms voltage has also been used as an indicator of the relative amount of AE energy by some researchers. Pencil-lead fracture method was used in order to calibrate the system prior to the actual run. Calibration eliminated the need to obtain the velocity of emitted waves. The detected signals were initially preamplified 60 dB to a total system gain of 80 dB. A floating threshold of 0.5 V was chosen to eliminate the background noise.

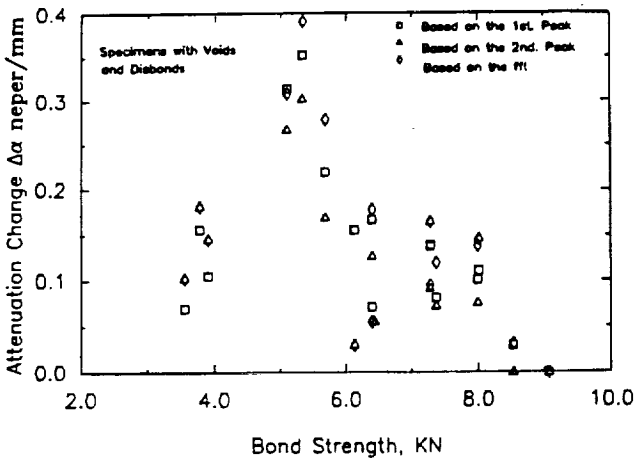

Fig. 11 Changes of longitudinal wave attenuation versus bond strength, for a pulse oscillator with the center frequency of 2 MHz, propagating through the lap thickness in steel-adhesive-steel specimens with symmetric void and disbond in the middle of overlap.

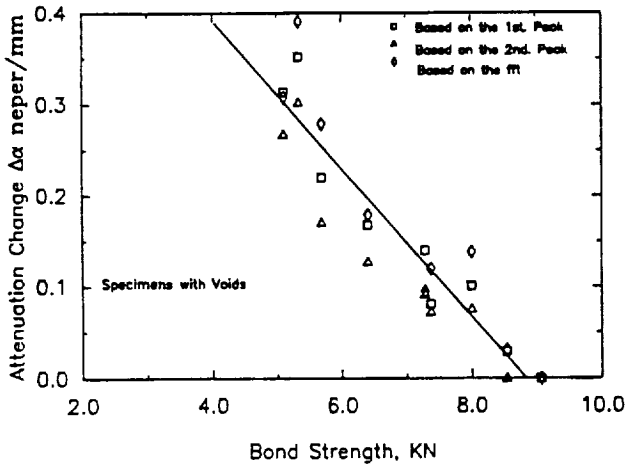

Fig. 12 Changes of longitudinal wave attenuation versus bond strength for a pulse oscillator with the center frequency of 2 MHz, propagating through the lap thickness in steel-adhesive-steel specimens with symmetric void in the middle of overlap.

7. Experimental Results and Discussion

For the steel bonded joint specimens the value of $\bar{\theta}$ from equation (10) is found to be 3.4. For this value of $\bar{\theta}$, the peak shear stress is affected by introduction of void and disbond in the overlap. It was suspected that the through transmission attenuation would be also affected in a similar way by the presence of void or disbond. Using both Panametric longitudinal and shear transducers with nominal element diameter of 19 mm, the attenuation changes for the entire overlap length (25.4 mm x 25.4 mm) were evaluated at frequency of 1 and 2 MHz. Transducers were coupled to the specimens by using either low or high viscosity Panametric couplant (low viscosity couplant when using

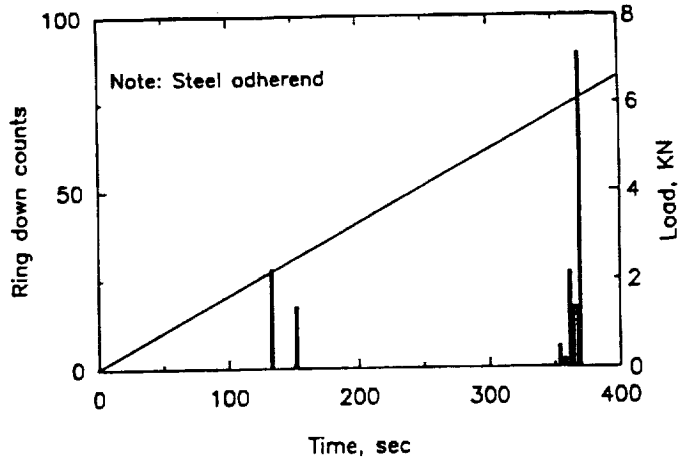

Fig. 13 Typical load and ringdown counts versus time (interval size = 2 s.)

the longitudinal transducers and high viscosity couplant when using the shear transducers). A load of 90 N was applied to each transducer by using a spring fixture device. Figure 11 shows the changes in longitudinal wave attenuation vs. bond strength. Similar pattern was also observed when plotting shear wave attenuation vs. bond strength. At first glance the data suggest no correlation between bond strength and attenuation change. However, closer examination of the data shows that, although disbonds and voids have similar effect on the bond strength, they have completely different effects on wave propagation characteristics. For specimens with a void, the transmitted wave is reflected significantly at the adherend void interface. A larger void results in more reflection and thus higher attenuation. However, the disbond is a weak bond between adherend and adhesive. The transmitted wave is not significantly affected by the presence of this region in the overlap. Furthermore, the attenuation change may not be very sensitive to the disbond length. Separating the data for specimens with voids and specimens with disbonds, and plotting attenuation change versus bond strength results in an excellent correlation between attenuation change and bond strength for specimens with voids; see Fig. 12. There was no correlation between attenuation change and bond strength for specimens with disbond, and the attenuation change was fairly constant over the disbond of 3 to 19 mm range. The correlations between the SWF and AUP, and the bond strength for these specimens were not clear. This may be explained by considering the dynamic response of the systems for an input wave at one edge and received wave at the other edge, as shown in Figs. 7 and 8. Here again, the peak amplitude of the signal is not an increasing function of disbond and void size. In contrast, bond strength is an increasing function of the void and disbond sizes.

In the AE experiments, we expected to find a good correlation between AE parameters and bond strength for all types of specimens with different defects (steel-adhesive-

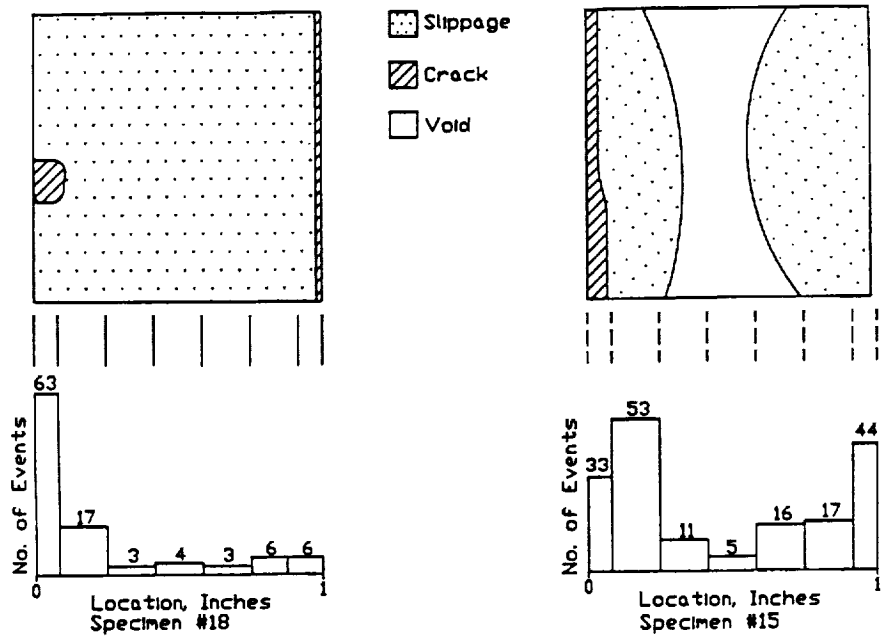

Fig. 14 Plots of the number of events along the lap joint for two typical specimens.

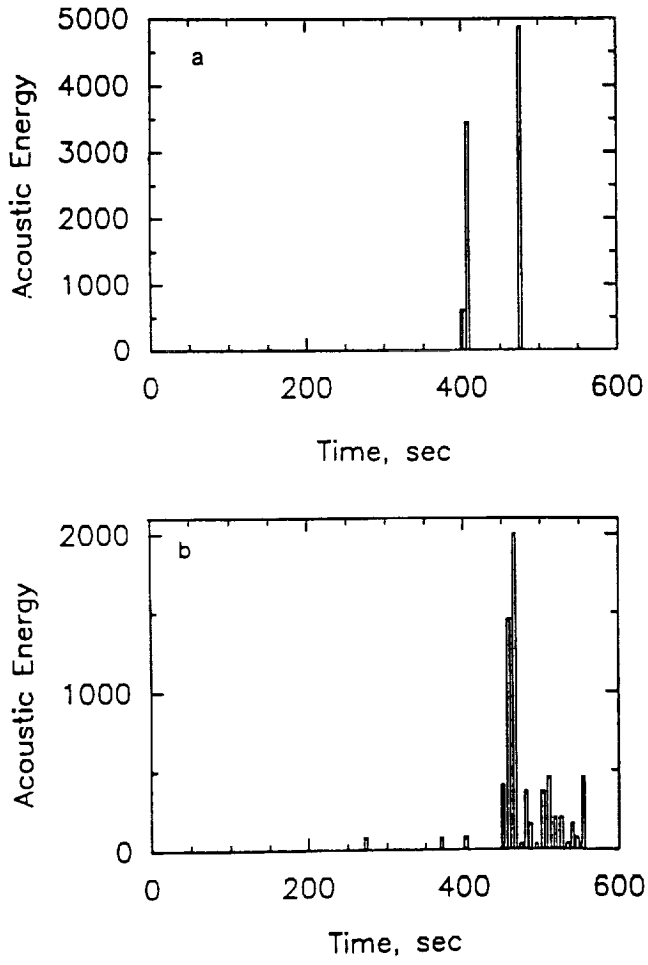

Fig. 15 Typical plot of AE energy vs. time for a) specimens with void or disbonds, b) perfect specimens.

steel specimens, with $\bar{\theta}$ = 3.4). This is due to the nature of failure location and mechanism, and energy released during failure. Since for symmetric voids and disbonds in the center of the overlap, stress distribution is almost identical, the bond strength and energy released can be assumed to be the same for specimen with identical void or disbond size. Furthermore, all detected released energy is associated with the high stress areas, which are the two edges of the overlap, which also control the bond strength. Figure 13 is a plot of a typical load-time curve of an adhesively bonded joint specimen along with its corresponding mean ringdown counts (number of threshold crossing) vs. time. There are three prominent peaks, the last of which corresponds to the time of failure. Having a lower amplitude, the first two peaks can be associated with crack initiation and preliminary crack growth. The source of these prominent peaks, recorded in real-time, was found to be near the end of the lap joint where the failure was originated. Furthermore, most of the AE activities were confined to the edges of the overlap; see Fig. 14.

Plots of energy vs. time compiled every four seconds during the period in which the specimens had reached their ultimate strength, exhibit two principal formats as shown in Fig. 15a. The specimens with a distinguished peak at failure, normally depicts specimens with artificial voids or disbonds. These specimens can be categorized as having failed in a brittle manner due to their short energy released duration. For these specimens, the energy released was relatively high at the peak compared to the perfect ones. Pollock and Lane (1968) showed that brittle materials exhibited high peak energy and short emission duration after

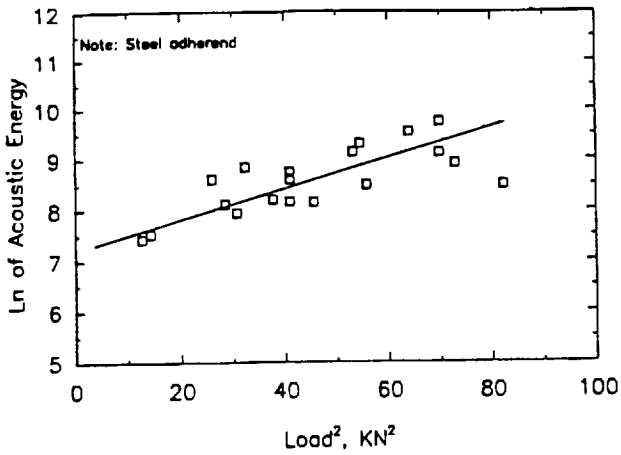

Fig. 16 Natural log of AE energy released at and immediately after the peak released energy vs. the square of maximum load (bond strength)^2 endured.

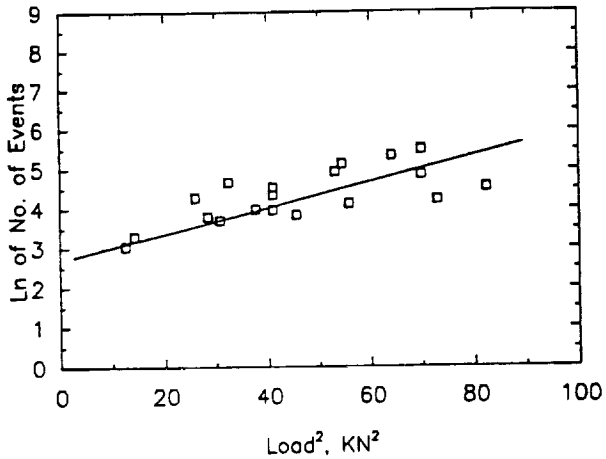

Fig. 17 Natural log of the number of events at and after peak event (failure point) vs. the square of the maximum load (bond strength)^2 endured.

the maximum load than ductile materials. This may be due to the fast fracture behavior in brittle materials and crack tip blunting (crack arrest) in ductile materials. For perfect specimens, fast fracture may have been prevented by having effective adhesive in the entire overlap. This is not true for specimens with void or disbond. Figure 15b depicts energy released for perfect specimens. Energy emission and the number of threshold crossings were sustained at a low level for some period after the time of the maximum peak of energy. This can be due to the crack or damage growth period in perfect specimens which is generally greater for the perfect specimens than specimens with a defect. Regression analyses of the total energy released and number of events at and after maximum peak energy show that these parameters can be related to the bond strength for all type of specimens; see Figs. 16 and 17. Analysis of the AE data further showed that the events with lower rise time were associated with the crack initiation while the one with

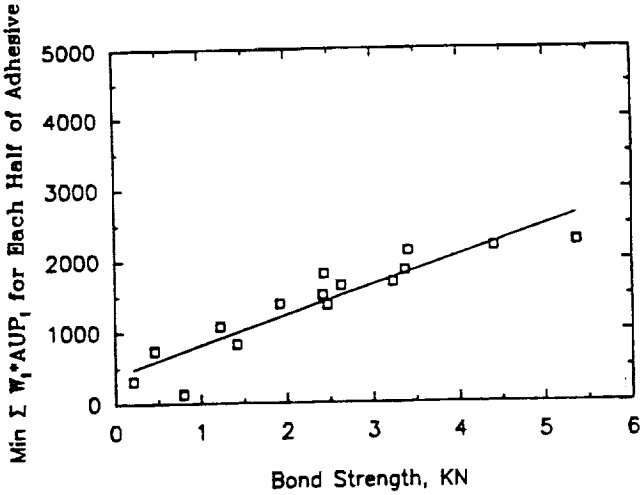

Fig. 18 Bond strength vs. minimum of Σ(weighted AUP) for aluminum-adhesive-aluminum specimens with various defects (mostly due to improper surface preparation and disbond).

higher rise time was associated with the crack (damage) propagation.

For the graphite epoxy composite-adhesive-graphite epoxy composite, $\bar{\theta}$ = 10. For this value of $\bar{\theta}$, it was expected that symmetric void or disbond up to 70% of the overlap length, to have a negligible effect on bond strength. Indeed there was little change in the bond strength for specimens with void up to 70% of the overlap length in the central region of the bonded joint (Nayeb-Hashemi and Rossettos, 1990). The peak amplitude of the received signal in an SWF setup experiment (Fig. 9), was found not to be very sensitive to the bond strength and showed a trend similar to the one exhibited by the dynamic analyses (Fig. 8). Other AU factors also failed to show any sensitivity to the bond strength.

To address more effectively the effects of disbond, improper adherend surface preparation, over cured and under cured adhesive, and deficient pressure during manufacturing of these specimens on bond strength, we set up an immersion experiment (Nayeb-Hashemi and Rossettos, 1993). As was described above, through transmission experiments utilizing a contact transducer resulted in little change in attenuation data for specimens with disbonds. Furthermore, disbonds or voids may not result in any change in bond strength as shown for composites. Disbonds right at the edge and a disbond in the middle of the bond have completely different effects on the bond strength. However, using contact transducers may not be a sensitive means to evaluate any changes in attenuation. To incorporate the location into attenuation, peak amplitude, SWF and AUP measurements, a weighting function $w(x) = \exp(\bar{\theta}\, x)$ was introduced. Here x is measured from the center of the overlap. Using focus transducers with center frequency of 2

MHz and adjusting transducer specimen distance, such that the focal point lies on the adhesive adherend interface, the peak amplitude, SWF and AUP at several locations of the overlap were measured, using a pulse with center frequency 2 MHz. New ultrasonic parameters were introduced as

$$\text{Peak}^* = \sum_{i=1}^{j} \exp(\bar{\theta} x_i)\text{Peak}(x_i) \qquad (21)$$

$$\text{SWF}^* = \sum_{i=1}^{j} \exp(\bar{\theta} x_i)\text{SWF}(x_i) \qquad (22)$$

$$\text{AUP}^* = \sum_{i=1}^{j} \exp(\bar{\theta} x_i)\text{AUP}(x_i) \qquad (23)$$

These parameters were also evaluated by considering the weighting function to be equal to unity. These parameters were either evaluated for the entire overlap or the over lap was divided in half and these parameters were evaluated for each half. The bond strength was assumed to be controlled by the section with a lower specific parameter value. For a variety of aluminum-adhesive-aluminum specimens with many surface defects, minimum AUP^* produced an excellent correlation with bond strength (Fig. 18). However, the correlation of the same data with the bond strength without incorporating weighting function (minimum of or total of $\sum \text{AUP}(x_i)$ vs. bond strength) was not good.

The results presented in this paper clearly show that the quest for an effective procedure for nondestructive evaluation of the adhesively bonded joint requires multidisciplinary approach. We believe that the immersion technique using focus transducers and incorporating the proper weighting function is the most effective method for bond quality interrogation. This procedure may be applied by using echo transducers. Further research has to be performed to substantiate the new parameters.

8. Conclusions

Defects such as voids, disbonds, improper adherends surface preparation and manufacturing procedures, may affect the bond strength of adhesive joints. In order to develop a proper acousto-ultrasonic method for bond quality interrogation, effects of defects such as void and disbond on (1) the stress distribution over the overlap, (2) the dynamic response, and (3) ultrasonic wave propagation must be understood.

The stress distribution in a single lap joint with and without voids is analyzed. For identical adherends, the stress distribution depends on a nondimensionalized parameter, $\bar{\theta}$. This parameter incorporates adherend and adhesive thicknesses and properties. The analyses show that for joints with $\bar{\theta} \geq 10$ the maximum shear stress is not affected by the presence of symmetric voids or disbond in the middle of overlap (void < 70% of overlap length). In contrast a finite element analysis shows that the dynamic response of a bonded joint is significantly affected by the presence of voids or disbonds in the overlap region. These results show that the measured ultrasonic parameters are affected by the defects. However, these measured values may or may not be related to the bond strength.

Through transmission longitudinal and shear wave attenuation changes in steel-adhesive-steel specimens ($\bar{\theta}$ = 3.4) with and without defects (symmetric voids and disbonds in the middle of overlap region) were measured using pulse oscillators with the center frequency of 1 and 2 MHz. The experimental results showed that the specimens with a larger void exhibited higher attenuation. These specimens also had lower bond strength. In contrast, specimens with disbonds in the same range size as voids exhibited little variation in the measured attenuation change. However their strength was affected in a similar way as those with voids. Various other AU factors also failed to show good sensitivities to the bond strength.

Since the location of defects has an important effect on the shear stress distribution and subsequent bond strength, a weighting factor $w(x_i) = \exp(\bar{\theta} x_i)$ was suggested. Using an immersion system with focused transducers many AU factors were evaluated. New ultrasonic parameters based on measured values and weighting function were proposed. It was shown that some of the new parameters produced a good sensitivity for bond quality prediction. However the sensitivity of the same parameters without weighting function was somewhat poor.

AE activities during the tensile tests were monitored and several time-domain variables were gathered for steel-adhesive-steel specimens. Two different formats of energy vs. time were observed. The specimens with a perfect bond showed an abrupt energy release at failure, followed by a short period of continuous AE activities. However, specimens with voids or disbonds also showed abrupt energy release, but followed with no additional activities. This behavior was related to the crack initiation and propagation. AE parameters were found to be a means for bond quality prediction.

Acknowledgment

This research was supported under NASA Grant NAG3-1129 with Dr. Alex Vary as monitor. The support is gratefully acknowledged.

References

R.D. Adams and N.A. Peppiatt (1974), "Stress Analysis of Adhesive-Bonded Lap Joints," J. Strain Analysis, 9(3), 185-196.

D.J. Allman (1977), "A Theory for Elastic Stresses in Adhesive Bonded Lap Joints," Quarterly J. Mechanics and Applied Mathematics, 30(4), 415-436.

P.A. Cooper and J.W. Sawyer (1979), "A Critical Examination of Stress in an Elastic Single Lap Joint," NASA TP 1507, September.

P. Dickstein, Y. Segal, E. Segal, and A.N. Sinclair (1989), "Statistical Pattern Recognition Techniques: A Sample Problem of Ultrasonic Determination of Interfacial Weakness in Adhesive Joints," J. Nondestructive Evaluation, 8(1), 27-35.

P.A. Dickstein, S. Giroshovich, Y. Sternberg, A.N. Sinclair, and H. Leibovitch (1990), "Ultrasonic Feature-Based Classification of the Interfacial Condition in Composite Adhesive Joints," Research in Nondestructive Evaluation, 2(4), 207-224.

P.A. Dickstein, J.K. Spelt, A.N. Sinclair, and Y. Bushlin (1991), "Investigation of Nondestructive Monitoring of the Environmental Degradation of Structural Adhesive Joints," Material Evaluation, December, 49(12), 1498-1505.

P.A. Dickstein, J.K. Spelt and A.N. Sinclair (1992), "Application of a Higher Order Crossing Feature of Nondestructive Evaluation: A sample Demonstration of Sensitivity to the Condition of Adhesive Joints," Ultrasonics, 29, September, 355-365.

J.C. Duke, Jr., E.G. Henneke, II, M.T. Kiernan and P.P. Grosskopf (1986), "Ultrasonic Stress Wave Characterization of Composite Materials," NASA CR 4178, May.

J.C. Duke, Jr., E.G. Henneke, II, W.W. Stinchcomb, and K.L. Reifsnider (1984), "Characterization of Composite Materials by Means of the Ultrasonic Stress Wave Factor," *Composite Structure 2*, ed., I.H. Marshall, Applied Science Publishers, London, England, pp. 53-60.

D.M. Egle, C.A. Tatro, and A.E. Brown (1981), "Frequency Spectra of Acoustic Emission from Nodular Cast Iron," Material Evaluation, 39, 1037-1044.

O.R. Gericke (1963), "Determination of the Geometry of Hidden Defects by Ultrasonic Pulse Analysis Testing," J. Acoust. Soc. America, 35(3), 364-368.

M. Goland and E. Reissner (1944), "The Stresses in Cemented Joints," J. Applied Mechanics, 11(1), A14-A27.
A.K. Govada, J.C. Duke, Jr., E.G. Henneke, and W.W. Stinchcomb (1985), "A Study of the Stress Wave Factor Technique for the Characterization of Composite Materials," NASA CR 174870. Feb.

L.J. Hart-Smith (1987), "Design of Adhesively Bonded Joints," *Joining Fibre-Reinforced Plastics*, ed. F.L. Matthews, Elsevier Applied Science, New York, pp. 271-311.

L.J. Hart-Smith (1985), "Designing to Minimize Peel Stresses in Adhesive-Bonded Joint," *Delamination and Debonding of Materials*, ASTM STP 876, ed. W.S. Johnson, ASTM, Philadelphia, pp. 238-266.

C.R. Heiple and S.H. Carpenter (1983), "Acoustic Emission from Dislocation Motion," *Acoustic Emission*, ed. J.R. Matthews, Gordon and Breach Sci. Publ., New York, pp. 15-103.

E.G. Henneke, J.C. Duke, W.W. Stinchcomb, A. Govada and A. Lemascon (1983), "A Study of the Stress Wave Factor Technique for the Characterization of Composite Materials," NASA CR 3670, February.

O. Ishai, D. Peretz and S. Gali (1977), "Direct Determination of Interlaminar Stresses in Polymeric Adhesive Layer," Experimental Mechanics, 17(7), 265-270.

P.A. Meyer and J.L. Rose (1974), "Ultrasonic Determination of Bond Strength Due to Surface Preparation Variations in an Aluminum-to-Aluminum Adhesive Bond System," J. Adhesion, 8, 145-153.

H. Nayeb-Hashemi and J.N. Rossettos (1990), "Nondestructive Evaluation of Adhesively Bonded Joints," Progress Report to National Aeronautics and Space Administration, Lewis Research Center, Cleveland, Ohio, September.

H. Nayeb-Hashemi, M.D. Cohen, and T. Erturk (1985), "Evaluation of Fatigue Damage on the Mechanical Properties of Fiber Reinforced Cement Pastes," J. Cement and Concrete Research, 15, Sept., 879-888.

H. Nayeb-Hashemi and J.N. Rossettos (1993), "Nondestructive Evaluation of Adhesively Bonded Joints by Acousto-Ultrasonic Technique and Acoustic Emission," *Proc. 2nd International Conf. on Acousto-Ultrasonics, Acousto-Ultrasonic Materials Characterization*, ed. Alex Vary, ASNT, Columbus, OH, June 24-25, Atlanta, GA.

A.A. Pollock and G. Lane (1968), "Prediction of the Strength of Adhesive Bonds and Diagnosis of Poor Adhesion by Means of Acoustic Emission," Information Sheet, Nondestructive Testing Center, Atomic Energy Research Establishment, Harwell, Oxfordshire, England.

J.L. Rose and P.A. Meyer (1973), "Ultrasonic Procedures for Predicting Adhesive Bond Strength," Material Evaluation, 31, 109-114.

J.L. Rose (1984), "Elements of a Feature-based Ultrasonic Inspection System," Material Evaluation, 42, February, 210-218.

J.L. Rose, M.J. Avioli Jr. and R. Bilgram (1983), "A Feasibility Study on the Nondestructive Evaluation of an Adhesively Bonded Metal to Metal Bond: An Ultrasonic Pulse Echo Approach," British J. NDT, 24(2), March, 67-71.

J.N. Rossettos, Y. Peng, and H. Nayeb-Hashemi (1991), "Analysis of Adhesively Bonded Composites Joints with Void and Thermal Mismatch," *Plastics and Plastic Composites: Material Properties, Part Performance, and Process Simulation*, ed., V.J. Stokes, ASME Winter Annual Meeting, AMD-Vol. 29, December, pp. 259-268.

J.N Rossettos, and E. Zang (1993), "On the Peak Shear ... es in Adhesive Joints with Voids," ASME J. Applied ...anics, 60(1), 559-560.

A. Sarrafzadeh-Khoee, M.T. Kiernan, J.C. Duke, Jr. and E.G. Henneke (1986), "A Study of the Stress Wave Factor Technique for the Nondestructive Evaluation of Composite Materials," NASA CR 4002, July.

C.V. Subramanian, M. Thavasimuthu, P. Palanichamy, D.K. Bhattacharya and Baldev Raj (1991), "Evaluation of Bond Integrity in Sandwiched Structures by Dry Couplant Ultrasonic Technique," NDT International, 24(1), 29-31.

T. Talreja, A. Govada, and E.G. Henneke, II (1984), "Quantitative Assessment of Damage Growth in Graphite Epoxy Laminates by Acousto-Ultrasonic Measurements," Review of Progress in Quantitative Nondestructive Evaluation, Vol. 3B, eds., D.O. Thompson and D.E. Chimenti, Plenum, pp. 1099-1106.

A. Vary (1987), "Acousto-Ultrasonics," *Non-Destructive Testing of Fiber-Reinforced Plastic Components*," Vol. 2, ed. J. Summerscales, Elsevier Applied Science, London, pp. 25-54.

A. Vary and K.J. Bowles (1979), "Use of an Ultrasonic-Acoustic Technique for Nondestructive Evaluation of Fiber Composite Strength," NASA TM73813, Feb.

A. Vary and R.F. Lark (1978), "Correlation of Fiber Composite Tensile Strength with Ultrasonic Stress Wave Propagation Factors," NASA TM78846, April (Also see (1979) J. Testing and Evaluation, 7(4), 185-191).

O. Volkersen (1938), "Die Nietkraftverteilung in Zugbeanspruchten Nietverbindungen mit Konstanten Laschenquerschnitten," Luftfahrtforschung, 15, 41-147.

J.H. Williams, Jr., H. Yuce and S.S. Lee (1984), "Ultrasonic Attenuation of a Void Containing Medium for Very Long Wavelengths," Materials Evaluation, 42(2), 219-224.

J.H. Williams, Jr., and S.S. Lee (1987), "Pattern Recognition Characterization of Micromechanical and Morphological Material State Via Analytical Quantitative Ultrasonics," *Materials Analysis by Ultrasonics*, ed. A. Vary, Noyes Data Corp., pp. 187-199.

R.S. Williams and P.E. Zwicke (1982), "Assessment of Adhesive Properties Using Pattern Recognition Analysis of Ultrasonic NDE Data," Material Evaluation, 40, March, 312-317.

ELSEVIER

Int. J. Adhesion and Adhesives 17 (1997) 55–63

0143-7496/97/$17.00

PII: S0143-7496(96)00023-1

Multiaxial fatigue life evaluation of tubular adhesively bonded joints

H. Nayeb-Hashemi, J.N. Rossettos and A.P. Melo
Department of Mechanical, Industrial and Manufacturing Engineering, Northeastern University, Boston, MA 02115, USA
(Accepted 21 May 1996)

The only viable method for joining plastic tubes and composite shafts is by bonding them adhesively. These structures are often subjected to complex cyclic loadings. Failure of these tubular joints not only depends on the applied loads, but also depends on the tube geometry, material properties of adhesive and tubes, and defects in the joint.

The shear stress distribution in the tubular joints is obtained for joints under axial and torsional loadings using the shear lag model. Under axial loading the adhesive is assumed to carry only shear stress and adherend to carry only axial load. However, the model considers the variation of the shear stress across the adhesive thickness. The effect of a void on the maximum shear stress is obtained.

A nondimensional θ_a parameter is defined and it is shown that the shear stress distribution not only depends on the value of θ_a but it also depends on cross sectional geometry of the tubes. For tubes with equal cross sectional area, the shear stress distribution along the bonded area is almost symmetric. For tubular joints with θ_a equal or greater than 6.7, a centrally symmetrical annular void with a size of at least 50% of the overlap length has little effect on the maximum shear stress and thus the failure load.

The shear stress under torsional loading is obtained by assuming the adhesive to shear in the circumferential direction only and neglecting its other deformations. The tubes are assumed to shear in the axial direction. The analysis considers the variation of the shear stress across the adhesive thickness. As in the case of axial loading, a new nondimensional parameter, θ_t, for tubes under torsion is defined. The results show that the shear stress in the bonded area not only depends on the θ_t value, but also depends on the polar moment of inertia, J_1 and J_2, of the tubes. The effect of annular voids on the shear stress distribution is evaluated for different void sizes and θ_t values.

The failure locus of adhesively bonded tubular specimens under axial, torsional and combined axial and torsional loadings is obtained. Based on these results a damage model for the tubular joints under combined axial and torsional cyclic loading is proposed. It is shown that this model can predict the fatigue life of the tubular joints reasonably well.

(Keywords: tubular joints; composites; destructive testing; stress analysis; fracture mechanics; destructive testing by lap-shear joints)

INTRODUCTION

Composite and polymeric tubes are becoming more popular in structural applications and transmission shafts. These tubes are often connected to each other with an adhesive. The bond strength and its degradation during service depend on the mechanical properties of the tubes and adhesive, the geometry of the tubes, defects present in the bonded area, and loading conditions. There are many theoretical analyses addressing the stress distribution in the tubular joints under axial and torsional loadings. However, few of these theoretical works have considered the effects of defects, such as a void in the adhesive, on the shear stress distribution. Furthermore to the best of our knowledge, there is no literature on the multiaxial fatigue life estimation of tubular joints under combined axial and torsional loadings.

Lubkin and Reissner have analyzed the stress distribution in tubular lap joints under axial load and gave solutions for both the shear stresses, τ_{zr}, in the adhesive layer and the normal stress, σ_n, across the thickness of the adhesive layer, due to adherend bending[1]. In the analyses, the two adherends were assumed to be thin, and hence the thin shell approximation was employed. The adhesive layer was assumed to be thin and much more flexible than the adherend, and was modeled as a series of infinitesimal tensile and shear springs. The work of the stresses, τ_{zr} and σ_{rr}, in the adherend is assumed to be negligible compared to the work of these stresses in the adhesive. The effect of defects in the analyses was also neglected.

The stresses in adhesively bonded tubular lap joints subjected to axial and torsional loads have been analyzed using axisymmetric quadratic isoparametric finite elements by Adams and Peppiat[2]. In the axial

where τ_a is the shear stress in the adhesive. Using the adhesive constitutive equation, equation (3) can be written in terms of adhesive displacement u_a as

$$G_a \frac{d^2 u_a}{dr^2} + \frac{G_a}{r} \frac{du_a}{dr} = 0 \quad (4)$$

where G_a is the shear modulus of adhesive. Assuming the displacements of adherend 2 and 1 are u_2 and u_1 at $r = R_3$ and $r = R_2$, respectively, equation (4) can be solved to obtain the adhesive displacement field across its thickness. This can be presented as

$$u_a = u_2 + \left[\frac{u_2 - u_1}{\ln R_3 - \ln R_2}\right](\ln r - \ln R_3). \quad (5)$$

Using equation (5) the shear stress at the inner and outer surfaces of adherend 2 and 1 can be found from,

$$(\tau_{rx})_2 = G_a \frac{du_a}{dr}\bigg|_{r=R_3} = G_a \left[\frac{u_2 - u_1}{\ln R_3 - \ln R_2}\right] \frac{1}{R_3} \quad (6)$$

$$(\tau_{rx})_1 = G_a \frac{du_a}{dr}\bigg|_{r=R_2} = G_a \left[\frac{u_2 - u_1}{\ln R_3 - \ln R_2}\right] \frac{1}{R_2} \quad (7)$$

Substituting (6) and (7) into (1) and (2) results in

$$E_2(R_4^2 - R_3^2) \frac{d^2 u_2}{dx^2} - 2G_a \left[\frac{u_2 - u_1}{\ln R_3 - \ln R_2}\right] = 0 \quad (8)$$

and

$$E_1(R_2^2 - R_1^2) \frac{d^2 u_2}{dx^2} - 2G_a \left[\frac{u_2 - u_1}{\ln R_3 - \ln R_2}\right] = 0 \quad (9)$$

Letting $x = \xi L$, where L is the length of the overlap, equations (8) and (9) can be written as

$$\frac{E_2(R_4^2 - R_3^2)}{L^2} \frac{d^2 u_2}{d\xi^2} - 2G_a \left[\frac{u_2 - u_1}{\ln R_3 - \ln R_2}\right] = 0 \quad (10)$$

and

$$\frac{E_1(R_2^2 - R_1^2)}{L^2} \frac{d^2 u_2}{d\xi^2} - 2G_a \left[\frac{u_2 - u_1}{\ln R_3 - \ln R_2}\right] = 0 \quad (11)$$

Equations (10) and (11) are valid for the bonded region of the joint when an adhesive layer is present. For the region without an adhesive layer, the equilibrium equations are

$$\frac{d^2 u_2}{d\xi^2} = 0 \quad (12)$$

and

$$\frac{d^2 u_1}{d\xi^2} = 0 \quad (13)$$

The solution of equations (10)–(13) gives displacements in different region of the overlap. The displacement fields in the region 1 where the adhesive layer is present, are

$$u_2(\xi) = C_3 e^{\theta_a \xi} + C_4 e^{-\theta_a \xi} - \frac{B(C_1 \xi + C_2)}{\theta_a^2} \quad (14)$$

$$u_1(\xi) = \frac{1}{E_1(R_2^2 - R_1^2)}[C_1 \xi + C_2 - E_2(R_4^2 - R_3^2)u_2] \quad (15)$$

and for the region (2) with a void are

$$u_2(\xi) = C_5 \xi + C_6 \quad (16)$$

$$u_1(\xi) = C_7 \xi + C_8 \quad (17)$$

and for region (3) where again an adhesive layer is present are

$$u_2(\xi) = C_9 e^{\theta_a \xi} + C_{10} e^{-\theta_a \xi} - \frac{B}{\theta_a^2}(C_{11} \xi + C_{12}) \quad (18)$$

and

$$u_1(\xi) = [C_{11} \xi + C_{12} - E_2(R_4^2 - R_3^2)u_2] \frac{1}{E_1(R_2^2 - R_1^2)} \quad (19)$$

where θ_a is a nondimensional parameter

$$\theta_a^2 = \frac{2G_a}{\ln R_3 - \ln R_2}\left[1 + \frac{E_2(R_4^2 - R_3^2)}{E_1(R_2^2 - R_1^2)}\right] \frac{L^2}{E_2(R_4^2 - R_3^2)} \quad (20)$$

and

$$B = -\frac{2G_a L^2}{(\ln R_3 - \ln R_2) E_1 E_2 (R_2^2 - R_1^2)(R_4^2 - R_5^2)} \quad (21)$$

Boundary and continuity conditions in the various regions of the overlap are at $\xi = 0$

$$u_1 = 0 \quad (22)$$

$$\frac{du_2}{d\xi} = 0 \quad (23)$$

at $\xi = l_1/L$

$$u_2|_{\text{region 1}} = u_2|_{\text{region 2}} \quad (24)$$

$$\frac{du_2}{d\xi}|_{\text{region 1}} = \frac{du_2}{d\xi}|_{\text{region 2}} \quad (25)$$

$$u_1|_{\text{region 1}} = u_1|_{\text{region 2}} \quad (26)$$

$$\frac{du_1}{d\xi}|_{\text{region 1}} = \frac{du_1}{d\xi}|_{\text{region 2}} \quad (27)$$

at $\xi = l_2/L$

$$u_2|_{\text{region 2}} = u_2|_{\text{region 3}} \quad (28)$$

$$\frac{du_2}{d\xi}|_{\text{region 2}} = \frac{du_2}{d\xi}|_{\text{region 3}} \quad (29)$$

$$u_1|_{\text{region 2}} = u_1|_{\text{region 3}} \quad (30)$$

and

$$\frac{J_2}{R_3} G_2 \frac{d^2 u_2}{dx^2} - 2\pi G_a \frac{u_2 - u_1}{\frac{1}{R_2} - \frac{1}{R_3}} = 0 \qquad (46)$$

Equations (45) and (46) can be normalized by letting $x = \xi L$ and then solving for u_1 and u_2 in terms of ξ. This results in

$$u_2(\xi) = C_3 e^{\theta_t \xi} + C_4 e^{-\theta_t \xi} - \frac{B}{\theta_t^2}(C_1 \xi + C_2) \qquad (47)$$

and

$$u_1(\xi) = \frac{R_2 L^2}{J_1 G_1}\left[C_1 \xi + C_2 - \frac{J_2 G_2}{L^2 R_3} u_2\right] \qquad (48)$$

where here again θ_t is a nondimensional parameter for the case of torsional loading, which combines adherend and adhesive mechanical properties and geometries,

$$\theta_t^2 = \frac{2\pi G_a}{R_3 - R_2}\left(1 + \frac{J_2 G_2 R_2}{J_1 G_1 R_3}\right) R_2 R_3^2 L^2 \qquad (49)$$

and B is a constant depending on adhesive and adherends mechanical properties and geometries

$$B = -2\pi G_a \frac{1}{R_3 - R_2} \frac{R_2^2 R_3^2 L^4}{(J_1 G_1) J_2 G_2} \qquad (50)$$

Equations (47) and (48) are valid in region of a tubular joint when adhesive layer is present. For a region with an annular void the rotational displacements u_1 and u_2 are

$$u_2 = C_7 \xi + C_8 \qquad (51)$$

$$u_1 = C_5 \xi + C_6 \qquad (52)$$

A similar procedure as that developed for axial loading can be used to obtain rotational displacements at various regions of the overlap. The boundary conditions are also similar to those for the axial case except that at $\xi = 1$

$$\frac{du_2}{d\xi} = \frac{TLR_3}{J_2 G_2} \qquad (53)$$

The shear stresses $(\tau_{r\theta})_{10}$ and $(\tau_{r\theta})_{2i}$ can then be obtained by substituting for u_1 and u_2 from equations (47) and (48) into equations (40) and (41). These stresses are evaluated for various θ and J_1 and J_2 values. The normalized shear stresses are defined as the ratio of the actual stress to the average stress, giving

$$SCF = \frac{(\tau_{r\theta})_{2i}}{(\tau_{av})_{2i}} = \frac{(\tau_{r\theta})_{10}}{(\tau_{av})_{10}} \qquad (54)$$

where $(\tau_{av})_{2i}$ and $(\tau_{av})_{10}$ are

$$(\tau_{av})_{2i} = \frac{T}{2\pi R_3^2 L} \quad \text{and} \quad (\tau_{av})_{10} = \frac{T}{2\pi R_2^2 L} \qquad (55)$$

EXPERIMENTAL INVESTIGATION

Figure 3 shows the specimen geometries used to investigate the failure locus and multiaxial fatigue properties of tubular bonded joints. Steel adherends were bonded using an adhesive with 50% epoxy and 50% hardener supplied by the Shell Company (Epoxy 828 and Hardener V40). The mixture was degassed for 3 min prior to its usage. For this mixture of the adhesive, the shear modulus of the adhesive was reported to be 791 MPa[18]. The adhesive was cured at 100°C for 1 h. The surfaces of both adherends were sand blasted and cleaned ultrasonically in acetone. This resulted in highly repeatable experimental data. A fixture was used to ensure alignment of adherends prior to adhesive curing. A rubber gasket was used between male and female adherends to retain adhesive during its curing and avoiding its leakage, *Figure 3*.

For the failure locus experiments, specimens were installed in an Instron tension/torsion machine (Model 1322) and pulled or twisted to failure at the rate of 70 N or (2 Nm)/s. Increasing or decreasing the loading rate two or three times did not result in any change in the failure loads. An analog/digital convertor was used to measure load/displacement. The data were stored in a PC for future analysis. For fatigue experiments, the specimens were subjected to sinusoidal loading with zero mean load at the frequency of 1 Hz. The experiments were conducted under constant displacement amplitudes. The failure was defined when either the axial load or the torque dropped by 10%. Most of the failure was initiated at the inner surface where stresses were maximum.

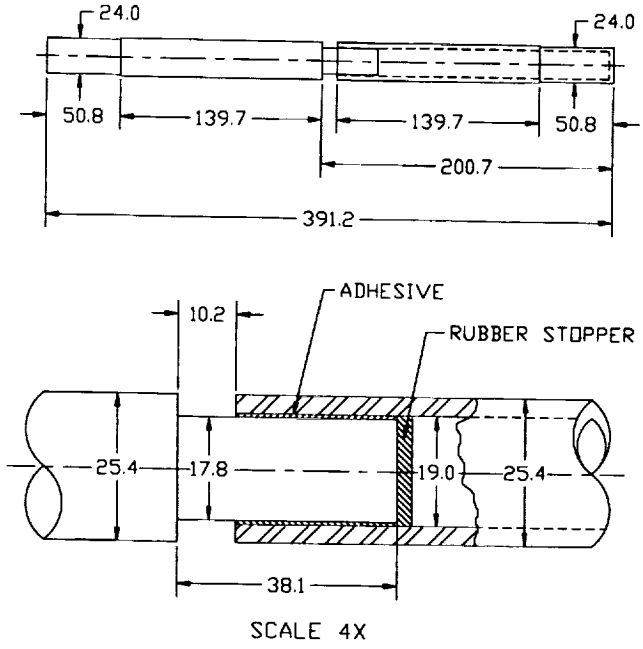

Figure 3 Schematic diagram of the steel–adhesive–steel tubular joint used in the experimental investigation

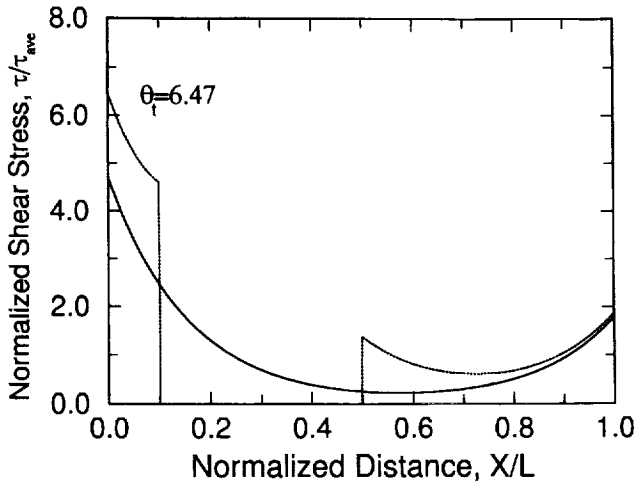

Figure 8 Normalized shear stress, $\tau_{r\theta}/\tau_{ave}$, distributions in a tubular bonded joint under torsion, with and without an annular void. The void is located at the edge where the torque is applied on the adherend with a smaller J value

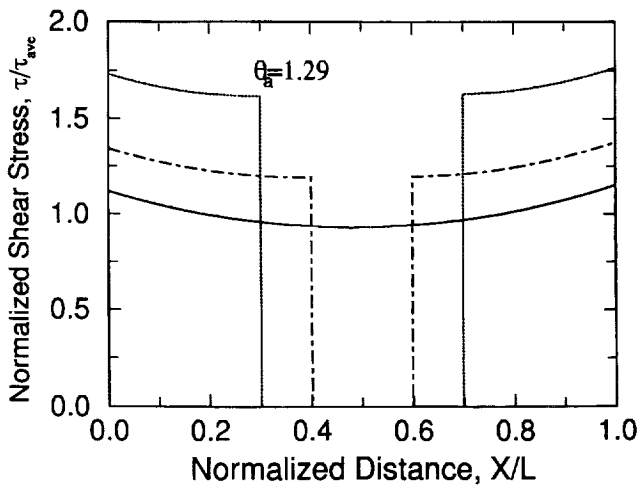

Figure 11 Normalized shear stress, τ_{rx}/τ_{ave}, distributions in a tubular bonded joint under tension, with a central annular void of different sizes

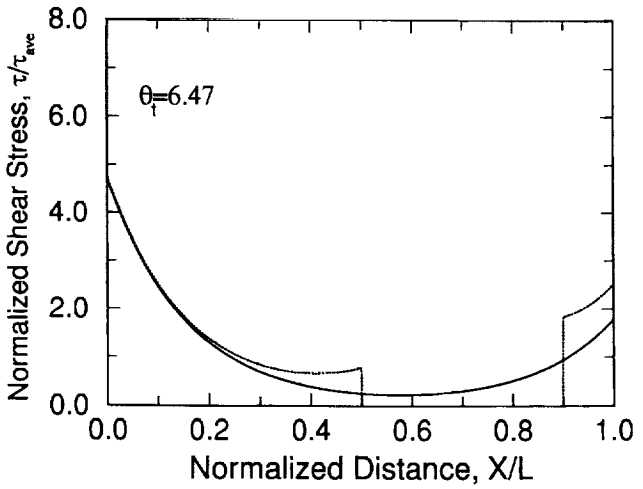

Figure 9 Normalized shear stress, $\tau_{r\theta}/\tau_{ave}$, distributions in a tubular bonded joint under torsion, with and without an annular void. The void is located at the edge where the torque is applied on the adherend with a larger J value

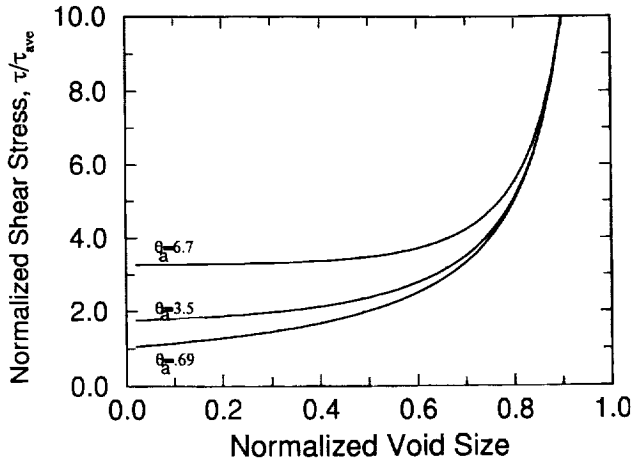

Figure 12 Normalized shear stress, $(\tau_{rx})_{max}/\tau_{ave}$, *versus* normalized void size in tubular joints under tension for several values of θ

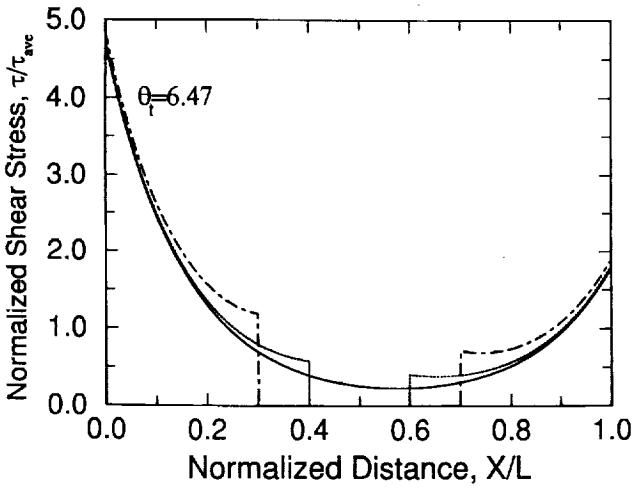

Figure 10 Normalized shear stress, $\tau_{r\theta}/\tau_{ave}$, distributions in a tubular bonded joint under torsion, with a central annular void of different sizes

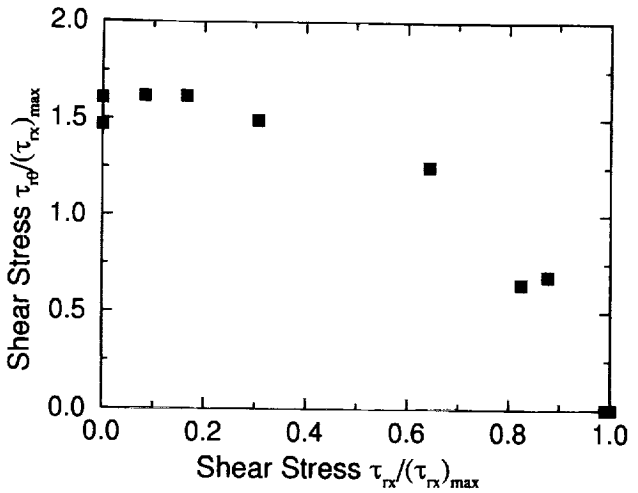

Figure 13 Failure locus of a steel–adhesive–steel tubular joint under in phase axial/torsional loading

7 Chen, D. and Cheng, S. *J. Appl. Mech., Trans. ASME* 1990, **57,** 78
8 Hart-Smith, L.J. NASA CR-112236, NASA, Huntsville, Ala. 1973
9 Nayeb-Hashemi, H. and Rossettos, J. *Int. J. of Acoustic Emission* 1994, **12**(1/2), 1
10 Rossettos, J.N., Lin, P. and Nayeb-Hashemi, H. *J. of Engineering Materials and Technology* 1994, **116,** 533
11 Rossettos, J.N. and Zang, E. *ASME J. of Applied Mechanics* 1993, **60**(2), 559
12 Lin, H., Nayeb-Hashemi, H. and Pelloux, R.M. *Int. J. Fatigue* 1992, **14,** 101
13 Hua, C.T. and Socie, D.F. *Fat. Fract. Eng. Mat. Struct.* 1987, **8,** 101
14 Brown, M.W. and Miller, K.J. *Proc. Instn. Mech. Engrs.* 1973, **187,** 745
15 Lin, H., Nayeb-Hashemi, H. and Pelloux, R.M. *Fat. Fract. Eng. Mat. Struct.* 1993, **16**(7), 723
16 Lin, H, Nayeb-Hashemi, H. and Berg, C. *J. Eng. Mat. Tec.* 1994, **116,** 27
17 Leese, G.E. ASTM STP 942, 1988, pp. 861–873
18 Mechanical Properties of Epoxy 828 and Hardener V40, NSERIES.BUL-1, Shell Oil Company, 1992

Theoretical and Experimental Evaluation of the Bond Strength Under Peeling Loads

Hamid Nayeb-Hashemi

Oussama Cherkaoui Jawad

Department of Mechanical Industrial and Manufacturing Engineering, Northeastern University, Boston, MA 02115

Reliable applications of adhesively bonded joints require understanding of the stress distribution along the bond-line and the stresses that are responsible for the joint failure. To properly evaluate factors affecting peel strength, effects of defects such as voids on the stress distribution in the overlap region must be understood. In this work, the peel stress distribution in a single lap joint is derived using a strength of materials approach. The bonded joint is modeled as Euler-Bernoulli beams, bonded together with an adhesive, which is modeled as an elastic foundation which can resist both peel and shear stresses. It is found that for certain adhesive and adherend geometries and properties, a central void with the size up to 50 percent of the overlap length has negligible effect on the peak peel and shear stresses. To verify the solutions obtained from the model, the problem is solved again by using the finite element method and by treating the adherends and the adhesive as elastic materials. It is found that the model used in the analysis not only predicts the correct trend for the peel stress distribution but also gives rather surprisingly close results to that of the finite element analysis. It is also found that both shear and peel stresses can be responsible for the joint performance and when a void is introduced, both of these stresses can contribute to the joint failure as the void size increases. Acoustic emission activities of aluminum-adhesive-aluminum specimens with different void sizes were monitored. The AE ringdown counts and energy were very sensitive and decreased significantly with the void size. It was observed that the AE events were shifting towards the edge of the overlap where the maximum peeling and shearing stresses were occurring as the void size increased.

Introduction

Adhesive bonding has been used extensively in the aerospace and other high-technology industries and has a great potential for applications in other areas of manufacturing. It is attractive because it distributes stress over the entire bond area and eliminates the stress concentrations which can occur with mechanical fasteners. Bonded joints have potential advantages of strength-to-weight ratio, design flexibility and ease of fabrication.

A Fokker Aerospace report [1] showed that many of the past failures of bonded structures involved poor design. Most often the poor design could be attributed to inadequate understanding of the adhesion failure mechanisms.

There are three dominant modes of mechanical failure in bonded joints: 1) adherend failure (including delamination if one of the adherends is a laminated composite), 2) interfacial failure between adhesive and an adherend and 3) cohesive failure within the adhesive. When an adhesively bonded joint is subjected to an out-of plane loading, the tearing of the adhesive which occurs is called peeling. Because this type of failure can be produced by normal loads which are relatively small compared to the shear loads which structural adhesives are capable of withstanding [2], peel strength of adhesively bonded joints is a property to be considered.

In its simplest form, an adhesively bonded structure consists of three components of different mechanical properties, namely the adhesive and the two adherends. Under most operating loads and environmental conditions, the adherends behave in a linearly elastic manner, however, the adhesive may exhibit viscoelastic or nonlinear behavior. The exact analytical solution of the problem regarding the stress distribution in the bonded area is complicated. The existing analytical studies are, therefore, based on certain simplifying assumptions with regard to the modeling of the adhesive and the adherends. The adherends are usually modeled as an isotropic or orthotropic membrane [3], plate [4], or elastic continuum [5]. The primary physical consideration used in the selection of a particular model is generally the adhesive-to-adherend and adherend-to-adherend thickness ratios and the ratio of the adherend-to-adherend thickness to its lateral dimensions.

Erdogan et al. [6] have analyzed a general plane strain problem of adhesively bonded structures which consist of two different orthotropic adherends. The thickness of the adhesive was assumed small compared to the thickness of the adherends which, in turn, are small compared to the length of the joint. The transverse shear stress effects in the adherends and the in-plane normal strain in the adhesive are taken into account. The solution is obtained by assuming linear stress-strain relations for the adhesive. The peak values of the shear as well as that of the normal stress in the adhesive are found to be at the edges of the overlap region. In another study [7], an adhesively bonded lap joint is analyzed by treating the adherends as linear elastic plates and the adhesive as linearly viscoelastic solid. The stress distribution in the adhesive layer is calculated for three different external loads, membrane loading, bending, and transverse shear loading. The results indicate that the peak value of the normal stress in the adhesive is not consistently higher than that of the corresponding shear stress, and its distribution decays slower than that of shear stress from the edge of the overlap. In [8], the governing equations for a step lap joint with a void are established using a modified shear lag model, where the adhesive can have extensional as well as shear deformations. The model considers a quadratic axial deformation across the adhesive thickness. This model was used in order to accommo-

Contributed by the Materials Division for publication in the JOURNAL OF ENGINEERING MATERIALS AND TECHNOLOGY. Manuscript received by the Materials Division February 4, 1996; revised manuscript received January 19, 1997. Associate Technology Editor: A. Freed.

date thermal mismatch between the adhesive and the adherend, where the adhesive can expand due to temperature changes. It was shown that relatively large void sizes have little effect on peak shear stress for sufficiently large values of one of the defined parameters, and the value of this parameter can be controlled by either changing the geometry of the bonded joint or its materials.

There are a substantial number of papers dealing with bond strength prediction using nondestructive evaluation techniques. Acoustic emission is a nondestructive evaluation technique that has been known to have a great success in predicting structural integrity of components.

Acoustic emission (AE) is the generation, propagation and detection of transient stress waves in materials as they undergo deformation or fracture. These waves propagate to the surface of the structure where they may be detected by an ultrasonic transducer. The output of the transducer is processed and the resulting signals are interpreted as the "AE" signals. Acoustic emission signals can take many forms depending upon the material and the failure mechanism in the material. AE signals from defects in composites and geological materials generally contain information at low frequencies 0.5–100 KHz, since attenuation is relatively high due to the complexity of these materials. Signals of significance in metals and brittle materials contain information between 100 KHz and 2 MHz. In this range, a good compromise is found for most testing applications because ambient noise is low [9].

A number of techniques are employed to isolate and validate signals from noise in the time domain. Times of arrival can be used to permit geometric elimination of obvious noise through gating, and acceptance of only those signals which arrive from a particular region of the structure. In time domain, acoustic emission data include: ringdown counts, rms voltage, number of events, energy rate, rise time, event duration, amplitude distribution, and numerous others.

Williams and Lee [10] in a comprehensive study of acoustic emission in fiber composites materials and structures, found that AE is capable of detecting potential failure sources and defects in complex structures independent of the location, type and orientation of the flaws. They also stated that in tests involving AE, both the geometry and materials may play an important role in the AE results. Accurate and reproducible results require calibrations of specimens or structures used. Hashemi et al. [9] monitored acoustic emission activities during tensile tests of steel single-lap joint specimens. Several time domain parameters were gathered and analyzed. They observed two different formats of energy versus time. The specimens with a perfect bond showed an abrupt energy release at failure, followed by a short period of continuous acoustic emission activities. However, specimens with voids or disbonds showed abrupt energy release, but followed with no additional activities. They reported that this behavior was related to the crack initiation and propagation and that acoustic emission parameters were found to be a means for bond quality prediction. Williams et al. [11] monitored acoustic emission in adhesively bonded automotive glass fiber composite single-lap joints. Their AE data obtained during monotonic loading was analyzed using the AE load delay concept. The concept of the "AE stress delay" as defined by Williams et al. [12–14] is used to characterize the AE-strength behavior of the specimens. The AE stress delay is defined as the stress required to produce a specified level of cumulative AE events. They found a linear relation between the AE load delay and the fracture strength of the bonded joints, independent of the flaw type in the specimens. Also, the AE load delay is found to be useful in distinguishing the delamination, interfacial and cohesive separation modes. The purpose of this research is to understand the effect of defects on the peel stress distribution and nondestructive evaluation of peel strength of bonded joints by acoustic emission and acousto-ultrasonic technique. A strength of materials approach and the finite element technique are used to find the stress distribution in single lap joints subjected to a direct peeling load.

Theoretical Investigation

The stress distribution in a single lap joint is derived using a strength of materials approach by assuming that the adherends behave as Euler-Bernoulli beams. The adherends in the bonded region are assumed to be supported by a continuous elastic foundation. When the adherends are deflected, the intensity of the distributed reaction at every point of the overlap is taken to be proportional to the difference in the deflections of the adherends at that point. Under such conditions, the reaction per unit length of the adherend can be presented as ky, where y is the relative deflection of the adherends at point x, k is the stiffness of the foundation and its value is obtained from $k = (E_a w/t)$ where E_a is the elastic modulus of adhesive layer, w is the width of the overlap, t is the adhesive thickness. In previous work [15], the adhesive layer was modeled as a combination of linear and torsional springs. The torsional spring constant of the adhesive was obtained by modeling the adhesive as a cantilever beam. The torsional spring constant k_t, depended on a scalar factor ranging from 0 to 1. In order to improve that model, the effect of the shear stress at the adhesive-adherend interface is taken into consideration without any assumption regarding its value. Figure 1 shows a single-lap joint geometry and dimensions. For a perfectly bonded joint with no void, the structure is divided into three regions, where the lateral deflection of adherend in region 1 and 2 is taken as y_1, and y_2 and that of adherend 2 in region 2 and 3 are taken as y_3, and y_4. Let V, M, and τ be the transverse shear load, moment and shear stress in the adhesive respectively. From the free body diagram in Fig. 2, the equilibrium equations in the region 2 can be written as:

$$\frac{dV}{dx} + k(y_2 - y_3) = 0 \tag{1}$$

$$V + \frac{\tau w h_1}{2} - \frac{dM}{dx} = 0 \tag{2}$$

Substituting for V from Eq. (1) into Eq. (2) results

$$\frac{dV}{dx} + \frac{wh_1}{2}\frac{d\tau}{dx} - \frac{d^2M}{dx^2} = 0 \tag{3}$$

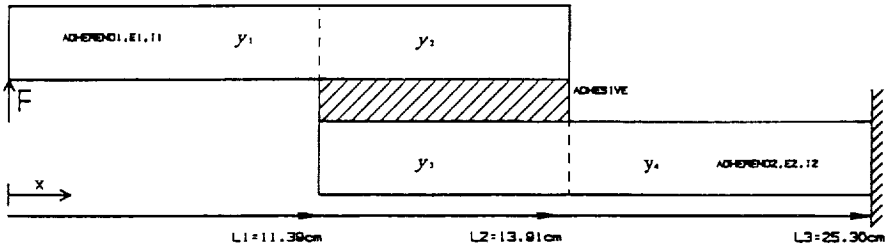

Fig. 1 Schematic diagram of a single lap joint

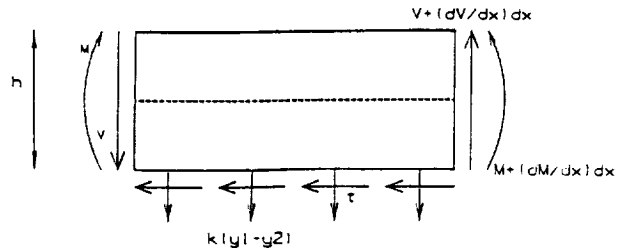

Fig. 2 Free body diagram of adherend 1 and adhesive

The bending moment and deflection are realted as

$$M = (EI)_1 \frac{d^2 y_2}{dx^2} \tag{4}$$

Substituting for M from Eq. (4) into Eq. (3) yields

$$(EI)_1 \frac{d^4 y_2}{dx^4} - \frac{wh_1}{2} \frac{d\tau}{dx} + k(y_2 - y_3) = 0 \tag{5}$$

The Shear strain γ_{ad} and shear stress τ at the adherend-adhesive interface can be determined by assuming that the shear strain in the adhesive is proportional to the relative slope of adherend 1 with respect to adherend 2. This can be written as:

$$\gamma_{ad} = \frac{\left[\frac{h_1}{2}\frac{dy_2}{dx} - \frac{h_2}{2}\frac{dy_3}{dx}\right]}{t} \tag{6}$$

The shear stress τ can then be obtained from:

$$\tau = G\gamma_{ad} = \frac{G}{t}\left[\frac{h_1}{2}\frac{dy_1}{dx} - \frac{h_2}{2}\frac{dy_3}{dx}\right] \tag{7}$$

Where G is the shear modulus of the adhesive, h_1, and h_2 are the thicknesses of adherend 1 and 2 respectively and (dy_2/dx) and (dy_3/dx) are the slopes of adherend 1 and 2. Substituting for τ from Eq. (7) into Eq. (5) results in a general form of a beam on an elastic foundation with a combined tensile and shear resistances.

$$(EI)_1 \frac{d^4 y_2}{dx^4} - \frac{wh_1}{2}\left[\frac{G}{t}\left(\frac{h_1}{2}\frac{d^2 y_2}{dx^2} - \frac{h_2}{2}\frac{d^2 y_3}{dx^2}\right)\right] + k(y_2 - y_3) = 0 \tag{8}$$

The modulus of bending rigidity of the adherends is denoted by $(EI)_1$ and $(EI)_2$. The governing deflection equations for the entire bonded joint with one end clamped and the other end subjected to a peeling force F can then be written as:

Region 1, adherend #1

$$(EI)_1 \frac{d^4 y_1}{dx^4} = 0 \tag{9}$$

Region 2, adherend #1

$$(EI)_1 \frac{d^4 y_2}{dx^4} + k(y_2 - y_3) - \frac{wh_1}{2}\frac{G}{t}\left[\frac{h_1}{2}\frac{d^2 y_2}{dx^2} - \frac{h_2}{2}\frac{d^2 y_3}{dx^2}\right] = 0 \tag{10}$$

Region 2, adherend #2

$$(EI)_2 \frac{d^4 y_3}{dx^4} - k(y_2 - y_3) + \frac{wh_2}{2}\frac{G}{t}\left[\frac{h_1}{2}\frac{d^2 y_2}{dx^2} - \frac{h_2}{2}\frac{d^2 y_3}{dx^2}\right] = 0 \tag{11}$$

Region 3, adherend #2

$$(EI)_2 \frac{d^4 y_4}{dx^4} = 0 \tag{12}$$

Boundary conditions:

- At $x = 0$

$$(EI)_1 \frac{d^3 y_1}{dx^3} = F \tag{13}$$

$$(EI)_1 \frac{d^2 y_1}{dx^2} = 0 \tag{14}$$

- At $x = l_1$

$$y_1 = y_2 \tag{15}$$

$$\frac{dy_1}{dx} = \frac{dy_2}{dx} \tag{16}$$

$$-(EI)_1 \frac{d^3 y_1}{dx^3} = -(EI)_1 \frac{d^3 y_2}{dx^3} + \frac{Gwh_1}{4t}\left[h_1 \frac{dy_2}{dx} - h_2 \frac{dy_3}{dx}\right] \tag{17}$$

$$(EI)_1 \frac{d^2 y_1}{dx^2} = (EI)_1 \frac{d^2 y_2}{dx^2} \tag{18}$$

$$-(EI)_2 \frac{d^3 y_3}{dx^3} - \frac{Gwh_2}{4t}\left[h_1 \frac{dy_2}{dx} - h_2 \frac{dy_3}{dx}\right] = 0 \tag{19}$$

$$(EI)_2 \frac{d^2 y_3}{dx^2} = 0 \tag{20}$$

- At $x = l_2$

$$-(EI)_1 \frac{d^3 y_2}{dx^3} + \frac{Gwh_1}{4t}\left[h_1 \frac{dy_2}{dx} - h_2 \frac{dy_3}{dx}\right] = 0 \tag{21}$$

$$(EI)_1 \frac{d^2 y_2}{dx^2} = 0 \tag{22}$$

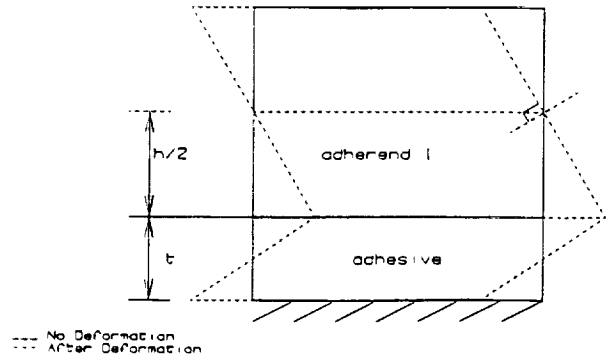

Fig. 3 Schematic diagram of the deformation field in the bonded joint where the shear strain was derived from

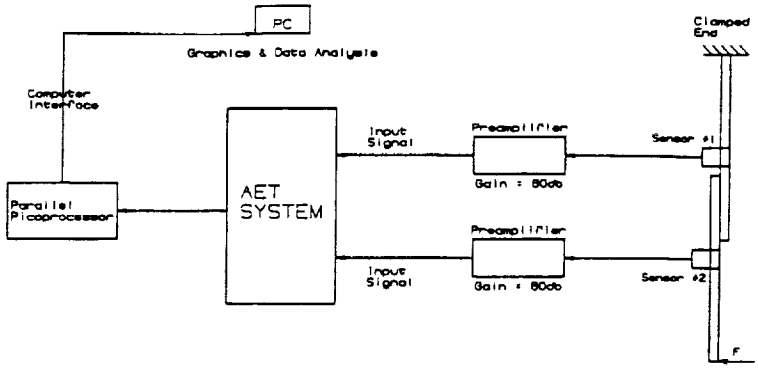

Fig. 4 Schematic diagram of the acoustic emission data acquisition system

$$-(EI)_2 \frac{d^3 y_3}{dx^3} - \frac{Gwh_2}{4t}\left[h_1 \frac{dy_2}{dx} - h_2 \frac{dy_3}{dx}\right] = -(EI)_2 \frac{d^3 y_4}{dx^3} \quad (23)$$

$$(EI)_2 \frac{d^2 y_3}{dx^2} = (EI)_2 \frac{d^2 y_4}{dx^2} \quad (24)$$

$$y_3 = y_4 \quad (25)$$

$$\frac{dy_3}{dx} = \frac{dy_4}{dx} \quad (26)$$

- At $x = l_3$

$$y_4 = 0 \quad (27)$$

$$\frac{dy_4}{dx} = 0 \quad (28)$$

Similar governing equations and boundary conditions can be written for the bonded joint with a void, by dividing the overlap into three regions. This analysis was performed and the effect of voids on the peel and shear stresses was derived.

In order to verify the results obtained for the peel and shear stresses from the model, these stresses were again obtained by finite element analyses, using ADINA finite element code. The bonded joint was modeled as 2 dim. structure, using 8 node isoparametric elements. The analysis was done for the same materials and geometry used in the experimental investigation. Voids were created by giving the modulus of the adhesive for elements in the void region a very small value. Adherends were 6061-T6 aluminum with elastic modulus of E = 69 GPa. The analyses were performed for joints with adherends of equal or different thicknesses. The adhesive layer was Hysol EA9689 adhesive with E = 2.2 GPa and a thickness of .13 mm. The overlap was 25.4 mm × 25.4 mm and symmetric central voids were introduced in the overlap. Effects of the mesh size in the overlap region were also investigated. Based on the results optimum mesh size was selected in the overlap region.

Experimental Investigations

Adhesively bonded joint specimens were prepared using aluminum 6061-T6 as adherends. Adherends were joined together in a single lap joint configuration using Hysol EA9689 epoxy film of .13 mm thickness. The adherend surfaces were sand-blasted and cleaned with acetone prior to bonding. The overlap area was 25.4 mm × 25.4 mm and upper and lower adherend thicknesses were 3.17 mm and 12.6 mm, respectively. Voids were introduced in the overlap by cutting and removing the adhesive film from the desired area of the boned joint and spraying a mold release agent over the void area before bonding. The specimens were cured at 170°C for 1 h, and dummy tabs and shims were used during the curing process to ensure that the adhesive layer in the specimens had the same thickness. Strain gages were also mounted on the surface of each specimen in order to monitor strain changes up to the specimen failure. Identical specimens were manufactured in order to ensure repeatability of the obtained data. An MTS model 810 servo-hydraulic testing system was used for the test.

The data for acoustic emission were monitored and collected using AET 5500 system. Two AE transducers, each with a center frequency of 175 KHz and nominal diameter of 22 mm, were used to detect events emitted from the specimens at a distance of 76 mm (center to center of transducers 98 mm)

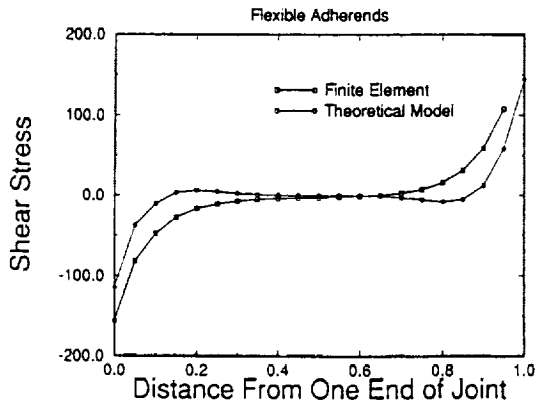

Fig. 5 Comparison of the shear stress distribution obtained from the theoretical model and finite element

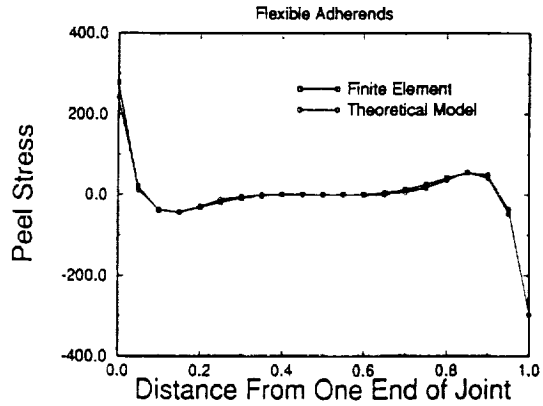

Fig. 6 Comparison of the peel stress distribution using theoretical model and finite element

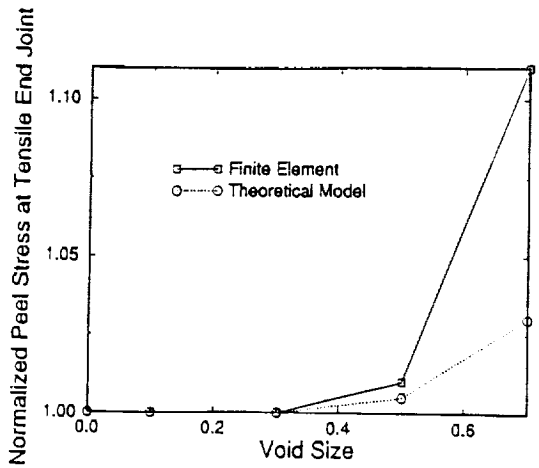

Fig. 7 Normalized variation of the maximum peel stress as a function of the void size

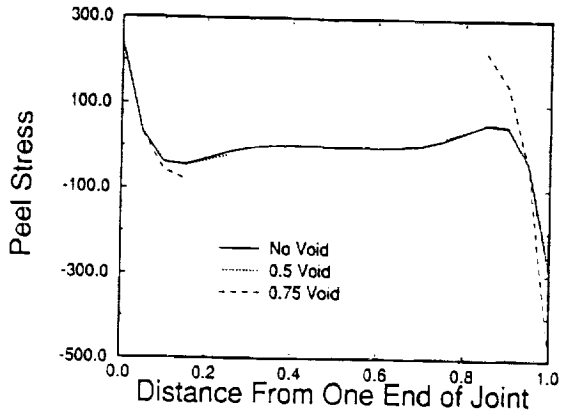

Fig. 9 Effect of a central void on the theoretical peel stress distribution

apart. Each sensor was coupled with the workpiece through a B-type panametrics couplant and held in position with the aid of 4 stiff springs as shown in Fig 4. Data collection were focused on the lap joint portion only and all the other AE activities were thus discarded. AE event locations were established using the difference in the arrival times of the signals received by the two sensors. ASTM standard of pencil lead fracture method [24] was used in order to calibrate the system prior to the actual run. Calibration eliminated the need to obtain the velocity of emitted waves. It is assumed that lead pencil fracture simulate stress waves generated by the actual failure and first arival wave is the longitudinal wave. The detected signals were preamplfied using two 60 db preamplifiers and a threshold of 0.5 V was chosen to eliminate the background noise. The entire wave forms and important features of the AE wave forms were recorded using a P.C. After completion of the tests, data were analyzed and processed using an AET 5500 software (Bawin™) and various AE parameters were extracted.

Theoretical Results and Effect of Voids on Stress Distribution

Figures 5 and 6 show the shear and peel stress distributions obtained from the theoretical and finite element analyses. The results show good agreement for shear and excellent agreement for peel stresses between the theoretical and finite element results. In our previous work, the peel and shear stress distribution in the bonded joint were obtained by modeling the adhesive layer as a combination of linear and torsional springs. The torsional spring constant was determined from a cantilever beam model which resulted in a spring constant with a scalar factor [15]. Although the model was capable of determining the peel stress, it resulted in a poor determination of the shear stress at the adhesive/adherend interface. Furthermore, the scalar factor for the torsional spring constant was determined from the solution obtained from the finite element results. The current analyses overcomes these deficiencies and provides excellent results for both peel and shear stresses without any assumptions and the need for a scalar factor. The model was further verified for different bonded joint dimensions and again good agreement was found between peel and shear stresses and those obtained from the finite element analyses. Results show that when both adherends are flexible and have the same thickness, both peel and shear can contribute to the failure of the joint when a void is introduced. But, when one adherend is flexible and the other is rigid, peel stress become dominant and contribute mainly to the failure. The effect of the void in the adhesive was also of interest in this investigation. It was found that for certain adhesive and adherend geometries and properties, a central symmetric void had a negligible effect on the peak peel and shear stresses. Figures 7 and 8 indicate the variations of the maximum normalized (normalized with respect to the maximum stresses for the case of no void) peel and shear stresses for a joint with a central void size up to 70 percent of the overlap length. Figure 9 show the effect of a central void on the peel stress distribution in the joint. These results are similar to those obtained for single lap joints under tension and tubular joints under tension/torsion.

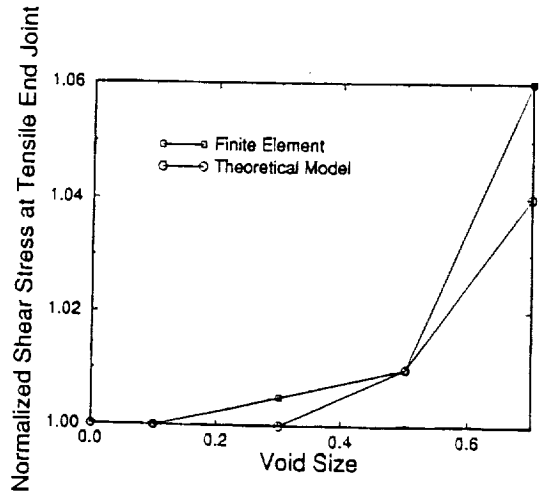

Fig. 8 Normalized variation of the maximum shear stress as a function of the void size

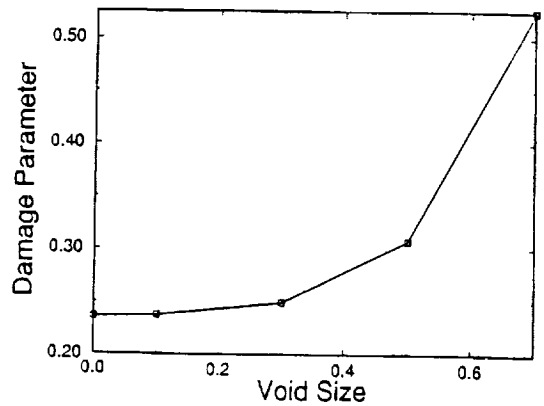

Fig. 10 Variation of the damage parameter with the void size using finite element results

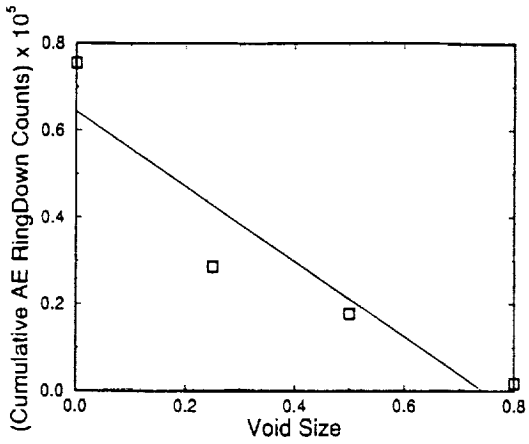

Fig. 11 Variation of cumulative AE ringdown counts with the void size

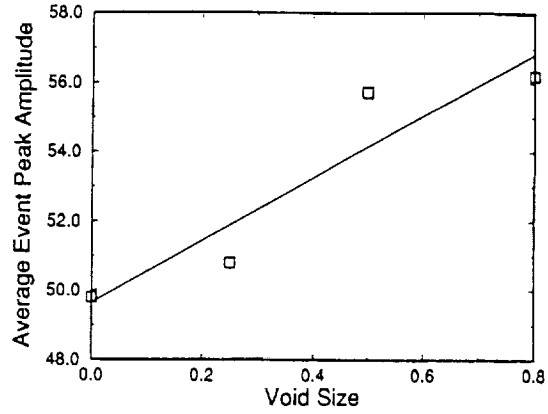

Fig. 13 Variation of peak amplitude with the void size

For these joints it was also found that the introduction of central symmetric void may have little effect on the bond failure [9, 25]. These results could not justify experimental data since significant changes in the failure loads were observed with the introduction of central voids in the bonded joint.

In order to obtain a failure criterion for the bonded joint, a damage parameter $D = \alpha\sigma^2 + \beta\tau^2$, where σ and τ are peel and shear stress at the tensile end joint was defined. The bonded joint is assumed to fail when $D = 1$. This concept is analogous to the failure criteria such as yielding. A material is considered to fail if $D \geq 1$. Similar models have been developed for fatigue life prediction of components under multiaxial loadings [25]. The values for α and β were obtained from the failure load on two specimens (a perfect specimen with no void and a specimen with 50% central void) and using the stresses obtained from the finite element results. After establishing the values of α and β the damage parameter D were found for different void sizes. Figure 10 shows that the damage parameter monotonically increases as the void size increases. It may be thus concluded that this is a better criterion to relate NDE parameters to the bond strength than the individual peel or shear stresses. Indeed our obtained AE data support this conclusion.

Experimental Results

Four specimens, one without a void and three with 6.3 mm, 12.6 mm and 20.2 mm wide voids were subjected to an increasing peeling load up to failure. At the same time, strains readings were recorded and acoustic emission activities were monitored. All detected events are associated with the high stress areas, which is the tensile edge of the joint which also controls the bond strength. Figures 11, 12 show that the Cumulative AE ringdown counts decreases with the void size, also that the AE energy exhibit the same behavior. Thus, these two parameters appear to be a good indication of the damage brought to the joint by the presence of the void in a set of specimens that otherwise are identical. The average of events peak amplitude is also sensitive to the presence of the void and increases with the void size as shown in Fig. 13. It is also found that the AE events are shifting towards the tensile end joint where the maximum peeling and shearing stresses are occurring as the void size increases as shown in Fig. 14. Further work is in progress to evaluate acousto-ultrasonic parameters for various bonded joints and relating them to the peel strength of the joint.

Conclusion

The stress distribution in a single lap joint under direct out-of plane loading with and without voids is analyzed by modeling the adherends as Euler-Bernoulli beams on an elastic foundation. The results show that the maximum peel and shear distributions are confined to the edge ends of the overlap. The results also show that for the type of adherend and adhesive analyzed, a void up to 50 percent of the overlap length has a negligible effect on the peak peel and shear stresses. The stress distribution in the joint is compared to the results obtained from the finite element analyses. The theoretical model and finite element results are in good agreement. A damage parameter was defined and shows promise as a criterion to relate NDE parameters to the bond strength.

Acoustic emission activities were also monitored and several parameters were extracted. Cumulative AE ringdown counts and energy were found to be sensitive and decreased significantly with the defect size.

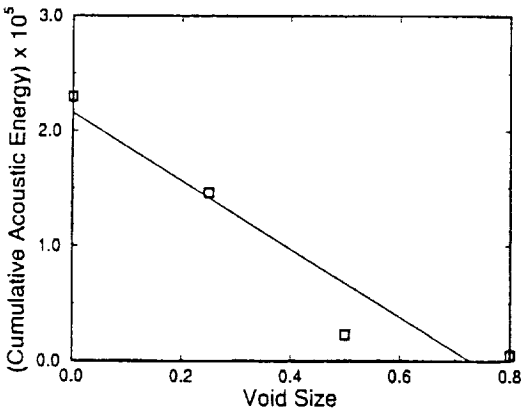

Fig. 12 Variation of AE cumulative energy with the void size

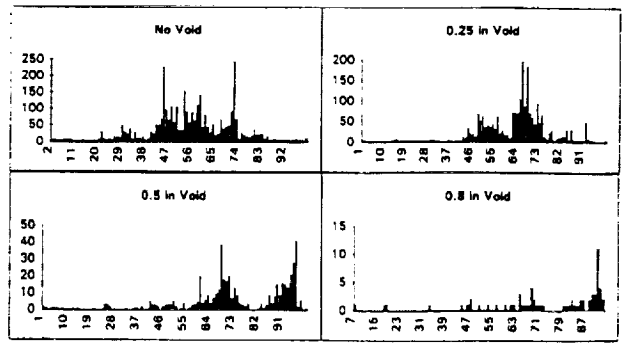

Fig. 14 Distribution of events by location in specimens with different void sizes

Acknowledgment

Authors express their sincere appreciations to Professor J. N. Rossettos for the review of the paper. This research was supported under NASA grant NAG3-1129 with Dr. Alex Vary as monitor, and is gratefully acknowledged.

References

1 Schlickelmann, R. J., "Past, Present, and Future of Structural Adhesive Bonding in Aerospace Application," *Trans. JSCM*, Vol. 5, No. 1–2, Dec. 1979.

2 Yurenka, S., "Peel Testing of Adhesive Bonded Metal," *J. of Applied Polymer Science*, Vol. 4, Issue No. 20, pp. 136–144, 1962.

3 Erdogan, F., and Ratwani, M., "Stress Distribution in Bonded Joints," *J. of Composite Materials*, Vol. 5, pp. 378–393, 1971.

4 Goland, M., and Reissner "The Stresses in Cemented Joints," ASME *Journal of Applied Mechanics*, Vol. 1, No. 1, pp. A.17–A.27, 1944.

5 Erdogan, F., and Civelek, M. B., "Contact Problem for an Elastic Reinforcement Bonded to an Elastic Plate," ASME *Journal of Applied Mechanics*, Vol. 41, pp. 1014–1018, 1974.

6 Delale, F., Erdogan, F., and Aydinoglu, M. N., "Stresses in Adhesively Bonded Joints: A Closed Form Solution," *J. of Composite Materials*, Vol. 15, May 1981, p. 249.

7 Delale, F., and Erdogan, F., "Viscoelastic Analysis of Adhesively Bonded Joints," NASA Contractor Properties, Part Performance, and Process Simulation, ASME 1991.

8 Rossettos, J. N., Lin, P., and Nayeb-Hashemi, H., "Comparison of the Effects of Debonds and Voids on Adhesive Joints," ASME JOURNAL OF ENGINEERING MATERIALS TECHNOLOGY, Vol. 116, pp. 533–538, 1994.

9 Nayeb-Hashemi, H., and Rossettos, J. N., "Nondestructive Evaluation of Adhesively Bonded Joints by Acousto-Ultrasonic Technique and Acoustic Emission," *J. of Acoustic Emission*, Vol. 12, Nos. 1/2, 1994.

10 Williams, J. H., and Lee, S., "Acoustic Emission Monitoring of Fiber Composite Materials and Structures," *J. of Composite Materials*, Vol. 12, Oct. 1978, pp. 348.

11 Williams, J. H., Lee, S., and Wang, T. K., "Nondestructive Evaluation of Strength and Separation Modes in Adhesively Bonded Automative Glass Fiber Composites Single Lap Joints," *J. of Composite Materials*, Vol. 21, Jan. 1987.

12 Williams, J. H., Lee, S. and Wang, T. K., "Quantitative Nondestructive Evaluation of Automative Glass Fiber Composites," *J. of Comp. Materials*, Vol. 16, pp. 20–39, Jan. 1982.

13 Williams, J. H., and Lee, S., "Acoustic Emission/Rupture Load Characterizations of Double-Braided Nylon Rope," *Marine Technology*, Vol. 19, No. 3, pp. 268–271, July 1982.

14 Williams, J. H., and Lee, S., "Acoustic Emission Characterization Using AE [Parameter] Delay," *Materials Evaluation*, Vol. 41, No. 8, pp. 961–966, July 1983.

15 Nayeb-Hashemi, H., and Jawad, Oussama, "Application of Acousto-Ultrasonic Technique and Acoustic Emission in Evaluation of Bond Strength," PVP-Vol. 295/NE-Vol. 16, Recent Advances in Structural Mechanics, ASME 1994.

16 Hart-Smith, J., "Analysis and Design of Advanced Composite Bonded Joints," NASA CR-2218, 1973.

17 Blichfeldt, B., and McCarthy, J. E., "Analytical and Experimental Investigation of Aircraft Metal Structures Reinforced with Filamentary Composites," NASA CR-2039, 1972.

18 Ishai, O., and Girshengorn, T., "Strength of Bonded Aluminum-CFRP Single Lap Joints," *Adhesive Age*, Vol. 21 (7), pp. 25–30, 1978.

19 Hart-Smith, L. J., "Designing Adhesive Bonds," *Adhesive Age*, pp. 32, Oct. 1978.

20 Crocombe, A. D., and Adams, R. D., "Peel Analysis Using the Finite Element Method," *J. Adhesion*, Vol. 12, pp. 127–139, 1981.

21 Olia, M., "Adhesively Bonded Joints," Ph.D thesis, Department of Mechanical Engineering, Northeastern University, Boston MA 02115.

22 Curtis, G. J., "Acoustic Emission Energy Relates to Bond Strength," *Nondestructive Testing*, Vol. 8, No. 5, pp. 249–257, Oct. 1975.

23 Hill, R., "The Use of Acoustic Emission for Characterizing Adhesive Joint Failure," *NDT International*, Vol. 10, No. 2, pp 63–72, Apr. 1977.

24 ASTM E976-94, "Standard Guide for Determining the Reproducibility of Acoustic Emission Sensor Response," ASTM, Philadelphia, PA 19103.

25 Nayeb-Hashemi, H., Rossettos, J. N., and Melo, A. P., "Multiaxial Fatigue Life Evaluation of Tubular Adhesively Bonded Joints," Accepted and will appear in the *Int. J. Adhesion and Adhesives*, Vol. 17, 1997.

Northeastern University

Department of Mechanical Engineering

Dr. Alex Vary
National Aeronautics and Space Administration
Lewis Research Center
Cleveland, Ohio 44135

December 2, 1994

Dear Alex:

Enclosed you will find our recent publications made possible by your continuous support. Regarding our current efforts, I will outline some of our progress for your information. Because our work is still progressing, I am requesting a no cost three month extension for our project.

Nondestructive Evaluation of Adhesively Bonded Joints

Our efforts have continued toward understanding factors affecting the tensile strength of single lap joints in tension as well as peel strength of bonded joints and their effects on the acousto ultrasonic parameters. The peel stress distribution in the bonded joint was obtained by modeling the single lap joint as a beam on an elastic foundation, Fig. 1. As with the case of the shear stress distribution in the single lap joint, the maximum peel stress was confined again to an area close to the edge of the lap joint. Central voids again had little effect on the maximum peel stress. Thus one may conclude again that the quality of the bond under peeling is controlled by the material close to the edge of the over lap, Fig.2. We have also studied wave propagation in the lap joint using finite element techniques, Fig. 3. This work was undertaken to address comments received from some reviewers, since the previous analysis was based on the steady state response of the lap joint rather than the transient response.

The stress wave finite element model resembled the acousto ultrasonic set-up. A broad band pulse with the center frequency of 2 MHz was introduced into the specimen and the received wave was analyzed, Fig. 4. Here as in the case of the vibration analysis reported earlier, the peak amplitude of the received signal decreased with increasing defect size, Fig. 5. However, as reported here and earlier, the peel and shear strength did not exhibit a similar trend. Thus, our previous conclusions hold, and using a weighting function in conjunction with the measured acousto-ultrasonic parameters appears to be justified.

We have also been involved in nondestructive evaluation of tubular bonded joints subjected to tension and torsion. The preliminary work is concentrated on nondestructive evaluation of adhesively bonded tubular aluminum tubes. Future work will consider tubular composite joints. The failure locus of aluminum joints under tension and torsion is found, Fig. 6. The effects of defects in the adhesive region on the tension and torsion strength of the joint and its relation with the acousto ultrasonic

334 Snell Engineering Center
Northeastern University
Boston, Massachusetts 02115
617-373-2982 (office) 617-373-2921 (fax)

properties are the focus of our investigation. The degradation of the bond during cyclic tension/torsion fatigue is another area of investigation.

Nondestructive Evaluation of Composite Materials Subjected to a Localized Heat Damage (Burning)

Unidirectional fiber glass epoxy composite panels with a thickness of 0.86 mm were manufactured and 12.7 mm strip composite specimens were cut from it. The mid point of the specimens was then subjected to 400 C by pressing a 6.35 copper cylinder at 400 C against the composite surface. The contact time was varied from 5 sec. to 9 min. Since the glass transition temperature of the E glass fiber in the composite was much higher than 400 C, most of the damage was associated with the matrix decomposition. The extent of the matrix decomposition depended on the exposure time. However, it seemed that after 2 min. exposure, the entire matrix in the mid section was decomposed and further exposure caused the decomposition of the matrix along the specimen length. The specimens were subsequently interrogated using an acousto ultrasonic set-up. A broad band pulse with the center frequency of 2 MHz was used as the transmitting signal. A resonant Panametric transducer with the center frequency of 2 MHz was used as the transmitting transducer. The receiving transducer was a Fc-500 AET transducer with a flat sensitivity in the frequency range of 100 kHz-2 MHz. Stress wave factor, SWF, and acousto ultrasonic parameter, AUP, were measured for these specimens. The specimens were then pulled to their failure, and acoustic emission activities of these specimens were measured. The results showed that there is no significant strength reduction beyond 2 minutes exposure at 400 C. This may be explained by the fact that the strength of the composites is controlled by the fiber strength. AUP of these specimens also showed a similar trend as those strengths versus the exposure time, figures 7, and 8. This may again be justified since the major part by of the stress wave energy is transmitted along the fiber. This phenomena is also reported in the literature. Specimens without heat exposure and those with exposure more than 1 minute showed different failure pattern and different acoustic emission activities. Figures 9 and 10 show events per location of perfect specimen and specimen with one minute heat exposure. The results show that most activities of the specimens are concentrated in the mid section of the specimens, while events from specimens with no heat exposure are distributed along the entire gage section of the specimen. Acoustic emission activities of specimens with two or more minutes of heat exposure were also relatively unchanged. We are currently analyzing our data and I will inform you about our results. This is an important area of research, since many composites may be subjected to localized burning due to malfunctions of electronic components attached to composites or heat from other sources.

A preliminary finite element stress analysis of this problem has also been performed, by conducting the static analysis of a long composite plate with a damaged region. The damaged region, where the matrix has deteriorated and the fibers are still in tact, is modeled by elements with reduced effective modulli. The stress distribution near the flawed region shows a tendency toward stress concentration, whose severity is related

to the values selected for the effective modulli, which in turn can be related to the degree of burning applied.

I would also like to inform you of some interesting and somewhat related work involved with the characterization and nondestructive evaluation of metal matrix composites. My colleague, Professor Blucher, has developed a new technique to manufacture metal matrix composites by continuous casting. We are interested in understanding the effects of manufacturing parameters, such as temperature, infiltration temperature, cooling rate, and matrix materials on the mechanical properties of these composites. We are also interested in predicting the mechanical properties of our composite using acousto ultrasonic technique and acoustic emission. We have acquired an imaging system and have used ICEPACK software to develop pattern recognition parameters to distinguish good and bad composites. We have broken some of our composites and have collected their acoustic emission activities. The acoustic emission activities of an alumina fiber reinforced 6061 aluminum is shown in Figure 11. The results show that the activities of the specimens increase exponentially up to .22% strain. However, beyond .22% strain the activities rate changes and becomes a linear function of strain. This change of activities may be related to the changes in micro mechanisms of failure. We are currently investigating the damage mechanisms at different strain levels, in order to be able to explain the change in the energy release mechanisms. One may postulate that the early events are associated with matrix yielding and fiber matrix debonding, and the later stages are associated with fiber fracture and linkage of cavities. Several specimens will be taken to different strain levels and then unloaded prior to their failures. These specimens will then be sectioned polished and studied under both optical and scanning electron microscope in order to reveal damage mechanisms at different strain levels.

We hope this gives some information about our progress. I will provide you with a comprehensive report on each project as soon as students finish their theses. In the mean time, may we take this opportunity to wish you a merry Christmas and a happy and healthy new year.

Sincerely yours,

Hamid N. Hashemi and John N. Rossettos

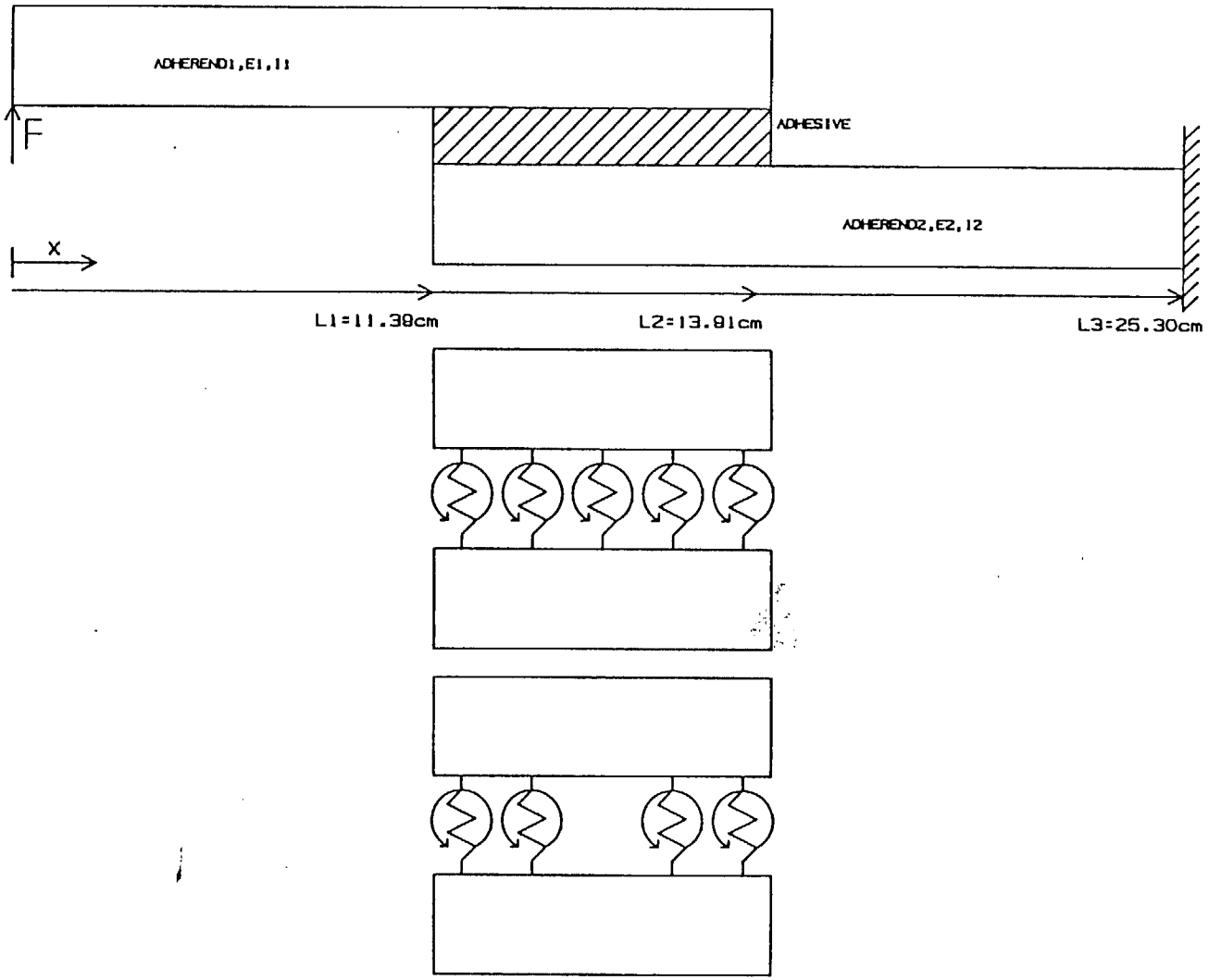

Fig. 1 Schematic diagram of the model for the peel stress analysis.

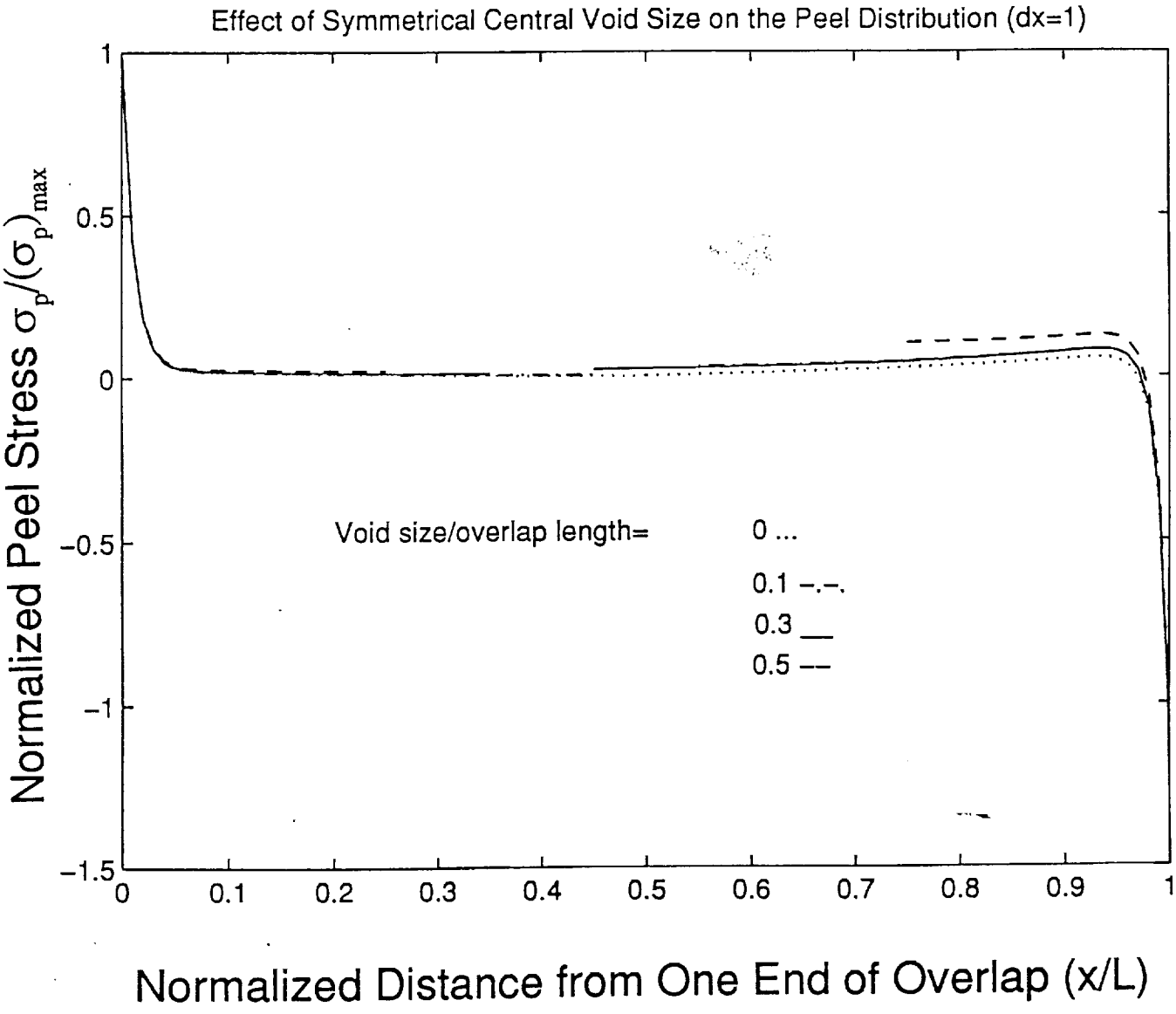

Fig. 2 Effect of symmetrical central void size on the peel stress distribution.

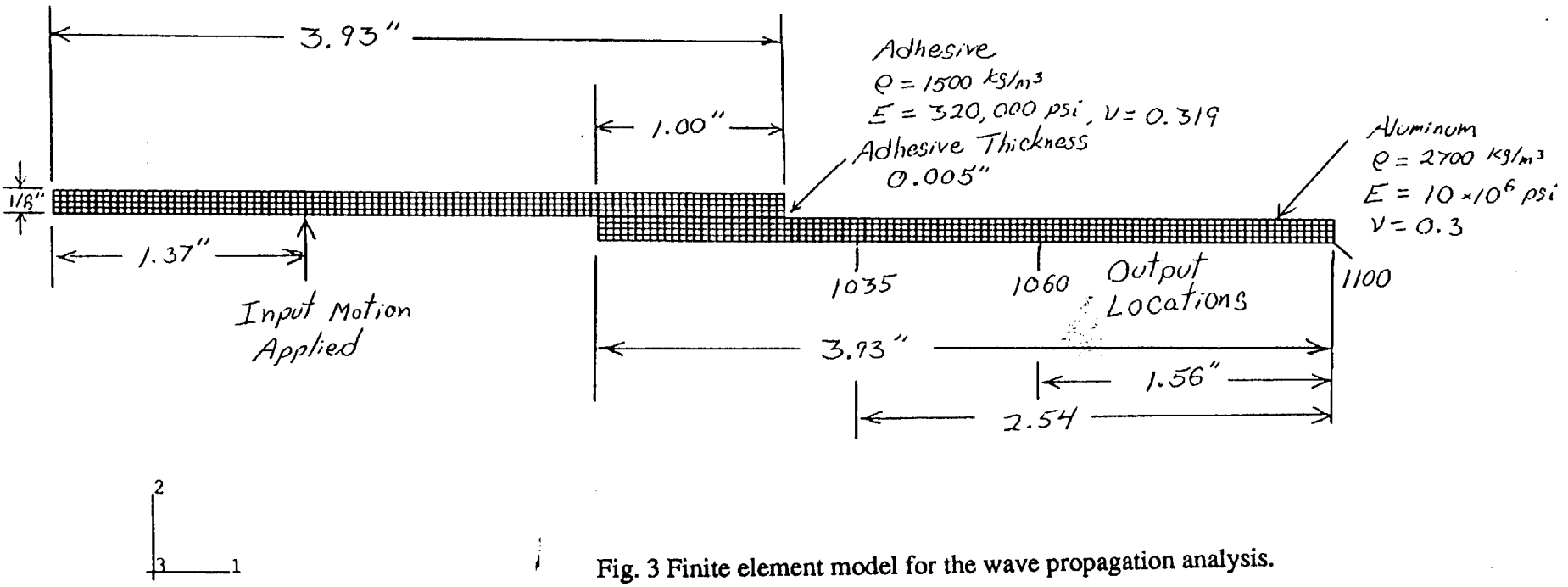

Fig. 3 Finite element model for the wave propagation analysis.

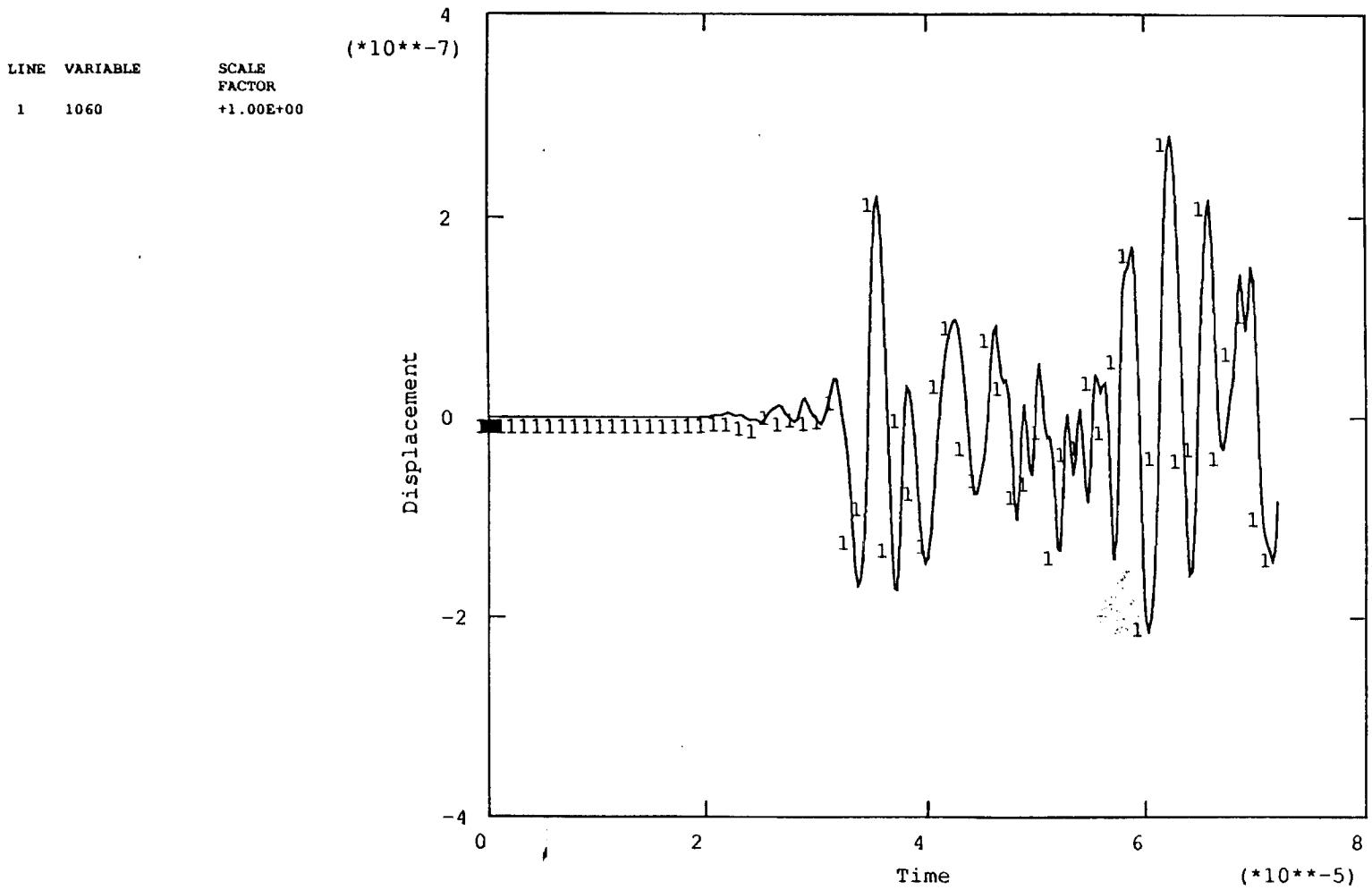

Fig. 4 The received wave form at node 1060, due to a broad band input pulse with the center frequency of 2 MHz for a specimen with 52% of the over lap symmetrical central void.

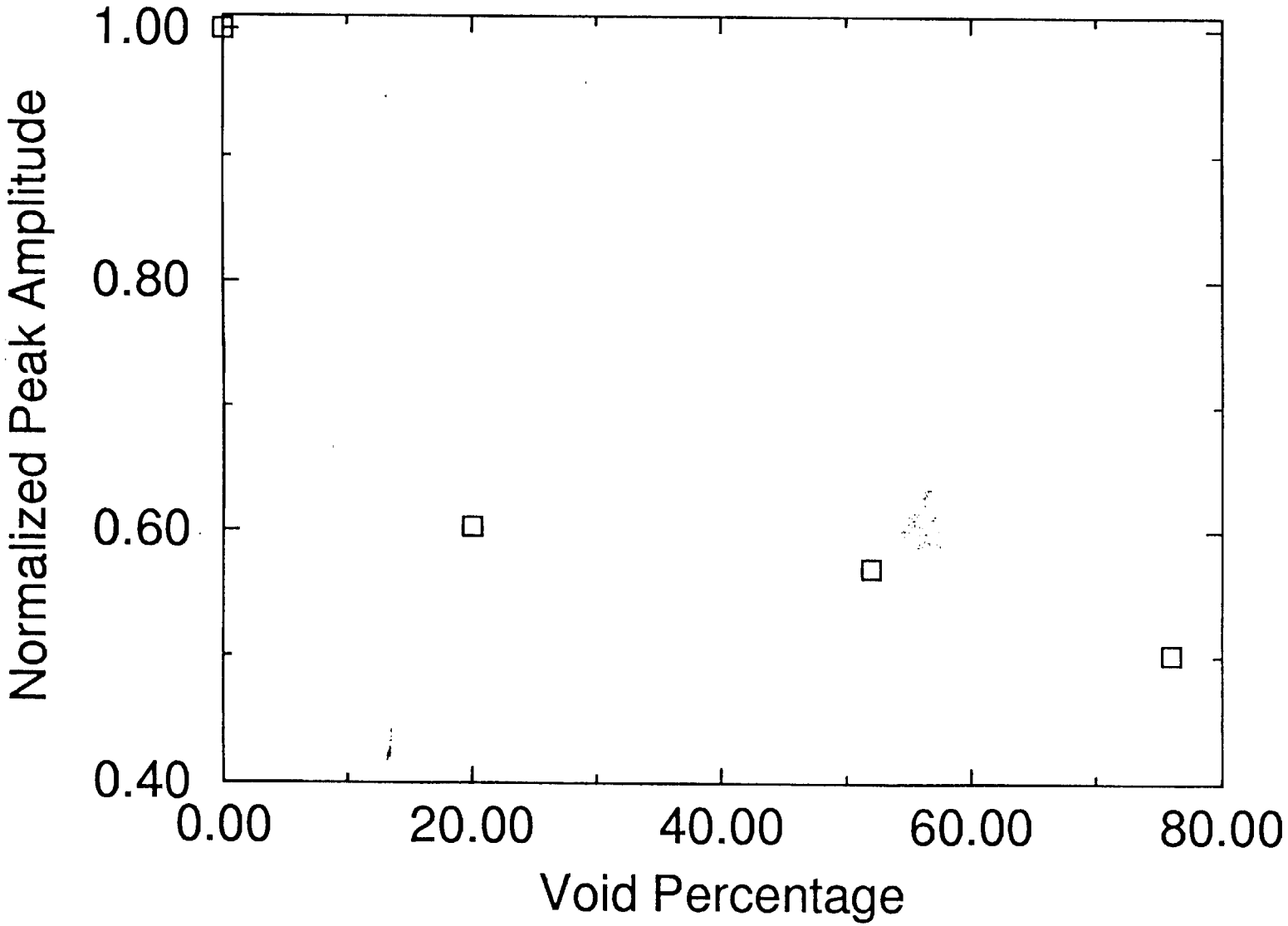

Fig. 5 Effect of symmetrical central void on the peak amplitude of the received wave at the node 1060.

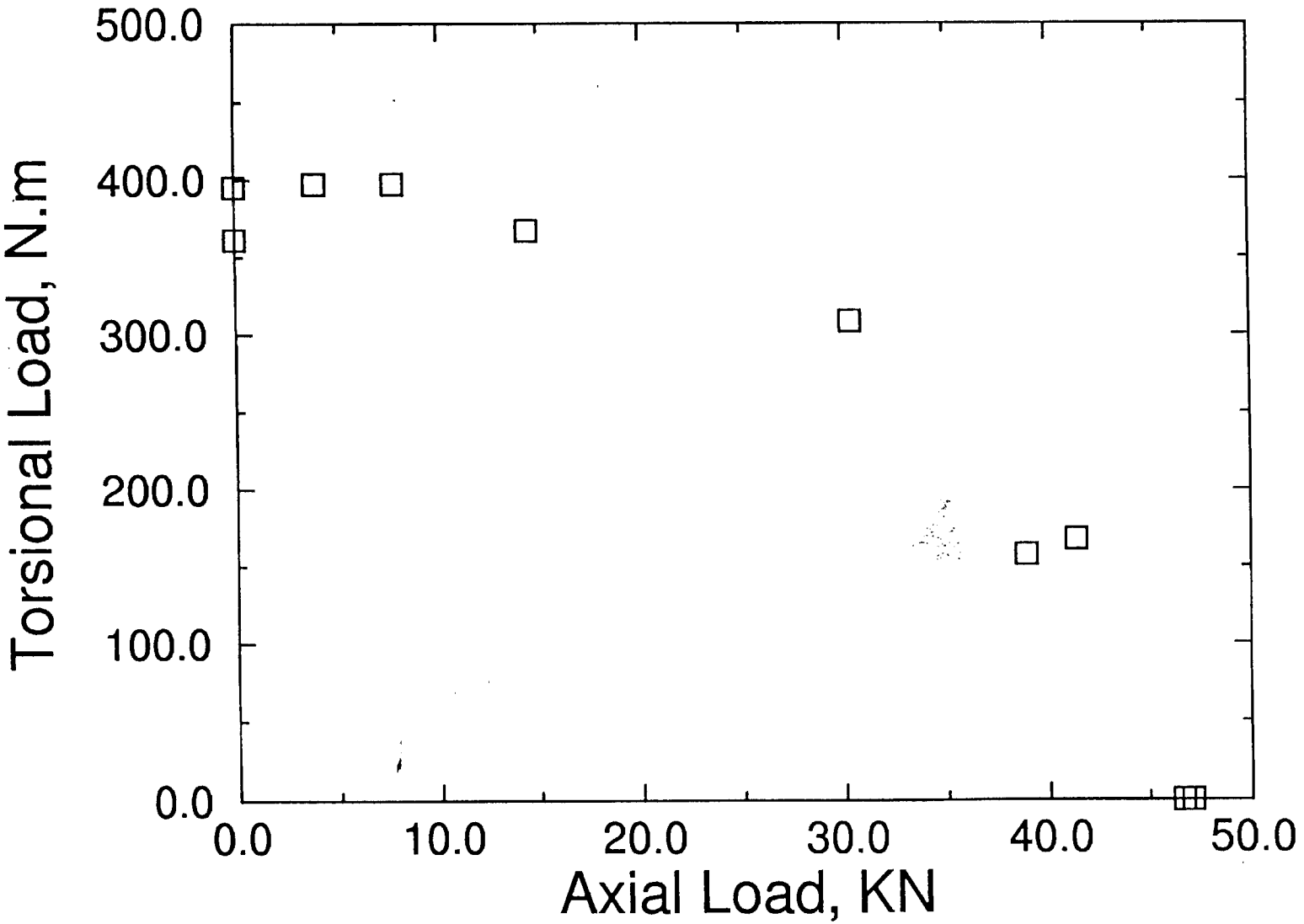

Fig. 6 Failure locus of a tubular bonded joint subjected to tension/ torsion.

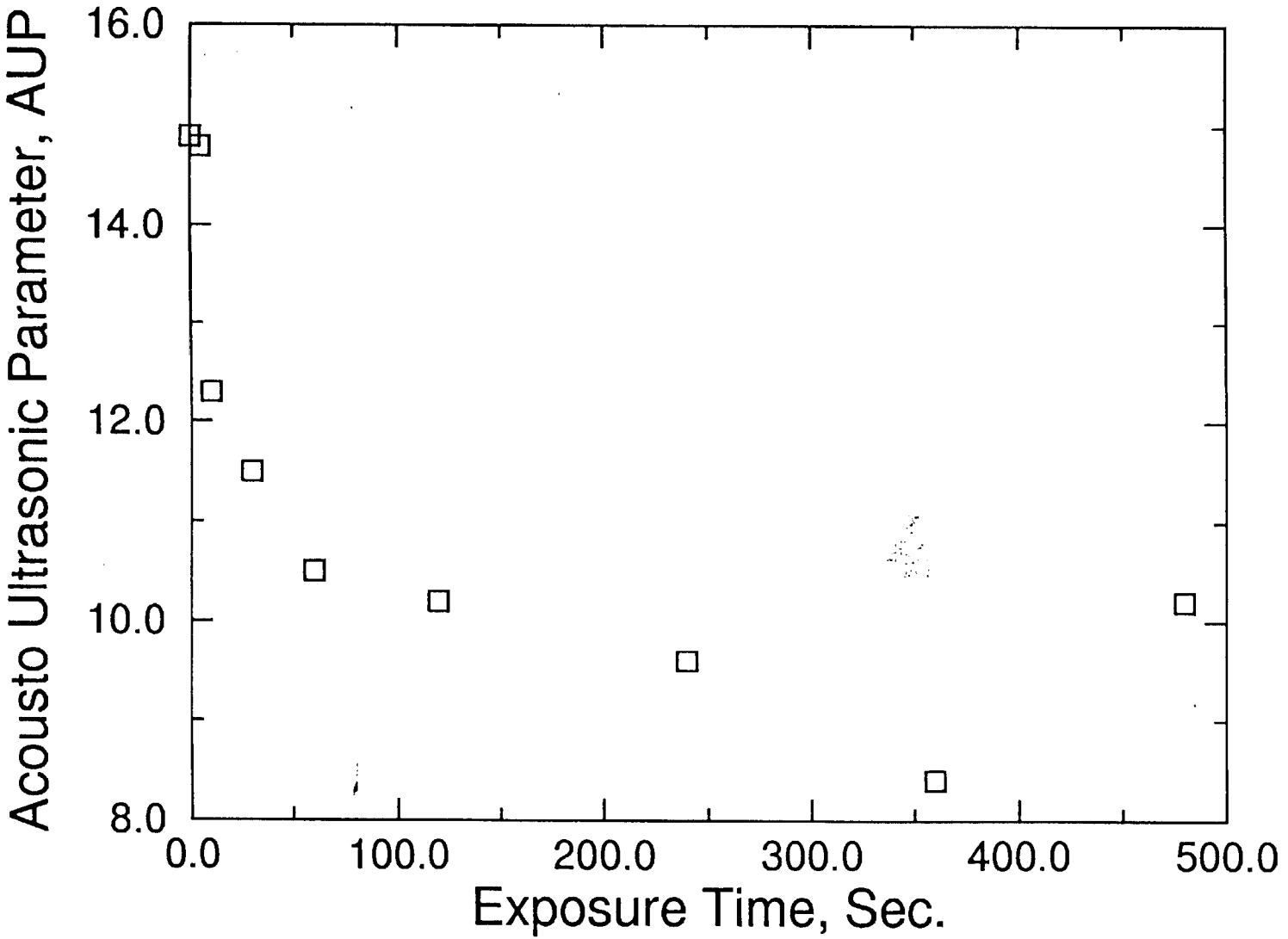

Fig. 7 Variation of the acousto ultrasonic parameter with the heat damage time of a fiber glass epoxy composite.

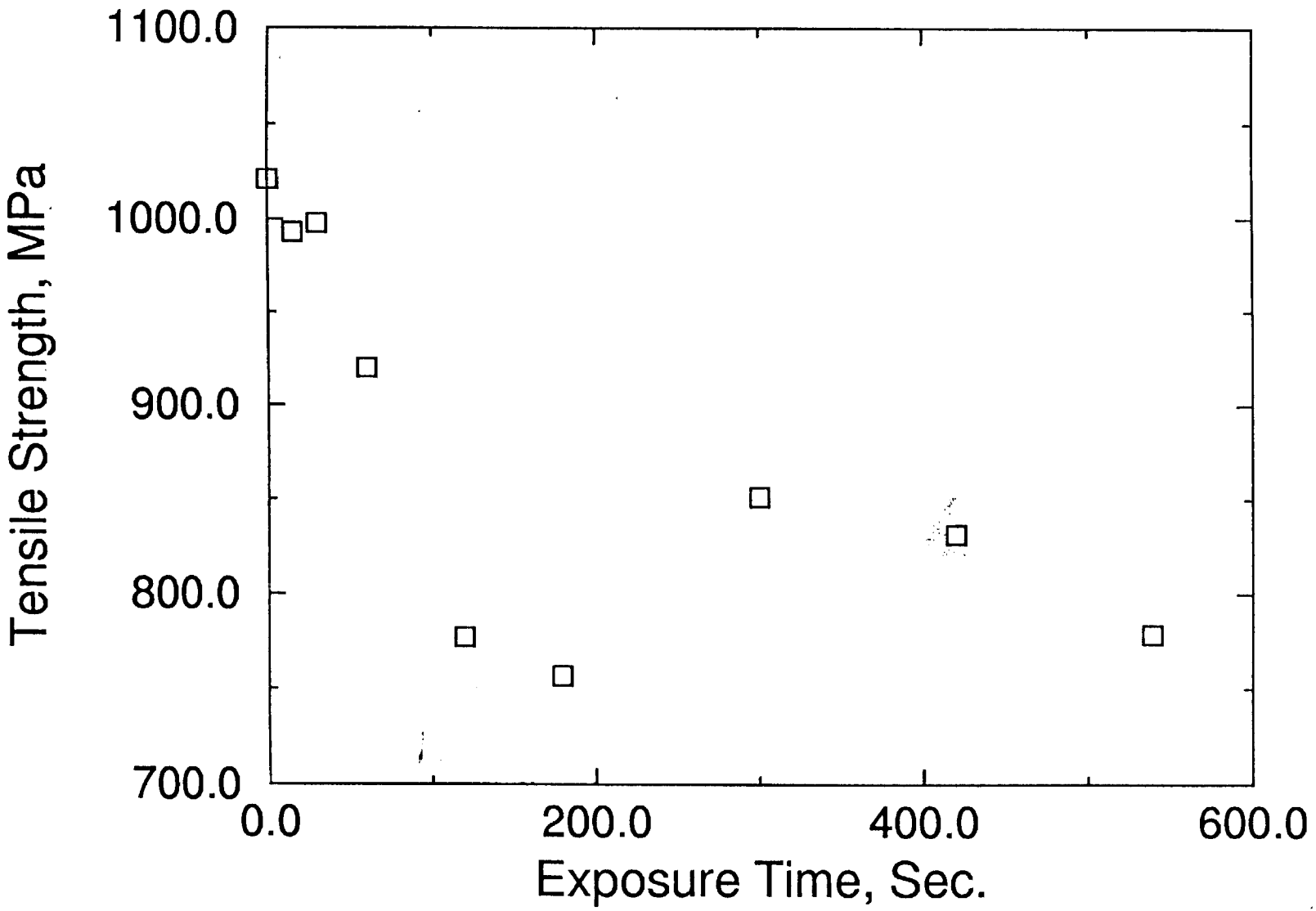

Fig. 8 Variation of the tensile strength with the heat damage time of fiber glass epoxy composites.

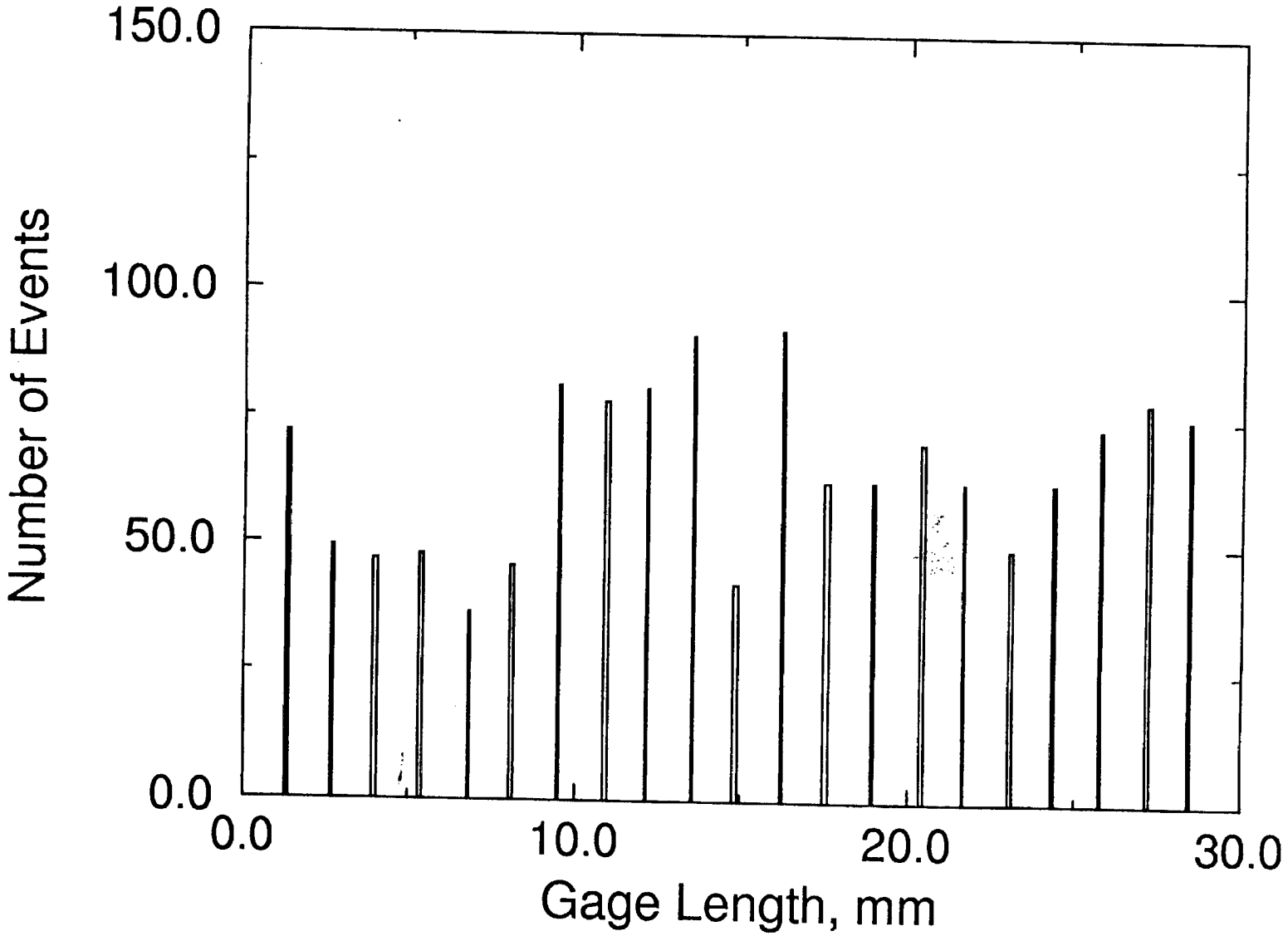

Fig. 9 Events per location of a fiber glass epoxy composite with no heat exposure.

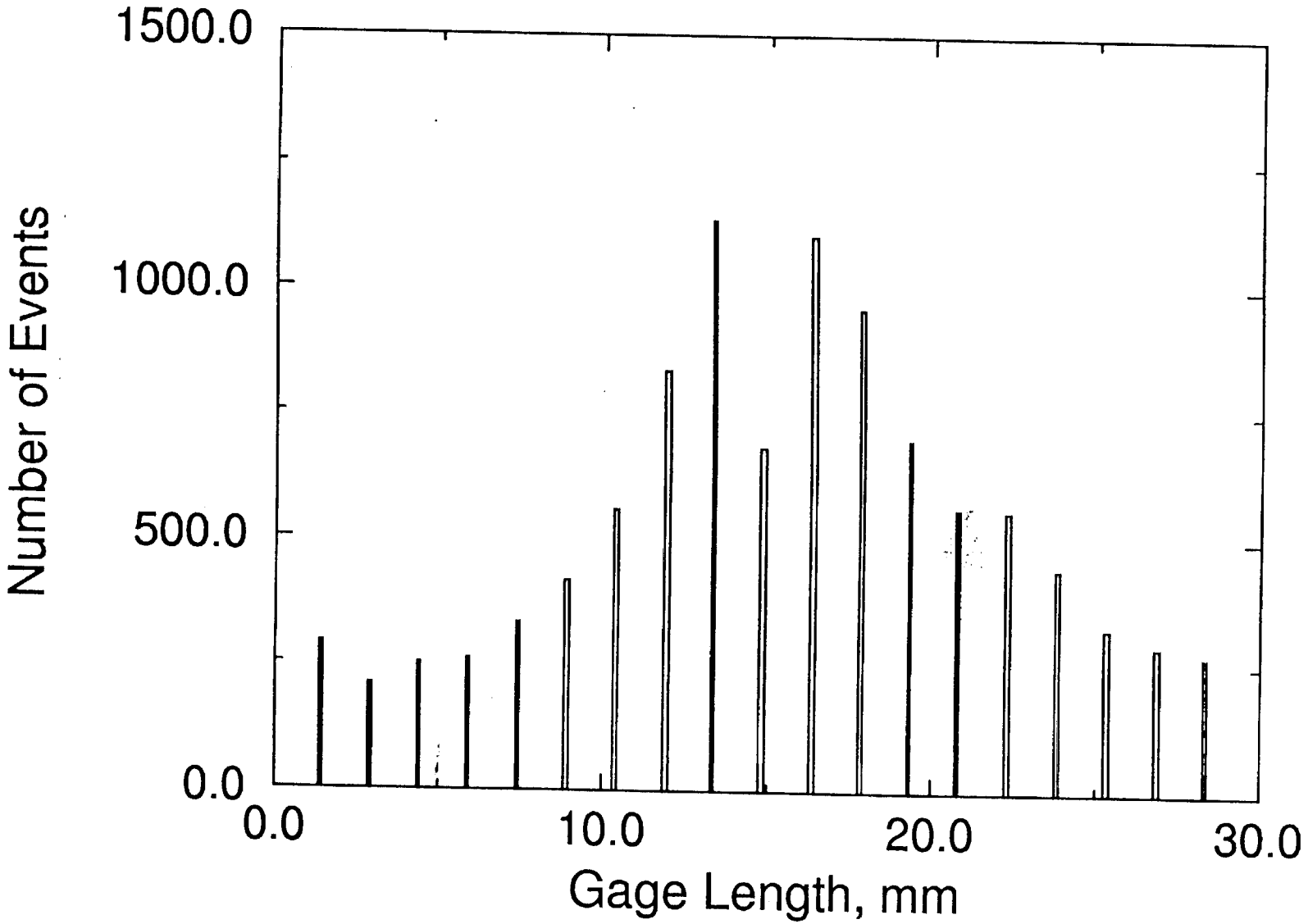

Fig. 10 Events per location of a fiber glass epoxy composite subjected to a localized heat exposure at 400 C for 1 minute.

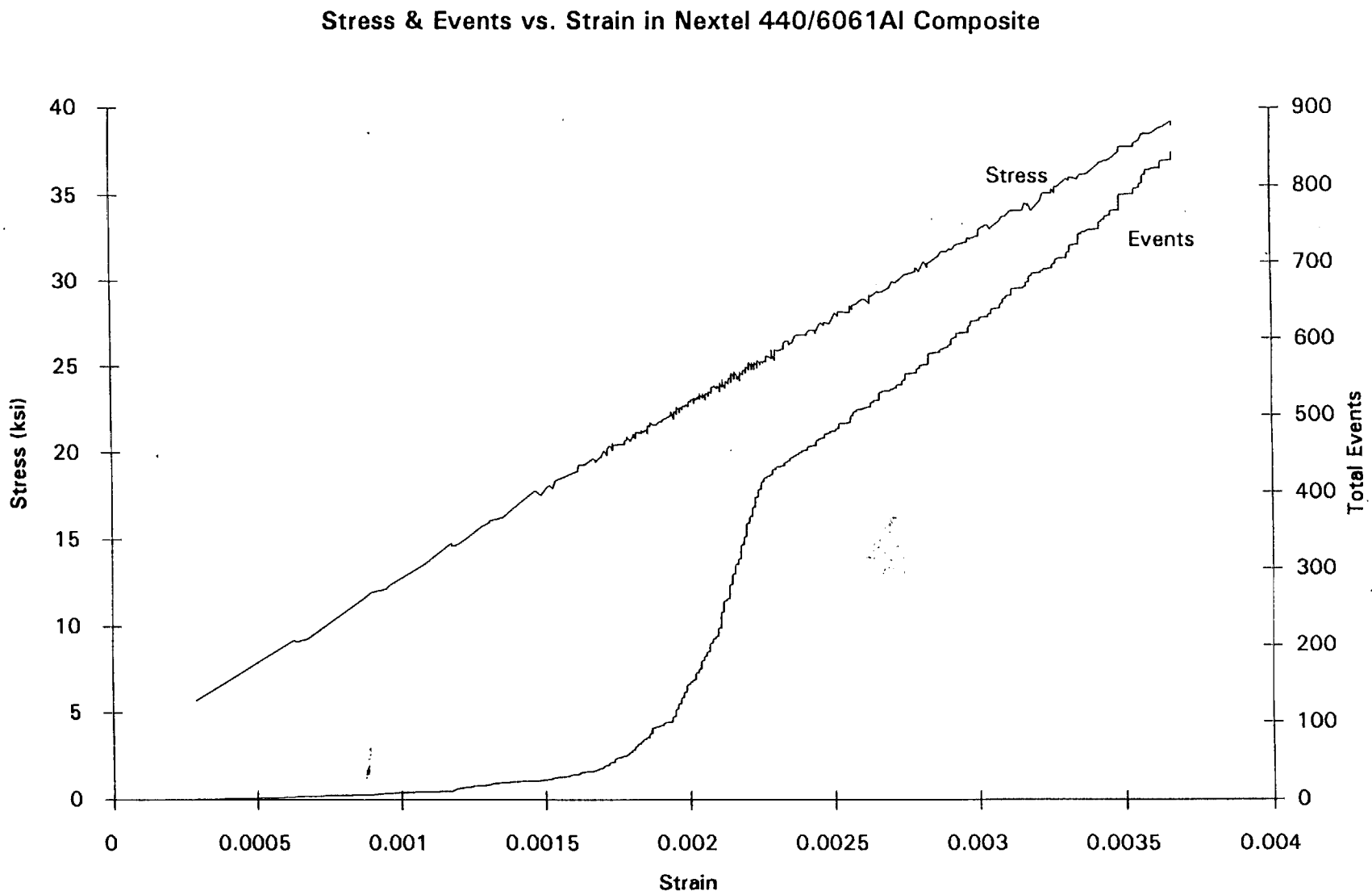

Fig. 11 Events versus applied strain in an alumina fiber reinforced aluminum metal matrix composite.